APPLICATION OF POLYETHYLENE-GLYCOL LINKED MULTI-WALLED CARBON NANOTUBES FOR IMPROVED STEM CELL DIFFERENTIATION

ZHAO CHUNYAN

NATIONAL UNIVERSITY OF SINGAPORE

2015

APPLICATION OF POLYETHYLENE-GLYCOL LINKED MULTI-WALLED CARBON NANOTUBES FOR IMPROVED STEM CELL DIFFERENTIATION

ZHAO CHUNYAN

(Master, Sichuan University)

A THESIS SUBMITTED

FOR THE DEGREE OF DOCTER OF PHILOSOPHY

DEPARTMENT OF PHARMACY

NATIONAL UNIVERSITY OF SINGAPORE

2015

Declaration

I hereby declare that this thesis is my original work and it has been written by me in its entirety. I have duly acknowledged all the sources of information which have been used in the thesis.

This thesis has also not been submitted for any degree in any university previously.

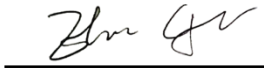

Zhao Chunyan
10 August 2015

Acknowledgements

I would like to express my deepest gratitude to my main supervisor, Dr. Ho Han Kiat, for his constant support and encouragement over the 4 years. Without his meticulous guidance, none of my accomplishments would have been possible. I have also been very fortunate to have had A/Prof. Giorgia Pastorin as my co-supervisor. I am honored that she entrusted me to work on this project, and I am grateful that she has been an invaluable source of continual guidance, stimulation discussion and help throughout this endeavor.

I would like to thank the members in my thesis advisory committee, Dr. CHIU Ngar Chee Gigi and Dr. CHOO Boon Hwa Andre, for their precious time and valuable advice about my work. I also greatly appreciate the help from A/Prof. EE Pui Lai Rachel and A/Prof. Dan Yock Young for cell supply, key equipment access and valuable discussions about my projects.

There have been many others to whom my gratitude is due. I would like to thank my collaborator, Henrik Andersen from the Department of Physics. Henrik helped tremendously with the physical characterization of PEG-CNT films. I would also like to thank A/Prof. Yap Von Bing for interesting discussions on statistics. My appreciation extends to Dr. Daniel Pickard and his lab members (Zhongkai, Hanfang, Fang Chao), for their assistance in characterization of PEG-CNT films by HIM. I would like to give my sincere thanks to Ms. Nur Halisah Bte Jumat and Dr. Zhou Lei for the help in hAEC work, to A/Prof. CHAN Chun Yong Eric and James for passing me HepaRG cells.

I am especially indebted to Li Jian and Priyankar for the help in PEG-CNT synthesis, to Sia Lee for showing me the cell culturing techniques, to Winnie, Lee Cheng, Angie

and Cheau Yih for the technical assistance in RT-PCR and western blot, to Tao Ran for guiding me through immunostaining assays. Besides them, my gratitude extends to the former and current members in the Laboratory of Liver Cancer and Drug-induced Liver Disease Research Group, especially Yi Yun, Yun Shan, Sheela, Jie Kai and Carrie, not only for their scientific guidance, but also for their great company and support. My heartfelt thanks also go to the former and present members in Giorgia Research Group, in particular Sudheer, Gopal, Yi Ming, Wei Jiang, Jie Ling, Qun Yuan, Aaron, Yang Zhi, Bertrand and Christopher, for their friendship and help in many ways. I would like to thank my FPY student, Vivien, for her technical assistance, energy and curious perspectives in PEG-CNT film project.

I am grateful to the financial support from NUS (research scholarship, NanoCore) which has enabled me to undertake this study. I am also grateful to the grants (NUS-FRC R-148-000-129-112 and R148-000-187-112) for monetary support in the scientific research. For helping with the administrative hurdles at NUS, I am thankful to the administration staff, lab technologies and support staff who have render their kind assistance at numerous occasions.

I also want to thank my friends and colleagues: Tao Ran, Kamila, Michelle, Ariana, Hui Li, Lu Qi, Chen Wan, Long Wei, Yuan Jie, Yang Xuan, Pan Jing, Hai Rui, Li Fang, Shi Qing, Wen Xia, Yan Bo and the others in S4 L3. You made my time at NUS Pharmacy enjoyable.

Finally, I would like to express my warmest gratitude to my family who made my education possible. To my parents, your support through the hard times was constant

and sure. I could not have made it without you. To Zhongkai, you were my source of inspiration. I would have never begun this path without you. Thank you for the loving support and tolerance during many difficult times in the course of my studies, especially during the thesis writing period. I am indebted to all of you.

Table of Contents

Summary

The cornerstone of successful tissue engineering rests upon a constructive interaction between cells and scaffolds. Stem cells have unique capabilities of self-renewal and multi-lineage differentiation to serve as a versatile cell source, while polyethylene glycol linked multi-walled carbon nanotubes (PEG-CNTs), with high conductivity, large surface-to-volume ratio, outstanding mechanical properties and nanotopographic features, have lately emerged as a promising candidate in producing scaffolds. This thesis, therefore, investigated the application of PEG-CNT-based scaffolds to modulate the differentiation of various stem cells into dedicated cell lineages for tissue engineering to address specific clinical needs.

PEG-CNT films were prepared on cover slips with nanoscale surface roughness, orderly arrangement of PEG-CNTs, high hydrophilicity and high mechanical strength. The influence of PEG-CNT films to modulate skeletal myogenic differentiation of human mesenchymal stem cells (hMSCs) was explored. Notably, PEG-CNT films alone could direct the skeletal myogenic differentiation of hMSCs, even in the absence of myogenic induction factors. The quantitative real-time polymerase chain reaction (RT-PCR) showed that the non-induced hMSCs plated on PEG-CNT films, compared to the negative control, presented significant up-regulation of general myogenic markers including MyoD, desmin and MHC. Corresponding protein analysis by immunoblot assays corroborated these results. Skeletal muscle-specific markers, TnC and Ryr, were also found significantly increased in the non-induced hMSCs on PEG-CNT films by RT-PCR. For these cells, the commitment to specific skeletal myoblasts

was further proved by the absence of enhanced adipogenic, chondrogenic and osteogenic markers. This study elucidated that PEG-CNT films supported a dedicated differentiation of hMSCs into a skeletal myogenic lineage.

To enhance the myogenic differentiation of hMSCs, we designed and fabricated a PEG-CNTs coated poly-acrylamide hydrogel with close stiffness to human muscle (CNT-PA-M). hMSCs demonstrated efficient attachment and maintenance on the CNT-PA-M. Additionally, spontaneous myogenesis of hMSCs on CNT-PA-M was observed by immunostaining of MyoD, desmin and MHC, indicating that scaffold stiffness adjustment could be a key parameter to fine-tune, in order to optimize stem cell differentiation.

As a result, PEG-CNTs coated poly-acrylamide hydrogel with calibrated stiffness that mimicked healthy human liver (CNT-PA-L) was prepared and examined for its effect on modulating differentiation of human amniotic epithelial cells (hAECs) into functional hepatocyte-like cells (HLCs). Firstly, the CNT-PA-L supported HLCs adhesion and growth, coaxing them to assume a hepatocytic polygonal morphology. Secondly, at the end of 18 days, the HLCs on CNT-PA-L lost pluripotent markers (Nodal, Nanog and OCT4) and up-regulated several hepatic markers (AFP, ALB, HNF4α, α1AT, CK18, G6P, CYP3A4, CYP2C9), some of which were even higher than that in HepG2 or HepaRG cells, through RT-PCR-based transcript analysis. Protein expression analysis by immunostaining substantiated these results. Furthermore, the HLCs on CNT-PA-L demonstrated functional capabilities of hepatocytes in terms of some ALB secretion, higher uptake of indocyanine green and comparable CYP3A4

enzymatic function and its inducibility as compared to HepG2 cells. Taken together, CNT-PA-L provides an efficient and scalable platform for the expansion of HLCs from hAECs.

Collectively, these landmark findings led us to conclude that PEG-CNTs could be a highly versatile coating material to enhance the course of stem cell differentiation towards dedicated lineages under suitable conditions by using proper stem cells as starting points (e.g., hMSCs or hAECs).

List of Tables

List of Figures

List of Abbreviations

α1AT	α1-anti-trypsin
AC	Alternating current
A-CNT-PA-L	Aligned PEG-CNTs coated liver stiffness mimicked poly-acrylamide hydrogel
A-CNT-PA-M	Aligned PEG-CNTs coated muscle stiffness mimicked poly-acrylamide hydrogel
AFM	Atomic force microscope
AFP	α-fetoprotein
ALB	Albumin
ALP	Alkaline phosphatase
AP2	Adipocyte protein 2
BDGF	Brain-derived neurotrophic factor
bFGF	Basic fibroblast growth factor
BME	β-mercaptoethanol
BMP	Bone morphogenetic protein
BSA	Bovine serum albumin
CD73	Cluster of differentiation 73
CD90	Cluster of differentiation 90
CD105	Cluster of differentiation 105/endoglin
CK18	Cytokeratin 18
CNTs	Carbon nanotubes
CNT-PA-L	PEG-CNTs coated liver stiffness mimicked poly-acrylamide hydrogel
CNT-PA-M	PEG-CNTs coated muscle stiffness mimicked poly-acrylamide hydrogel
Col-I	Collagen type I
Col-II	Collagen type II
CSM	Continuous stiffness measurement
CYP	Cytochrome P450
DAPI	4, 6-diamidino-2-phenylindole
DMEM	Dulbecco's Modified Eagles Medium
DMF	Dimethylformamide
DXM	Dexamethasone
ECM	Extracellular matrix
EGF	Epidermal growth factor
ELISA	Enzyme linked immunosorbent assay
FBS	Fetal bovine serum
FGF-2	Fibroblast growth factor-2
G6P	Glucose-6-phosphatase
GAPDH	Glyceraldehyde 3-phosphate dehydrogenase
GDNF	Glial cell line-derived neurotrophic factor

hAECs	Human amniotic epithelial cells
HCM	Hepatocyte culture medium
hESCs	Human embryonic stem cells
HGF	Hepatocyte growth factor
HIM	Helium ion microscope
HLCs	Hepatocyte-like cells
hMSCs	Human mesenchymal stem cells
HNF4α	Hepatocyte nuclear factor-4-alpha
HSCs	Hematopoietic stem cells
ICG	Indocyanine green
LDR	Luminescence Detection Reagent
LPL	Lipoprotein lipase
MHC	Myosin heavy chain
MSCs	Mesenchymal stem cells
Myf5	Myogenic factor-5
MyoD	Myoblast differentiation protein
NPCs	Neural progenitor cells
NSCs	Neuronal stem cells
NTA	Nicotinamide
OCN	Osteocalcin
OCT4	Octamer-binding transcription factor 4
OPN	Osteopontin
PCL	Polycaprolactone
PDGF	Platelet-derived growth factor
PEG-CNTs	Polyethylene glycol linked multi-walled carbon nanotubes
PLGA	Poly-(D, L-lactic-co-glycolic acid)
PLLA	Poly-L-lactic acid
PMMA	Poly-(methyl methacrylate)
PTFE	Poly-tetrafluoroethylene
PVA	Poly-vinyl alcohol
PVDF	Poly-vinylidene difluoride
RA	Retinoic acid
RMS	Root Mean Square
RT-PCR	Real-time polymerase chain reaction
Ryr	Ryanodine receptor 1
SEM	Scanning electron microscope
SKMCs	Human skeletal muscle cells
Sox9	SRY (sex determining region Y)-box 9
sulfo-SANPAH	Sulfosuccinimidyl 6-((4-azido-2-nitrophenyl) amino) hexanoate
TGF-β	Transforming growth factors β
TGA	Thermogravimetric analysis
TnC	Fast skeletal troponin C

CHAPTER 1. Introduction

1.1 Tissue engineering

Organ/tissue transplantation is often the only treatment for end stage organ/tissue failure, which cannot otherwise be adequately treated pharmacologically (1). In terms of organs, the kidneys are the most frequently transplanted organs, followed by the liver and then the heart. Diabetes, hypertension and inherited kidney diseases such as polycystic kidney disease are the most common causes of kidney failure requiring transplants (2). In addition, liver failure can be caused by viral infections, genetic disorders or even alcoholism. These conditions result in cirrhosis, which forms scar tissue that blocks blood flow and thus impedes essential liver functions in terms of detoxification, protein synthesis and digestive biochemical production. Liver transplantation is thus required when the liver failure severely impairs patients' health and life quality (3). Moreover, a number of heart diseases, including coronary artery diseases, cardiomyopathy or heart muscle weakening, may render transplantation necessary (4). In the situation of tissue transplantation, cornea and musculoskeletal grafts are the most commonly transplanted tissues. A corneal graft can restore sight in corneal blindness; bone and tendon transplantation can be carried out to replace or reconstruct tissues destroyed by tumors, trauma or infection, thus saving limbs that would otherwise be amputated.

Based on the source of the donor, the living organs/tissues transplantation can be divided into autografts (implants from patient to himself/herself) or allografts (implants from a donor). Both autografts and allografts require the removal of healthy

organ/tissue to replace the damaged parts, and therefore they are severely limited by crucial tissue shortage and can lead to donor-site morbidity, which further causes functional loss (5). Furthermore, allografts are often associated with an immune rejection and expose the patients to higher risk of viral infections.

Artificial grafts such as man-made blood vessels and artificial joints have been developed and applied clinically (6, 7). However, they cannot recapitulate all the functions of real tissues and may not be able to undergo tissue repair, hence limiting their long-term viability (8). Moreover, adverse inflammatory and immune reactions or even direct toxicity provoked by an artificial implanted material can jeopardize their applications. For example, infections are common among patients with artificial joints (9); silicone breast implants could also cause a systemic inflammatory disorder in clinic (10).

The need for improved treatments has motivated research on tissue engineering and has now emerged as a potential preference to organ/tissue transplantation. Tissue engineering is defined by Prof. Williams as "the creation or formation of new tissue for the therapeutic reconstruction of the human body, by the deliberate and controlled stimulation of selected target cells through a systematic combination of molecular and mechanical signals" (11). For therapeutic applications, the engineered tissue is either grown in patients (e.g., chondrocytes embedded in a matrix to form the expected functional cartilage tissue) or outside the patients and transplanted subsequently (e.g., fully functional liver tissue). This tissue technology could regenerate patients' tissues or organs that are biocompatible, biofunctional, immunologically compatible and

easily available. In addition to these attributes, tissue engineering may provide a stable resource of tissue for *in vitro* applications, such as pharmaceutical testing (e.g., uptake, metabolism and toxicity of drugs), investigating the pathogenicity of diseases, industrial production of insulin by bioartificial pancreas, generation of blood cells to reduce the need for blood donors etc. (12).

To regenerate new tissues, the two most essential components are cells and scaffolds. The cells, which may be a part of an engineered tissue [e.g., human mesenchymal stem cells (hMSCs) encapsulated inside a hydrogel matrix for muscle tissue engineering *in vitro* (13)] or recruited *in vivo* with the help of scaffolds [poly-L-lactic acid (PLLA)/demineralized bone powders (DBPs) scaffolds alone repaired rat skull defects *in vivo* (14)], constitute the "prototype" of the living tissue to generate and to synthesize matrices for repopulation; the scaffolds provide an appropriate environment to facilitate intercellular contact and signaling, and consequently enable the cells to effectively engraft into host tissues and recapitulate endogenous functions. In some cases, cells and scaffolds could collaborate with differentiation inducing factors, such as proteinaceous growth factors and chemical inducers, which function as "switches" for facilitating and committing the cells to differentiate into the respective cell lineages and attain the fully functionalized new tissue (15).

1.2 Stem cells in tissue engineering

Although several tissues are important sources of therapeutically relevant differentiated cells, the inevitable problems are the difficulty in harvesting sufficient cells for

implantation. Lineages such as neurons and cardiac cells, being terminally differentiated and non-regenerative, impose the biggest challenge. In this light, pluripotent stem cells have attracted much attention due to their unique capabilities of self-renewal in an undifferentiated state for prolonged duration and multi-lineage differentiation with proper stimuli (16).

Intuitively, the foremost resource of pluripotent stem cells are the embryonic stem cells (ESCs). They are obtained from the inner cell mass of blastocysts and can generate all cell types in the body. Due to the tumorigenic potential of ESCs (17) as well as the legal and ethical considerations associated with their usage (18), the application of ESCs in tissue engineering at large remains rudimentary as of today.

Recent establishment of induced pluripotent stem cells (iPSCs) generated directly from adult cells (e.g., epithelial cells) emphasizes their potential to derive patient-specific ESC equivalents. The technology of introducing four specific genes (Oct3/4, Sox2, c-Myc, and Klf4), which encode transcription factors, could convert adult cells into iPSCs, as published by Shinya Yamanaka's lab in 2006 (19). The iPSCs exhibit similar features to ESCs, including cell morphology, cell markers, growth properties, telomerase activity (20, 21) and giving rise to every other cell type in the body (19). These iPSCs seemingly present fewer ethical concerns than hESCs since they can be derived directly from adult tissues, thus bypassing the need for manipulating embryos. Moreover, each individual could have his/her own pluripotent stem cell line by a patient-matched manner. However, the major concern with the potential clinical application of iPSCs is their propensity to form tumors (22). Thus, more research is

still required to reveal the nature and the therapeutic usefulness of iPSCs to achieve the stage where therapeutic transplants can be deemed safe.

Fortunately, these concerns are less pervasive in adult stem cells because of minimal tumorigenicity concerns (23). Moreover, adult stem cells are isolated from various tissues (including bone marrow, adipose tissue, umbilical cord and umbilical cord blood) and differentiate into cells of their own lineages or even atypical lineages in some cases (24). The main function of adult stem cells is to maintain and repair the tissue in which they are found. Some of the commonly applied adult stem cells in tissue engineering are mesenchymal stem cells (MSCs) (25), neuronal stem cells (NSCs) (26), hepatic stem cells (27) and hematopoietic stem cells (HSCs) (28) from both human or non-human sources. The most explored adult stem cells are human MSCs (hMSCs), owing to their wide range of sources and multiple differentiation abilities (Figure 1.1). They are attractive, being readily isolated from bone marrow (29), glomeruli (30), umbilical cords (31), umbilical cords blood (32), lacrimal glands (33) and other easily accessible sources such as adipose tissue (34) and peripheral blood (35). Under appropriate conditions, mainly *via* biochemical inducers, MSCs can differentiate into osteocytes, chondrocytes, adipocytes, myocytes and even trans-differentiate into hepatocytes, cardiomyocytes and neurons (23). Comparing to ESCs, adult stem cells have morelimited pluripotency and are often restricted to differentiate into lineages within germ layer. The ability of adult stem cells from one germ layer to differentiate into cell types from different germ layers is called trans-differentiation (36). By using the patients' own hMSCs, it is possible for an autologous transplant and thus avoids

tissue rejection effects (37).

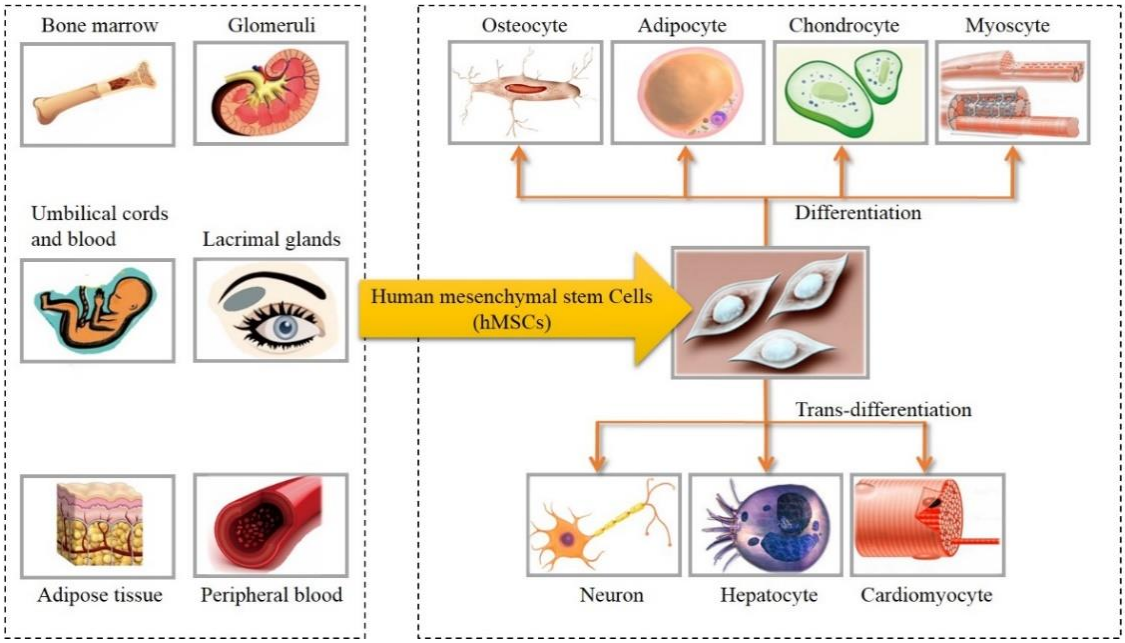

Figure 1.1 hMSC sources and capability of differentiation and trans-differentiation.

Different multipotent stem cells are also found in amniotic fluid and amniotic membrane (38-40). The amniotic fluid contains a heterogeneous mixture of multipotent cells, such as MSCs, embryonic-like stem cells and HSCs (41). Additionally, human amniotic epithelial cells (hAECs) can be isolated from the amniotic membrane and have shown multipotent potential, being able to differentiate into neural and glial cells (42), osteoblasts (43) and hepatocytes (44, 45). The amniotic fluid and amnion derived stem cells have non-tumor forming property, which is a similarity shared with adult stem cells. This property could be an advantage over hESCs and iPSCs when medical applications are considered (41). More importantly, ethical issues pertaining to the isolation of these cells could be minimized.

1.3 Nanomaterials in tissue engineering

In most native tissues, cells are organized in a tissue-specific, three dimensional (3D) extracellular matrix (ECM), which comprises a complex network of nanoscale fibers forming highly structured local microenvironments (46). Cellular communication, transport of oxygen and nutrients, removal of wastes and cellular metabolites require such environment, where cellular orientation can be polarized and movement of contents can be directional. Hence, in tissue engineering, most of the engineered organs/tissues need support, named scaffold, for their formation from cells. These scaffolds usually serve the purposes of supporting cell proliferation and differentiation, enabling diffusion of vital cell nutrients and expressed products, and exerting certain mechanical and biological influences to the cells. It is generally hypothesized that a close imitation to the natural ECM could provide scaffolds with a more conducive environment to support the adhesion, migration, proliferation and differentiation of stem cells (47, 48). Many physicochemical properties of ECM can exert subtle effects on the surrounding cells' biological cues. For one, we should notice the nanostructural features intrinsic to the natural ECM: (1) many tissues' basement membranes exhibit enormous nanotopographies, which affect cellular behaviors including adhesion, proliferation, migration and differentiation (49); (2) ECM molecules, such as collagen and hydroxyapatite crystals in bone, exhibit several nanostructures which are hypothesized to contribute to cell matrix signaling (50). In order to better mimic the nanostructures in natural ECM, engineered nanomaterials, which are defined by the size of materials with at least one dimension less than 100 nm (51), have recently

emerged as promising candidates in producing scaffolds that resemble the ECM and efficiently replace defective tissues. For manipulating stem cells' commitment, scaffolds derived from nanomaterials have been investigated over the past decade.

Nanofibers are one the suitable nanomaterials for stem cell engineering. They are ranging from synthetic biodegradable polymers [PLLA (52), poly-(D, L-lactic-co-glycolic acid) (PLGA) (53), polyvinyl alcohol (PVA) (54) or polycaprolactone (PCL) (55)] to natural materials such as collagen (56), gelatin (57) and chitosan (58). Besides biocompatibility and biodegradability, nanofibrous scaffolds are amenable to various functional modifications and can be prepared with 3D scale and highly porous network towards enhancing stem cell survival and proliferation or directing specific stem cell fates. Their utilization for nerve (59), cardiac, bone (60), skin, vascular and cartilage tissue engineering are intensively discussed in publications (61, 62). However, the intrinsic properties of these polymers generally lack additional multifunctional attributes such as adequate mechanical support, ability to guide/induce specific cellular processes (e.g., stem cell differentiation) (63).

More recently, a carbon-based material, **carbon nanotubes (CNTs)**, has been at the forefront of nanotechnology due to their unique properties, such as high conductivity, large surface-to-volume ratio, outstanding mechanical properties as well as nanotopographic features (64). Thus, their multifunctional characteristics have been exploited for the development of novel scaffolds to modulate stem cell differentiation for a range of applications in the field of tissue engineering. For example, CNTs are suitable materials for bone scaffolds due to their low density, high thermal conductivity

and elastic modulus (stiffness), and remarkable flexibility (65, 66). For the first time, a former study from A/P Giorgia Pastorin's lab found that the thin films of polyethylene glycol (PEG) linked multi-walled CNTs (PEG-CNTs) were not cytotoxic and accelerated the osteogenic differentiation of hMSCs, to a similar extent as compared to hMSCs cultured with a commonly used growth factor, the bone morphogenetic protein-2 (BMP-2) (67). This was demonstrated by quantitative real-time polymerase chain reaction (RT-PCR) analysis, immunostaining and alizarin red quantification (calcium mineralization). It was hypothesized that these regular nanoscale undulations on PEG-CNT film surface, which resembled the nanoarchitecture of the natural ECM, favored an efficient growth of hMSCs and eventually stimulated their further differentiation into bone cells. In neural engineering, CNTs are attractive materials because of their excellent electrical conductivity. Laminin/CNT thin films were developed and found to support human NSC (hNSC) growth and to be conducive to hNSC differentiation and successful excitation, from the observation of (1) extensive formation of functional neural network as indicated by the presence of synaptic connections; (2) generation of action potentials upon applying a lateral current through the CNT substrate by calcium imaging (68). The combination of CNT-based scaffolds and stem cells were also employed in cardiac muscle engineering for adjustment of the conductivity and mechanical strength of scaffolds to influence cardiomyocyte development. The research by Crowder SW *et al*. is a relevant example (69): as compared to the tissue culture polystyrene and PCL scaffolds, the electrospun PCL/CNT scaffolds enhanced the cardiomyogenic differentiation of hMSCs in the presence of 5-azacytidine (69).

More examples about the combination of CNT-based scaffolds and stem cells for tissue engineering are summarized in Table 1.1.

Table 1.1 Application of CNT-based scaffolds and stem cells in tissue engineering

Scaffold	Stem cells	Application areas	References
Oxidized CNTs (single-walled)	Murine ESCs	Bone engineering	(70)
PLGA/oxidized CNT (multi-walled) nanocomposites	Rat MSCs	Bone engineering	(71).
CNT (multi-walled) array	hMSCs	Bone engineering	(72)
CNTs (multi-walled)	Human adipose-derived stem cells	Bone engineering	(73)
PCL/CNTs (multi-walled) composite	hMSCs	Bone engineering	(74)
Aligned CNTs (single-walled)	hMSCs	Bone engineering	(75)
PLLA/CNT (single-walled) nanocomposite	hMSCs	Bone engineering	(76)
PEG-CNT (multi-walled) films	hMSCs	Bone engineering	(67)
CNT (single-walled) films	hMSCs	Neural tissue engineering	(77)
Laminin/CNT (single-walled) films	hNSCs	Neural tissue engineering	(68)
Poly-methacrylic acid grafted CNT (multi-walled) films	hESCs	Neural tissue engineering	(78)
Poly-acrylic acid grafted CNT films	hESCs	Neural tissue engineering	(79)
Silk/CNT (multi-walled) composite	hESCs	Neural tissue engineering	(80)
PDMS/CNT (multi-walled) sheets	Rat adipose-derived stem cells	Neural tissue engineering	(81)
PLLA/CNT (multi-walled)/silk fibroin nanofibers	Human adipose-derived stem cells	Neural tissue engineering	(82)

Table 1.1 Application of CNT-based scaffolds and stem cells in tissue engineering (continued)

Scaffold	Stem cells	Application areas	References
Collagen/CNT (single-walled) fiber	Human decidua parietalis placental stem cells	Neural tissue engineering	(83)
Collagen/CNT (multi-walled) hydrogels	Rat MSCs	Neural tissue engineering	(84)
Oxidized CNTs (multi-walled)	hMSCs	Neural tissue engineering	(85)
CNT (Single-walled) rope	Rat NSCs	Neural tissue engineering	(86)
PCL/CNT (multi-walled) composite	hMSCs	Cardiac tissue engineering	(69)
PCL/thiophene-CNTs (multi-walled) meshes	Murine cardiac stem cells	Cardiac tissue engineering	(87)
PLLA/oxidized CNT (single-walled) nanofibers	hMSCs	Cardiac tissue engineering	(88)

CNTs can be seen as cylindrical tubes of rolled graphene sheets (Figure 1.2). Based on the composition of a single tube or concentric cylinders, CNTs are divided into single-walled CNTs or multi-walled CNTs, both of which have similar properties in general. During chemical modification, the outer walls of multi-walled CNTs can protect the inner CNTs from surface modification, thus preserving the intrinsic properties. However, the electrical and mechanical properties of single-walled CNTs can change upon functionalization, due to the structural defects of C=C bond breakages through chemical process (89). Other advantages of multi-walled CNTs over single-walled CNTs include higher tensile strength (90, 91), ease of mass production and low product cost. Therefore, multi-walled CNTs are more frequently used than single-walled CNTs in tissue engineering (Table 1.1).

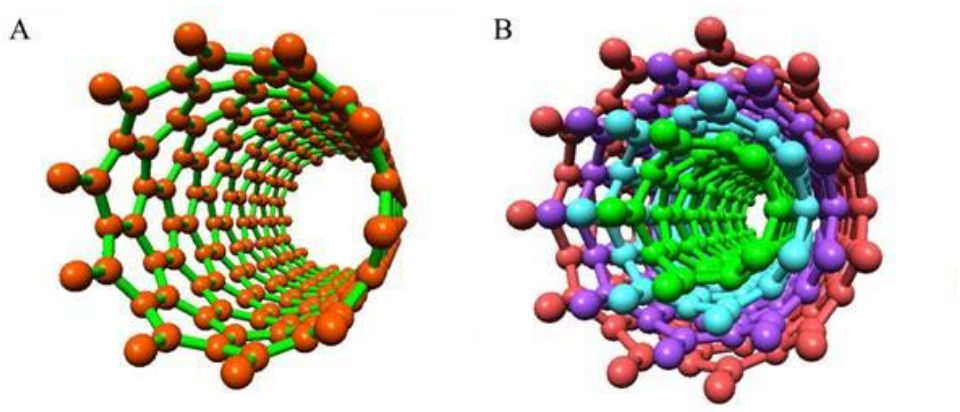

Figure 1.2 Schematic illustration of (A) single-walled and (B) multi-walled CNTs.

In the past several years, CNT toxicity to cells and tissues has received a great deal of attention (92, 93). CNTs were shown to inhibit proliferation of HEK293 cells and to decrease cell adhesion in a dose- and time-dependent manner (94). In another study, the potential pulmonary toxicity of CNTs in mice was investigated and it was considered that chronic inhalation and/or exposure to CNTs could be a serious occupational health hazard (95). However, controversy exists with some studies reporting that CNTs are non-cytotoxic and excellent substrates for cellular growth. Mooney *et al*. reported that CNT suspension displayed good biocompatibility with hMSCs, and supported proliferation as well as differentiation of hMSCs in the presence of an induction medium (96). In addition, exposure of adipose-derived stem cell (ADSCs) to a wide range of dispersed CNTs (0.1, 1, 10, 20, 50, 100 μg/ml) for 3 and 7 days revealed that low-dose CNTs (0.1 and 1μg/ml) increased viability and proliferation in mild ranges, but a high dose of CNTs inhibited proliferation and reduced the viability of ADSCs (97). Nowadays, there have been extensive efforts,

through synthesis, purification and functionalization, toward mitigating nanotube cytotoxicity and improving their biocompatibility (98-100). For example, a non-covalent functionalization scheme was exploited to allow carboxylic acid moieties to be attached to the CNT surface, thereby creating stable aqueous dispersions and limiting cytotoxicity (101). Additionally, Allen *et al*. demonstrated biodegradation of CNTs through natural enzymatic catalysis using horseradish peroxidase (102). Furthermore, Dumortier *et al*. demonstrated that CNTs functionalized with PEG chains did not show toxic effects when tested in a wide variety of immune cell types (103). Therefore, few clear conclusions have emerged from this body of work to date, due in part to the large degree of inherent variability between the fabrication methods, purity and functionalization of CNTs, as well as differences concerning the dose, mode of administration and type of exposure to cells and tissues (104).

Graphene is another carbon-based nanomaterial with a one-atom-thick sheet of carbon atoms arranged in a 2D honeycomb structure. It has received increasing attention for biomedical applications because of the remarkable properties like high surface area, high mechanical strength, and ease of functionalization (105). More importantly, graphene can be synthesized in a relatively pure form, making cell testing to be less affected by impurities (106). Although studies on graphene materials are still at a nascent stage, graphene has been widely used to help the development of stem cell engineering research. For example, a graphene substrate was observed to work as a promoter for human NSCs differentiation into neurons (107); Graphene (108) and 3D graphene foams (109) had the ability to facilitate the osteogenic differentiation of

hMSCs; Lee *et al*. reported that graphene enhanced the cardiomyogenic differentiation of human ESCs (110).

1.4 Differentiation induction factors for stem cell differentiation

To induce different lineage commitment, stem cells may require the appropriate extracellular signals to trigger or to promote this process. Differentiation induction factors from protein and chemical origins can constitute an important class of such stimuli. From protein sources, biological growth factors have been widely demonstrated to induce the differentiation of stem cells. For example, bone morphogenetic proteins (BMPs), such as BMP-2 and BMP-7, are known as the most potent growth factors for directing the osteogenesis of stem cells like MSCs and enhancing bone formation (111); transforming growth factors β1 and 3 (TGF-β1 and TGF-β3) can be utilized to enhance the differentiation of MSCs into chondrocytes (112); brain-derived neurotrophic factor (BDGF), platelet-derived growth factor (PDGF), glial cell line-derived neurotrophic factor (GDNF) (113) and basic fibroblast growth factor (bFGF) (114) are used to induce neural differentiation of NSCs, while epidermal growth factor (EGF) and bFGF can be utilized to promote neural trans-differentiation of MSCs (115); hepatocyte growth factor (HGF), EGF, TGF and insulin-like growth factor are employed to help MSCs to trans-differentiate into hepatocytes (116-118). Additionally, many non-proteinaceous chemicals are frequently used in the specific differentiation of stem cells *in vitro*. For instance, dexamethasone (DXM), ascorbic acid and β-glycerophosphate are typical osteogenic

inducers for MSCs (119); retinoic acid (RA) is used for neural differentiation of ESCs (120) and β-mercaptoethanol (BME) is utilized for neural trans-differentiation of MSCs (115); DXM, RA, sodium butyrate and nicotinamide (NTA) act as inducers for hepatic trans-differentiation of MSCs (116-118).

The devoted growth factors are either locally or systemically produced *in vivo*, and circulated to ECM to exert a paracrine or autocrine effect at injured sites for tissue formation or maturation. In contrast, some of the chemical differentiation induction factors such as DXM and BME cannot be generated *in vivo* and are mainly used *in vitro* stem cell culture. To support tissue regeneration in an *in vitro* setting, these biochemical agents can be loaded into scaffolds to promote or to induce differentiation of stem cells. However, the employment of differentiation inducers is dispensable under specific circumstances where only stem cells and scaffolds remain successful in tissue engineering. For example, oxidized CNTs were demonstrated to induce and to maintain neural differentiation of hMSCs without any exogenous differentiating factors, as evidenced by the protein expression (85). This outcome represents a development that accentuates the role of the scaffold in substituting some functions of differentiation factors besides just serving as structural support.

Beside differentiation inducer factors, physical cues from the immediate environment, such as stiffness or the surface roughness of the surrounding structure, can alter or enhance the fate and differentiation of the stem cells (121). Related knowledge will be discussed in the following chapters.

Overall, CNT-based scaffolds have been demonstrated to support or to enhance the attachment, growth and differentiation of various stem cells *in vitro* (Figure 1.3). The combination of CNT-based scaffolds and stem cells is a versatile strategy and can cover a broad range of applications (i.e., bone, nerve, and cardiac muscle, Table 1.1), with or without the differentiation induction factors (Figure 1.3). The permutation of this combination is not exhaustive. For this reason, more explorations in other tissue types, such as skeletal muscle and liver can be done and this needs further investigation. It is expected that the combination of stem cells and CNT-based scaffolds will develop into a powerful tool in tissue engineering for the innovative treatment of many diseases. This thesis will focus on a couple of these possibilities.

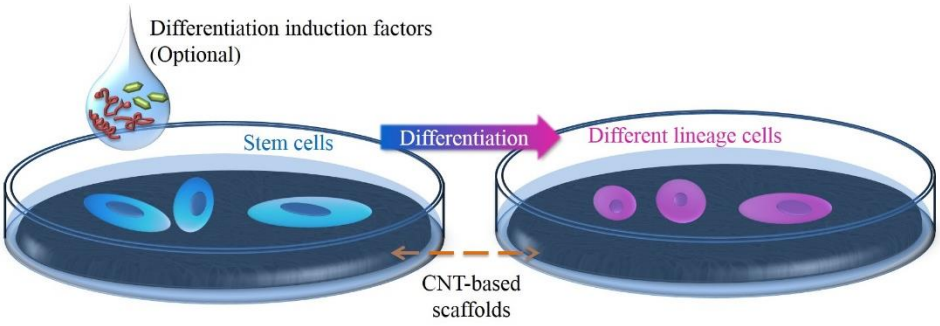

Figure 1.3 CNT-based scaffolds supported or enhanced the attachment, growth and differentiation of various stem cells *in vitro*.

CHAPTER 2. Hypotheses and objectives

2.1 Thesis rationale and hypotheses

As we discussed in Chapter 1, carbon nanotube (CNT)-based scaffolds supported cell growth and enhanced differentiation of stem cells into diverse lineages. Despite these potential biomedical applications, one challenge in using pristine CNTs is that they are extremely hydrophobic and rapidly precipitate in aqueous solutions, thus mitigating their beneficial characteristics. To improve the property of CNTs, polyethylene glycol (PEG) can be used to modify CNTs' surfaces and increase their hydrophilicity to facilitate scaffold preparation, cell adherence and growth (67, 122). Moreover, PEG linked multi-walled carbon nanotube (PEG-CNT) films were demonstrated to accelerate the osteogenic differentiation of human mesenchymal stem cells (hMSCs) by A/P Giorgia Pastorin's group (67). Therefore, it was hypothesized that PEG-CNTs may be a versatile coating material which provides nanoscale surface roughness and thus enhances the course of various stem cell differentiation towards dedicated lineages under suitable conditions. However, many of these possibilities have not been tested.

(1) CNTs have been used as an auxiliary material to modulate the conductivity or mechanical strength of scaffolds towards myotube formation from skeletal muscle progenitor cells in skeletal muscle engineering (123, 124). However, whether or not the intrinsic properties of CNTs themselves can influence the myogenesis of stem cells has not been fully investigated. Therefore, it is a novel and bold idea to determine the influence of PEG-CNTs to the skeletal myogenesis of hMSCs which have multi-lineage differentiation ability. The result would subsequently guide us towards successful

design of CNT-based scaffolds for engineering specific skeletal muscle tissues.

(2) Besides the surface features, the stiffness of scaffolds plays a critical role in the process of stem cell differentiation. Given the fact the PEG-CNT films were much stiffer than human muscle, we hypothesized the development of PEG-CNTs coated poly-acrylamide hydrogel (PA) with stiffness mimicking muscle (CNT-PA-M) would improve the myogenesis of hMSCs for skeletal muscle engineering.

(3) With the aim to further challenge the capability of PEG-CNT coating in directing stem cells' lineages and on the basis of importance of scaffold's stiffness, it was deduced that the PEG-CNTs coated PA with customized stiffness (CNT-PA-L) would be able to recreate the environmental profile of a healthy liver and could enhance the hepatic differentiation of a different stem cell source, the human amniotic epithelial cells (hAECs).

2.2 Objectives

Based on the rationale and hypotheses, the overall aim of this thesis is to explore the versatility of PEG-CNTs as a coating material in enhancing the differentiation of stem cells into dedicated lineages under proper conditions. Therefore, we propose the following specific objectives:

(1) Preparation and characterization of PEG-CNT films, and investigation of the influence of PEG-CNT films in modulating skeletal myogenic differentiation of hMSCs;

(2) Development and characterization of CNT-PA-M, as well as examination of the

effect of CNT-PA-M towards myogenic differentiation of hMSCs;

(3) Fabrication and characterization of CNT-PA-L, followed by determination of whether CNT-PA-L can enhance the hepatic differentiation of hAECs.

2.3 Experimental design

To achieve these objectives, three studies were designed and summarized in Figure 2.1. In Chapter 3, we will describe how we improve the PEG-CNT film preparation method and comprehensively characterize the films' surface roughness, hydrophilicity and stiffness. After culturing hMSCs on PEG-CNT films, cell viability will be tested to ensure the safety of application of PEG-CNT films in tissue engineering. The myogenic differentiation of hMSCs (with/without myogenic induction medium) on PEG-CNT films will be investigated through comparison with controls (cover slips) by quantitative real-time polymerase chain reaction (RT-PCR) and western blot assays. The osteogenesis, chondrogenesis and adipogenesis of hMSCs on PEG-CNT films will be determined to address if the myogenesis is lineage specific.

In Chapter 4, we will fabricate a novel scaffold of CNT-PA-M which has PEG-CNTs as the coating and muscle stiffness mimicked PA as the basement membrane. Since collagen is often used as a default ECM protein for surface coating in facilitating cell attachment, growth, differentiation, migration, and tissue morphogenesis, collagen-I (Col-I, the most abundant type of collagen in the body) coated PA with skeletal muscle mimicked stiffness (Col-PA-M) will be prepared as a control (125). To ensure successful development of scaffolds, characterization such as surface morphology and

stiffness will be performed. Finally, the myogenic differentiation of hMSCs (with/without myogenic induction medium) on CNT-PA-M, Col-PA-M and cover slips will be examined by cell viability and immunostaining studies.

In Chapter 5, PA with liver stiffness will be used as the basement support to be coated with PEG-CNTs (CNT-PA-L) and Col-I (Col-PA-L). After characterization of these scaffolds in terms of surface morphology and stiffness, hAECs will be seeded on CNT-PA-L, Col-PA-L and cover slips, and cultured in hepatic induction medium. The hepatic differentiation of hAECs on different substrates will be compared with cell viability, RT-PCR, immunostaining and hepatic function assays.

We will finally sum up the overall findings and future perspectives in Chapter 6.

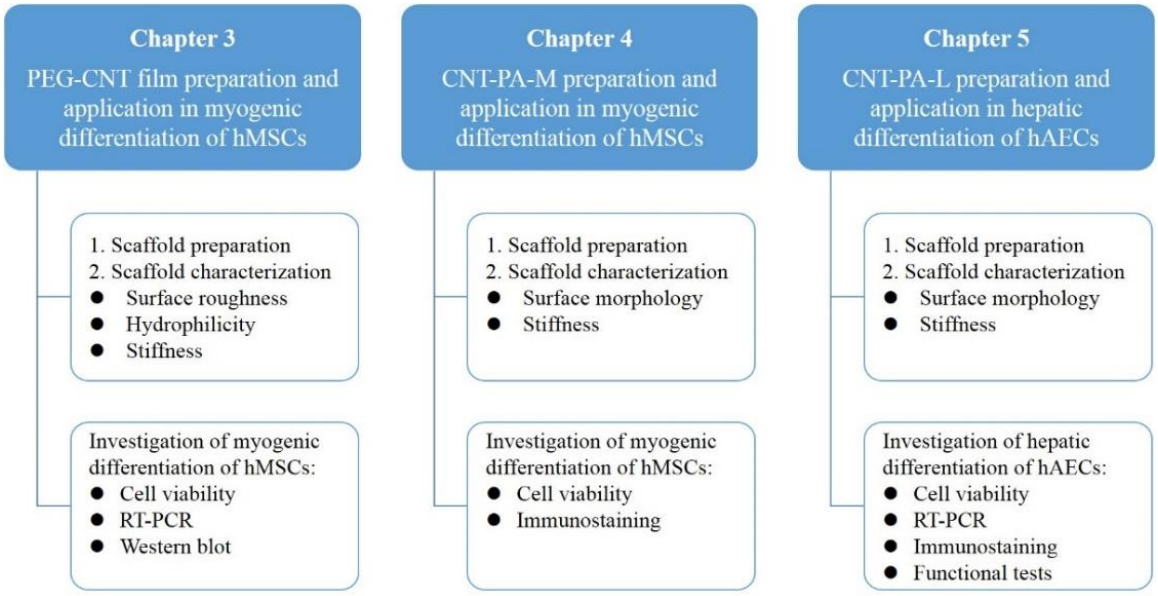

Figure 2.1 Thesis experimental design outline.

CHAPTER 3. Spontaneous and specific myogenic differentiation of human mesenchymal stem cells on polyethylene glycol-linked multi-walled carbon nanotube films for skeletal muscle engineering

3.1 Introduction

3.1.1 Skeletal muscle injury and therapy

Skeletal muscles, which are approximately 40% of all muscles and located throughout the human body, are responsible for the control of voluntary movement as well as the maintenance of structural contours and postures of the body (126). Skeletal muscle abnormalities can arise from a multitude of conditions including developmental anomalies, trauma, rhabdomyolysis of skeletal muscle, muscular dystrophy, diabetic tissue damage, irradiative injuries and physical injuries (127-129). As skeletal muscle tissues show limited regeneration capacity, these conditions, coupled with substantive surgical ablations, often result in permanent damage and loss of physical mobility (130). The current remedy for replacing skeletal muscle tissues involves autografts (implants from patient to himself/herself), allografts (implants from a donor) or artificial grafts. Considering the severe limitations of these therapies, such as limited supply (autografts), potential immune rejection and viral infections (allografts), adverse inflammatory and immune rejections or even direct toxicity (artificial grafts) (detailed discussion in Chapter 1, section 1.1, page 1), much effort was given to skeletal muscle engineering.

3.1.2 Cells in skeletal muscle engineering

Skeletal muscle cells (SKMCs) are produced when multiple myoblasts, muscle progenitor cells, differentiated and fuse together to form a fiber, within which each myoblast contributes one nucleus (131). The myoblasts that do not form SKMCs usually spontaneously dedifferentiate back into satellite cells. The satellite cells are specialized myoblast sub-population located between the sarcolemma and the basal lamina of the muscle fibers and are considered the muscle-specific stem cells (132). They are capable of intrinsic repair of the mature skeletal muscle and are involved in scar tissue formation which leads to a loss of functionality in the injured areas (133, 134). Satellite cells represent the natural first choice in cellular therapeutics for skeletal muscle due to their intrinsic myogenic commitment, and thus they are frequently used in skeletal muscle engineering (135, 136). However, the application of satellite cells is problematic because of invasive harvesting method, difficult purification, low expansion capability with low yield (13) and limited source due to low incidence of satellite cells in skeletal muscle (i.e., 1%–5%) (137, 138).

In this light, human mesenchymal stem cells (hMSCs) have attracted much attention due to their wide range of sources and capabilities of self-renewal in an undifferentiated state for prolonged time and multi-lineage differentiation, which has been discussed in details before (Chapter 1, section 1.2, page 5). The hMSCs were frequently investigated for skeletal muscle engineering because they have minimal tumorigenicity or ethic concerns, and can be coaxed to differentiate into myocytes upon proper stimuli (23).

A simple way to induce skeletal myogenesis of hMSCs is to culture hMSCs in

myogenic medium supplemented with chemical inducers such as dexamethasone (DXM), hydrocortisone (127, 139) and 5-azacytidine (15, 140). However, most chemical differentiation inducers including those mentioned above are controversial exogenous agents with potential to cause unexpected effects to the differentiation of hMSCs. In one study, Merrison *et al.* reported that collagen substrates and medium supplemented with multiple growth factors increased the expression of skeletal muscle markers in hMSCs as demonstrated by quantitative real-time polymerase chain reaction (RT-PCR) (141). Unfortunately, immunostaining revealed no change in expression of muscle-related proteins including desmin, myoblast differentiation protein (MyoD), myogenic factor-5 (Myf5) in hMSCs, indicating that these conditions only partially stimulated myogenic differentiation pathways. Alternatively, the use of conditioned media prepared from primary muscle precursor cell culturing media has been shown to improve the efficiency of skeletal myogenic differentiation of MSCs from human and mouse (15, 142). However, such method requires invasive harvesting of primary SKMCs, which is hard to implement in clinical settings. Therefore, the potential use of hMSCs for skeletal muscle engineering awaits an efficient and minimally-invasive protocol that guides hMSCs towards prescribed skeletal myogenic differentiation in a controlled and reproducible manner.

3.1.3 Carbon nanotubes (CNTs) as scaffolds in skeletal muscle engineering

Because of the unique mechanical and electrical properties, CNTs have been used in skeletal muscle engineering as an auxiliary material to modulate the conductivity or the

mechanical strength of scaffolds towards the myotube formation from fusion of myoblasts (123, 124, 143, 144). For instance, electrospun polyurethane/CNTs (multi-walled and single-walled) scaffold was used to modulate skeletal myotube formation from murine SKMCs (143); polycaprolactone (PCL)/oxidized CNT (multi-walled) hydrogel was demonstrated to support the proliferation of rat SKMCs and displayed more myotube cells comparing to the CNT free hydrogel (123); a recent study found that murine SKMCs grown on vertically aligned CNTs (multi-walled) within methacrylated gelatin hydrogels yielded a higher number of myotubes than cells cultured on hydrogels with randomly or horizontally aligned CNTs, respectively (124). However, the cells employed in these studies were skeletal muscle progenitor cells, which are harvested from skeletal muscle and have an inherent predisposition towards myotube formation (134). Additionally, there is no research investigating the sole influence of CNTs in skeletal muscle engineering. Therefore, we envisage to determine the influence of CNTs to the skeletal myogenesis of hMSCs which have multi-lineage differentiation ability. The result would subsequently guide us towards successful design of CNT scaffolds for engineering specific skeletal muscle tissues.

As we discussed in Chapter 2 (Section 2.1, page 15), pristine CNTs are extremely hydrophobic and thus the more hydrophilic polyethylene glycol-linked multi-walled carbon nanotubes (PEG-CNTs) were used in this study. **We aimed to prepare and comprehensively characterize PEG-CNT films, and to investigate the role of the films in spontaneous skeletal myogenic differentiation of hMSCs.**

3.2 Materials and methods

3.2.1 Synthesis and characterization of PEG-CNTs

Multi-walled CNTs (courtesy of Professor S. Ramaprabhu, Indian Institute of Technology Madras, Indian) were prepared by chemical vapor deposition method as previously reported (145). The outer diameter of CNTs was 30-40 nm with an average internal diameter of about 10 nm, and the CNT length ranged from a few hundred nm to 1 μm. Pristine CNTs were functionalized to synthesize PEG-CNTs according to the procedure reported by Zhao *et al.* (146) and illustrated in Figure 3.1. Briefly, 100 mg of pristine CNTs were oxidized by sonicating (Sono Swiss, Switzerland) in the mixture of 5 ml of concentrated nitric acid (Fluka Analytical, USA) and 15 ml of sulfuric acid (Merck Chemicals, Germany) for 6 hours. The obtained oxidized CNTs were thoroughly washed with distilled water until the pH value was around 6. The product was then filtered through 0.2μm pore size polytetrafluoroethylene (PTFE) membrane (Millipore, Germany) and re-suspended in a small amount of distilled water. The oxidized CNTs were finally lyophilized to get dry powder.

The oxidized CNT powder (100 mg) was added to anhydrous dimethylformamide (DMF, Sigma Aldrich, USA) and sonicated for 30 minutes to give a homogenous suspension. Oxalyl chloride (4 ml, Sigma Aldrich, USA) was then added drop wise into the oxidized CNT suspension at 0 ℃. The mixture was stirred at 0 ℃ for 2 hours and then at room temperature for another 2 hours. Finally, the temperature was increased to 85 ℃, and the mixture was stirred for overnight to remove excess oxalyl chloride. PEG (1 g, Sigma Aldrich, USA, MW=600) was added to the suspension and stirred at 100 ℃

for 5 days. When cooled to room temperature, the mixture was filtered through 0.2μm pore size PTFE membrane and thoroughly washed with distilled water. The black PEG-CNTs were collected in a small amount of distilled water and lyophilized.

Thermogravimetric analysis (TGA, TA instrument 2960 SDT V3.0F, USA) was employed to determine if the successful conjugation of PEG to CNTs was achieved. Samples were heated to 1000 ℃, ramping at 5 ℃/min at atmosphere pressure in air.

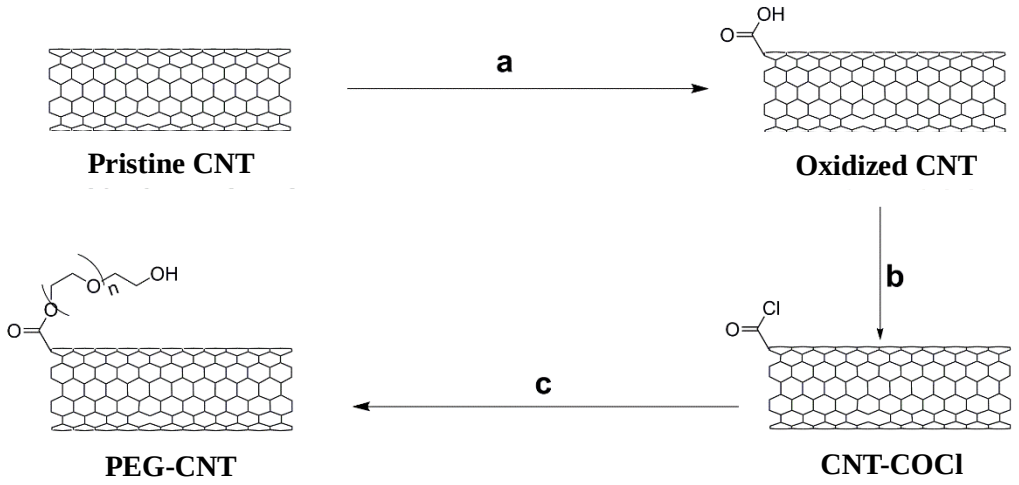

Figure 3.1 Schematic representation of the synthesis of PEG-CNTs. (a) HNO_3/H_2SO_4 (v/v, 1:3), sonication for 6 hours; (b) $(COCl)_2$ (2 hours at 0 ℃, 2 hours at room temperature, overnight at 85 ℃); (c) PEG (100 ℃, 5 days).

3.2.2 Preparation and characterization of PEG-CNT films

The PEG-CNT films were prepared by a drop-drying method. Briefly, PEG-CNTs were sonicated in DMF to obtain 2 mg/ml suspensions. The suspensions were subsequently dropped onto pre-heated round cover slips maintained at 160 ℃. After the evaporation of DMF, PEG-CNT films were formed and the films were kept at 160 ℃ for another 5 minutes to remove residual DMF. The deposited PEG-CNT amount on cover slips was

around 2.8 μg/mm^2.

The PEG-CNT film surfaces were imaged by helium ion microscope (HIM, Carl Zeiss, Germany) and then measured under atomic force microscope (AFM, Dimension FastScan, Bruker, Germany) for surface roughness characterization with bare cover slips as a control. The static contact angle measurements of PEG-CNT films and cover slips were conducted by applying a 1 μl drop of deionized water to the surface and capturing an image parallel to the image plane at high magnification (WV-CP300 Day/Night Fixed Indoor Camera, Panasonic, Japan). Analysis was carried out with ImageJ software (National Institutes of Health, USA) by fitting an ellipsis to the water droplet and measuring the angle to the substrate surface baseline. The PEG-CNT film thickness was detected by scanning electron microscope (SEM, JSM-6701F, JEOL, Japan) at the cross-section of the films. Mechanical strength of PEG-CNT films and cover slips was determined by MTS Nanoindenter XP (Agilent, USA). Loading rate was fixed at constant strain rate at 0.05 s^{-1} and the holding time at maximum load was 10 s. The unloading rate was the maximum loading rate incurred during loading. Continuous stiffness measurement (CSM) method was used to measure the Young's modulus and hardness. The reported values were averaged in depth range of 400-500 nm.

3.2.3 Cells and culture condition

Human MSCs (hMSCs, Lonza, Switzerland) were expanded at 5000 cells/cm^2 in growth medium consisting of high glucose-Dulbecco's Modified Eagles Medium

(DMEM, Sigma Aldrich, USA), 10% fetal bovine serum (FBS, PAA Technologies, Austria), 1% penicillin/streptomycin (Pan Biotech, Germany), 1 mM sodium pyruvate (Gibco, USA) and 1 mM non-essential amino acid (Sigma Aldrich, USA). For all experiments, hMSCs at passage 5 were used. Human SKMCs (Lonza, Switzerland) were seeded at 3500 cells/cm^2 in SKGM Bullet Kit (Lonza, Switzerland). All cells were maintained at 37 ℃, 5% CO_2 air atmosphere and medium was replaced twice per week. Sub-culturing was conducted when cells reached 80-90% confluence with 0.25% trypsin–EDTA (Invitrogen, USA).

For myogenic induction, hMSCs were cultured up to 21 days. The hMSCs at 3000 cells/cm^2 were seeded on various substrates and maintained in growth medium for 7 days. Myogenesis was then induced by changing growth medium with myogenic medium for another 14 days. The myogenic medium consisted of growth medium supplemented with 100 nM DXM (Sigma Aldrich, USA) and 50 μM hydrocortisone (Sigma Aldrich, USA) (147). For the non-induced hMSCs, growth medium was used throughout the study. We included 4 experimental groups: (1) non-induced hMSCs plated on cover slips as a negative control; (2) myogenically-induced hMSCs plated on cover slips; (3) non-induced hMSCs plated on PEG-CNT films; (4) myogenically-induced hMSCs plated on PEG-CNT films.

3.2.4 Cell viability of non-induced and myogenically-induced hMSCs

The cell viability was determined on day 1, 7, 14 and 21 by staining the cells with fluorescent live/dead viability/cytotoxicity kit (Invitrogen, USA) according to the

manufacturer's instruction. Briefly, a mixture of 2 μM calcein-AM and 4 μM EthD-1 was added to the hMSC samples after washing with PBS at each time point. The samples were incubated in dark at 37 ℃ for 45 minutes and then examined by a confocal microscope (Olympus, Japan).

This fluorescent live/dead viability/cytotoxicity kit was also used for a quantitative test of cell viability. For this study, hMSCs were seeded on a 96-black-walled, clear bottom plate. On the day of experiment (day 1, 7, 14 and 21), cells were gently washed with PBS three times and 100 μl PBS was left after the last wash. The reagent containing 2 μM calcein-AM and 4 μM EthD-1 (100 μl) was added into the wells. The samples were incubated in the dark at room temperature for 45 minutes and the fluorescence was measured by a plate reader (EnSpire Multimode Plate Reader, Perkin Elmer, USA). The calcein-AM was read at an excitation wavelength of 485 nm and emission wavelength of 530 nm while the EthD-1 was read at an excitation wavelength of 530 nm and emission wavelength of 645 nm. The fluorescence intensity of non-induced hMSCs plated on cover slips and PEG-CNT films at day 1 were used as control for cover slip and PEG-CNT film samples respectively. Values of cell viability were expressed as a fold change of that from the control. Results represented 5 independent biological replicates.

3.2.5 Quantitative RT-PCR

At the end of 21 days of incubation, hMSCs were processed for the isolation of total RNA using RNeasy Mini Kit (Qiagen, Netherlands) according to the protocol given by

the manufacturer. Total RNA concentration and purity were determined (OD 260/280 within 1.9-2.1) using Nanodrop (NanoDrop-ND1000, USA). cDNAs of respective samples were synthesized from RNA using SuperScript III first-strand synthesis system (Invitrogen, USA).

Quantitative RT-PCR was performed with Fast SYBR Green mater mix (Qiagen, Netherlands) and primers using iCycler iQ Real Time PCR Detection System (Bio-Rad Laboratories, USA). The primers for myogenic and osteogenic markers as well as hMSC-feature genes were designed by web-based Primer 3 software (http://frodo.wi.mit.edu/) and the sequences were listed in Table 3.1. The cycle thermal profile comprised an enzyme activation at 50 ℃ for 2 minutes, followed by an initial denaturation at 95 ℃ for 10 minutes, 40 cycles of 95 ℃ for 15 s and 60 ℃ for 1 minute. The primer and cycle thermal profile for adipogenic and chondrogenic markers were cited from references and the primer sequences were shown in Table 3.2. Expression changes of various genes were analyzed using Livak ($2^{-\Delta\Delta CT}$) method to normalize gene expression to the reference gene GAPDH and expressed as fold change as compared to the negative control (148). Results represented 5 independent biological replicates.

Table 3.1 Sequences of primers used in RT–PCR analysis of hMSC-feature genes, myogenic and osteognenic markers

Gene	Reference sequence number	Forward primer sequence (5'->3')	Reverse primer sequence (5'->3')	Product size (bp)
CD73	NM_001204813.1	GCC GCT TTA GAG AAT GCA AC	CTC GAC ACT TGG TGC AAA GA	234
CD90	NM_006288.3	CCC AGT GAA GAT GCA GGT TT	CAG CCT GAG AGG GTC TTG TC	183
CD105	NM_001114753.1	CAC TAG CCA GGT CTC GAA GG	CTG AGG ACC AGA AGC ACC TC	165
MyoD	NM_002478.4	CCG CTT TCC TTA ACC ACA AAT	CGG CTG TAG ATA GCA AAG TGC	98
Desmin	NM_001927.3	TCG GCT CTA AGG GCT CCT C	CGT GGT CAG AAA CTC CTG GTT	194
MHC	NM_001100112.1	GAT GGC ACA GAA GTT GCT GA	CTT CTC GTA GAC GGC TTT GG	177
TnC	NM_003279	TGG GGA CAT CAG CGT CAA G	CCA AGA ACT CCT CGA AGT CGA T	137
Ryr	NM_000540.2	TGG CTC ACC TAT GCT GCT C	GAC AGT GCG TCG TCC ATG T	101
Col-I	NM_000089.3	TCC AAA GGA GAG AGC GGT AA	CAG ATC CAG CTT CCC CAT TA	112
OCN	NM_199173.4	GAC TGT GAC GAG TTG GCT GA	CTG GAG AGG AGC AGA ACT GG	119
OPN	NM_000582.2	CAT CAC CTG TGC CAT ACC AG	GCC ACA GCA TCT GGG TAT TT	87
ALP	NM_001127501.2	CCT CCT CGG AAG ACA CTC TG	CCA CCA AAT GTG AAG ACG TG	64
GAPDH	NM_002046.4	ATG TTC GTC ATG GGT GTG AA	TGT GGT CAT GAG TCC TTC CA	144

CD73=cluster of differentiation 73, CD90=cluster of differentiation 90, CD105=cluster of differentiation 105/endoglin, MHC=myosin heavy chain 2, TnC=fast skeletal troponin C, Ryr=ryanodine receptor 1, Col-I=collagen type I, OCN=osteocalcin, OPN=osteopontin, ALP=alkaline phosphatase, GAPDH=glyceraldehyde 3-phosphate dehydrogenase

Table 3.2 Sequences of primers used in RT–PCR analysis of adipogenic and chondrognenic markers

Gene	Forward primer sequence (5'->3')	Reverse primer sequence (5'->3')	Reference
Sox9	GCC TTT TTG TCC ATC CCT TTT TTC	CTC CAG GTA GCC TCC CTC ACT CC	(149)
Aggrecan	CAC GGC TTC TGG AGA CAG GAC TG	TGT TGG GGA GGT GGC TGT TTC G	(149)
Col-II	ACC TCA CGC CTC CCC ATC ATT G	ACA TCA GGT CAG GTC AGC CAT TCA G	(149)
AP2	CCA GGG ACT TTG GGT ACG TG	GGT TGA GAA ATT CAG CTA CTG CT	(150)
Adiponectin	TCC TGC CAG TAA CAG GGA AG	GGT TGG CGA TTA CCC GTT TG	(151)
LPL	TCA TTC CCG GAG TAG CAG AGT	GGC CAC AAG TTT TGG CAC C	(150)

Col-II=collagen type II, AP2=adipocyte protein 2, LPL=lipoprotein lipase, Sox9= SRY (sex determining region Y)-box 9

3.2.6 Western blot

After 21 days of incubation, cells on the substrates were lysed with cell lysis buffer (50 mM HEPES pH 7.5, 150 mM NaCl, 1 mM EDTA, 10% Glycerol, 10% Triton X-100, 10 mM sodium pyrophosphate, 100 mM sodium fluoride, 2 mM sodium orthovanadate, 2 mM PMSF, 0.1 µg/ml aprotinin). The BCA protein assay (Thermo Scientific Pierce, USA) was performed to determine protein concentration. Equal protein lysates (~20 µg) were resolved by SDS-poly-acrylamide gel and transferred to polyvinylidene difluoride (PVDF) membranes (Bio-Rad, USA) for western blot. Primary antibodies were anti-MyoD (1:1000, mouse monoclonal, Abcam, UK), anti-desmin (1:500, rabbit monoclonal, Abcam, UK), anti-myosin heavy chain (MHC, 1:200, mouse monoclonal, Santa Cruz, USA) and anti-β-actin (1:10000, Abcam, UK). Secondary antibodies were anti-mouse and anti-rabbit horseradish peroxidase conjugated secondary antibodies (Thermo Scientific Pierce, USA) at 1:10000 dilution. Each membrane was exposed to

SuperSignal West Femto chemiluminescent substrate (Thermo Scientific Pierce, USA). Protein bands were then detected with enhanced chemiluminescence by feature-SRX-101A (Konica Minolta, USA).

3.2.7 Myogenic differentiation of hMSCs on graphene sheets

The graphene coated cover slips were provided by Barbaros Ozyilmaz's lab, Graphene Research Center, National University of Singapore. Graphene grown by chemical vapor deposition (CVD) on Cu-foil was transferred to cover slips by poly-(methyl methacrylate) (PMMA) mediated wet transfer and using ammonium persulfate to etch the Cu-foil, as described elsewhere (152). Both of non-induced hMSCs and myogenically-induced hMSCs were cultured on cover slips and graphene sheets. At the end of 21 days incubation, cells were processed to mRNA isolation, cDNA synthesis and RT-PCR analysis of myogenic markers. Results represented 3 independent biological replicates.

3.2.8 Statistical analysis

For each experiment, replicates were averaged and presented as mean ± standard deviation (SD). Statistical significance was determined with SPSS. Cell viability and the fold changes of each gene in RT-PCR study were analyzed using a two-way ANOVA with substrate and induction as independent variables. The *P*-values less than 0.05 denotes statistical significance.

3.3 Results

3.3.1 Synthesis and characterization of PEG-CNTs

Figure 3.2 showed the TGA graphs and the derivative curves of pristine CNTs, oxidized CNTs and PEG-CNTs. Compared with pristine CNTs and oxidized CNTs, an additional peak was observed from 400 ℃ to 450 ℃ in the derivative curve of PEG-CNTs, as shown by the arrow. It was postulated that this peak was due to the decomposition of PEG from PEG-CNTs, which was in agreement with the results obtained previously in A/P Giorgia Pastorin's lab (67).

3.3.2 Characterization of PEG-CNT films

The typical HIM top-view image showed that PEG-CNT films prepared using a drop-drying method displayed a homogenous and smooth surface with nanorange undulations (Figure 3.3A). Moreover, the film surfaces exhibited an orderly fashion of PEG-CNTs. The AFM scan of 1 μm^2 of surface topology substantiated the HIM results as the representative PEG-CNT film showed a small nanoscale Root Mean Square (RMS)-roughness of 75 ±9 nm with the waviness of PEG-CNT bundles. Comparing to this, the plain cover slip was extremely smooth and displayed surface roughness within 2 nm (Figure 3.3B). The hydrophilicity of each substrate was evaluated by water contact angle as presented in Figure 3.3C. The contact angle was found to be 17.0 ±3.1 ° for PEG-CNT films whereas 63.1 ±5.6 ° for cover slips, indicating that PEG-CNT films were more hydrophilic than cover slips.

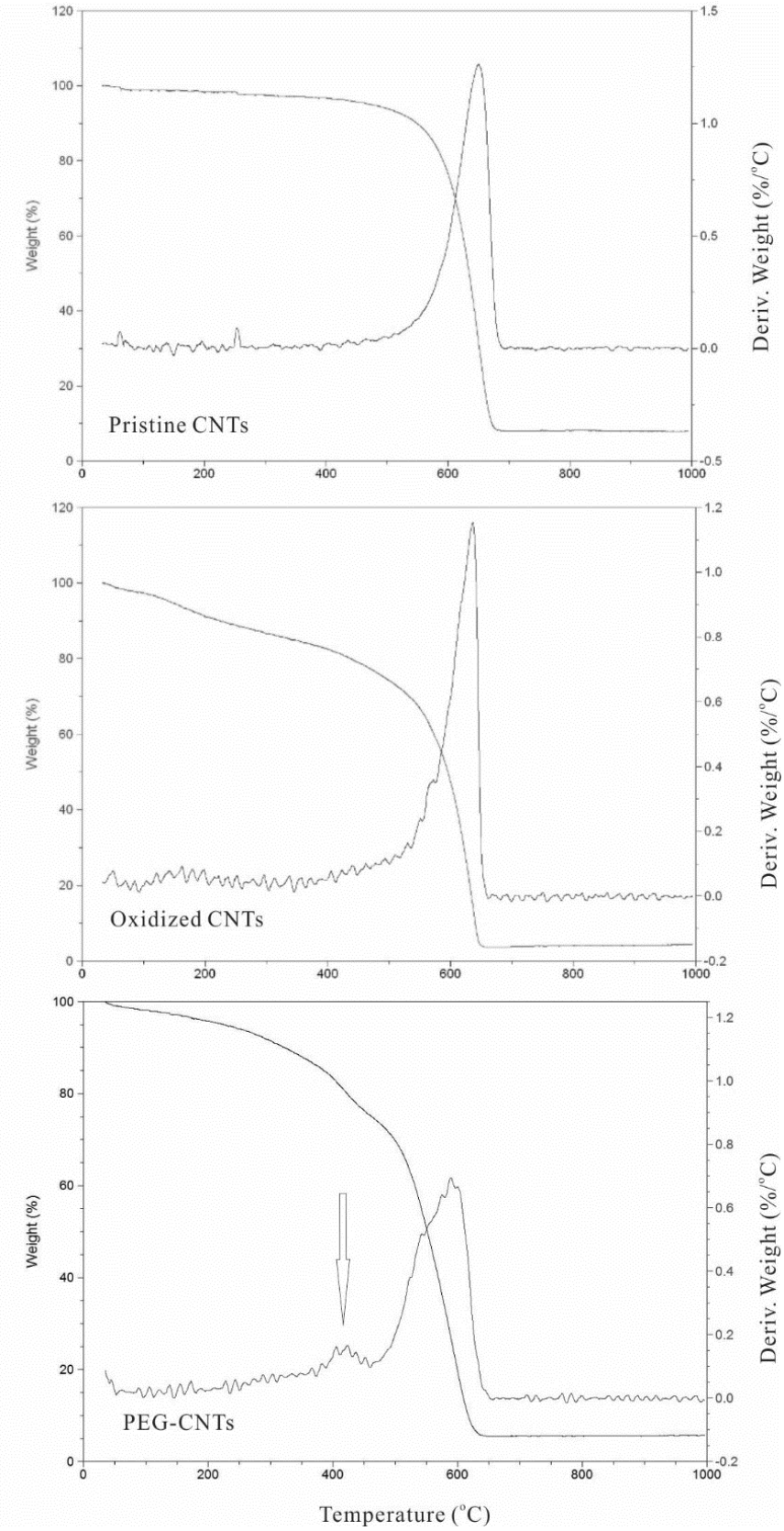

Figure 3.2 TGA graphs and derivative curves of pristine CNTs, oxidized CNTs and PEG-CNTs.

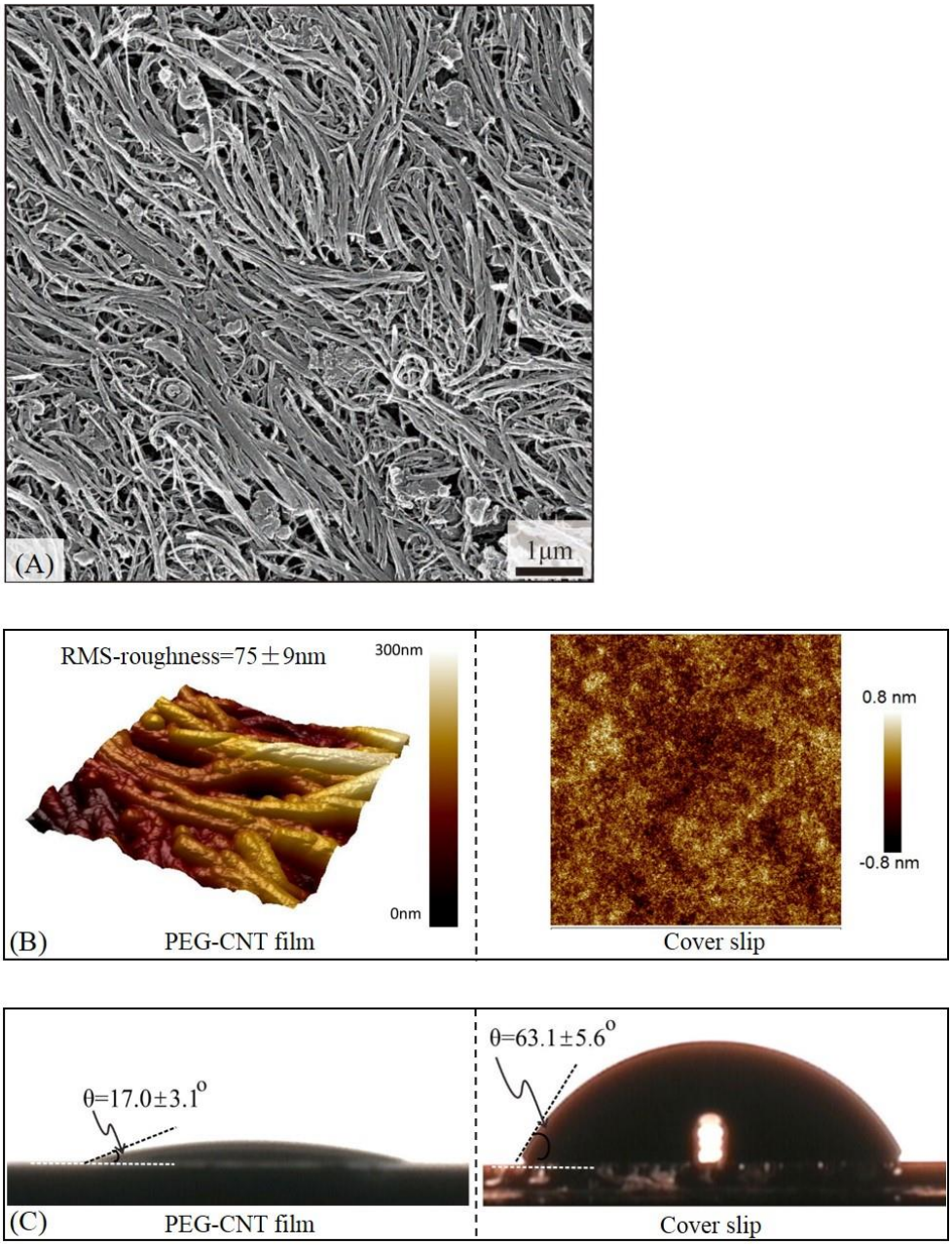

Figure 3.3 (A) HIM image of the surface topography of PEG-CNT films; (B) AFM image of PEG-CNT film and cover slip surface at 1 μm^2; (C) representative contact angles of water on a PEG-CNT film and a cover slip.

Figure 3.4A showed SEM images at the cross section of PEG-CNT films, which did not possess stratified layers but rather formed blended and porous films. The estimated thickness of PEG-CNT film was around 5 μm. The typical load–depth curves for PEG-CNT films and cover slips obtained from nanoindentation tests were illustrated in

Figure 3.4B and C. It revealed the average Young's modulus and hardness of PEG-CNT films to be 557.3±70.0 MPa and 26.3±3.0 MPa, respectively, indicative of high mechanical strength. Cover slips alone exhibited much higher stiffness than PEG-CNT films, with Young's modulus of 71.1±1.2 GPa and hardness of 6.8±0.1 MPa.

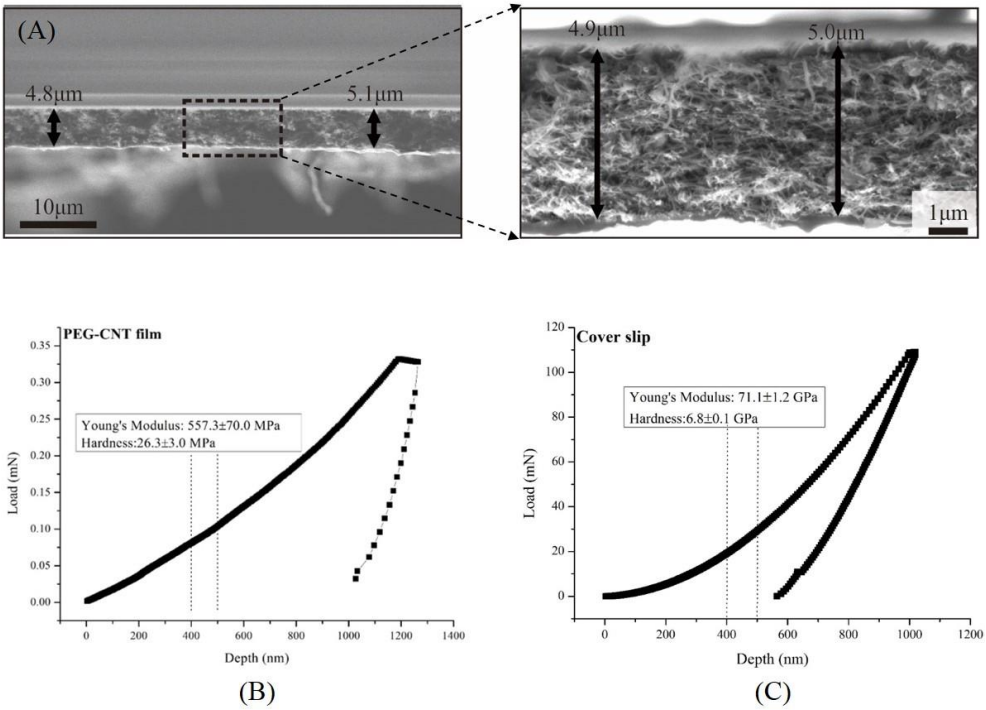

Figure 3.4 (A) SEM image at the cross section of PEG-CNT films, left: 2000× magnification; right: zoom in view at 10000× magnification; representative load-depth curves of (B) PEG-CNT films and (C) cover slips by nanoindentation tests.

3.3.3 Viability of non-induced and myogenically-induced hMSCs

The fluorescent live/dead staining (Figure 3.5A) indicated that both cover slips and PEG-CNT films well supported hMSC attachment and maintained the cell viability without any dead cell staining. Congruent with this result, the EthD-1 reading for dead cells was minimal in every sample for the quantification. Therefore, only the reading

of calcein-AM, which symbolizes viable cells, was taken in account for the calculation of cell viability.

Figure 3.5B showed that the cell number of non-induced hMSCs on cover slips increased rapidly after 7 days to an increase of 2.24 ± 0.08 folds as compared to day 1. The cell number reached a plateau of 2.49 ± 0.24 folds at day 14 and decreased marginally to 2.07 ± 0.08 folds at day 21. The myogenic induction decreased hMSC number to 2.22 ± 0.17 folds at day 14 and 1.63 ± 0.06 folds at day 21. Likewise, PEG-CNT films adequately supported hMSC attachment and growth over 21 days of incubation (Figure 3.5B). The cell number on PEG-CNT films gradually increased to 1.17 ± 0.06 folds at day 7, 1.32 ± 0.09 folds at day 14 and 1.29 ± 0.05 folds at day 21 for non-induced hMSCs. With myogenic induction, the fold change of cell number were 1.12 ± 0.10 at day 14 and 1.21 ± 0.07 at day 21. Two-way ANOVA was used to investigate the influence of substrate and induction to the cell viability of hMSCs. Both PEG-CNT films and myogenic induction exerted significant effects to the reduced cell viability at day 14 and day 21 (Figure 3.5B).

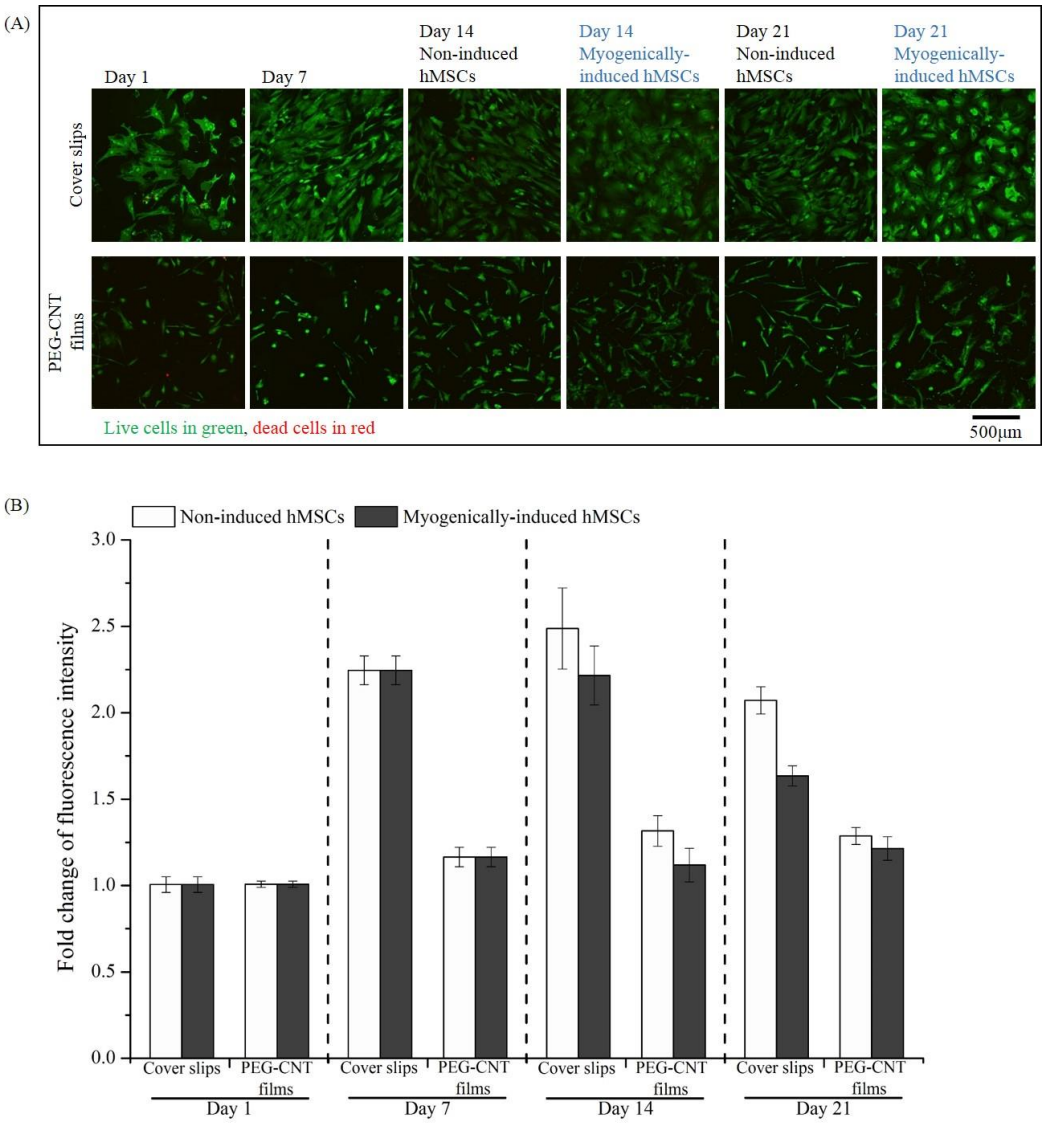

Figure 3.5 (A) Live and dead staining; (B) quantitative viability of hMSCs (induced to myogenic differentiation or not, n=5) on cover slips and PEG-CNT films during 21 days incubation. For quantitative analysis, two-way ANOVA showed substrate term $P<0.001$ for day 14 and day 21, induction term $P<0.01$ for day 14 and day 21, two-way interaction term $P>0.05$ for day 14 and $P<0.001$ for day 21. The P-values less than 0.05 denotes statistical significance.

3.3.4 Gene expression analysis by RT-PCR

To determine if the treated hMSCs repressed the hMSC features and acquired myogenic gene markers distinctive in myogenesis, RT-PCR analysis was performed after 21 days of incubation. For the investigation of hMSC features (Figure 3.6),

myogenic induction significantly depressed the expression of cluster of differentiation 73 (CD73), cluster of differentiation 90 (CD90) and cluster of differentiation 105/endoglin (CD105). On the other hand, PEG-CNT films alone exerted significant effect to the reduction of CD90, but not to CD73 and CD105 (Figure 3.6). Therefore, myogenic induction was necessary for the repression of hMSC-feature markers. The *P*-value from two-way ANOVA for two variables of substrate and induction was illustrated in Table 3.3.

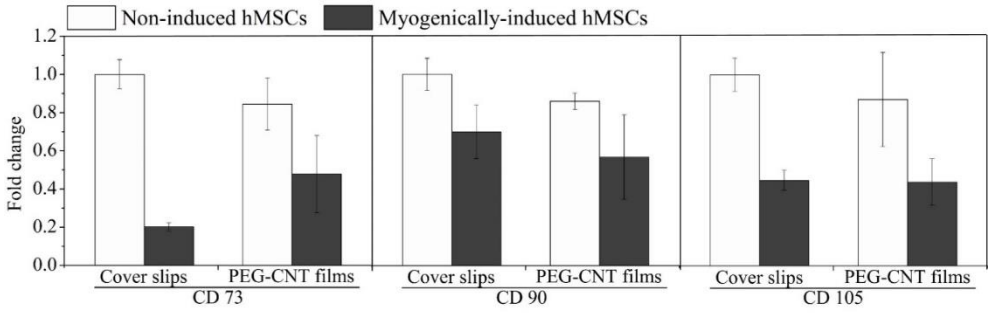

Figure 3.6 Depressed hMSC-feature genes, n=5. Two-way ANOVA showed substrate term $P<0.05$ for CD90 while $P>0.05$ for CD73 and CD105, induction term $P<0.001$ for CD73, CD90 and CD105, two-way interaction term $P<0.01$ for CD73 while $P>0.05$ for CD90 and CD105. The *P*-values less than 0.05 denotes statistical significance.

Looking at the acquisition of myogenic phenotype, the expression of early myogenic markers of MyoD and desmin as well as the late phase gene of MHC was significantly up-regulated by about 2-fold in hMSCs plated on PEG-CNT films as compared to the negative control (Figure 3.7A). However, the myogenic differentiation of hMSCs was not influenced by myogenic induction as there was no significant difference in myogenic marker expression between non-induced and myogenically-induced groups. Additionally, between the two variables, only PEG-CNT film was responsible for the

significant up-regulation of fast skeletal troponin C (TnC) and ryanodine receptor 1 (Ryr) (Figure 3.7B).

Overall, there was no myogenic differentiation of hMSCs on cover slips and the myogenic induction could not improve the myogenesis of hMSCs on PEG-CNT films. These results indicated PEG-CNT films played a vital role in skeletal myogenic differentiation of hMSCs and a spontaneous skeletal myogenic differentiation of non-induced hMSCs on PEG-CNT films was observed.

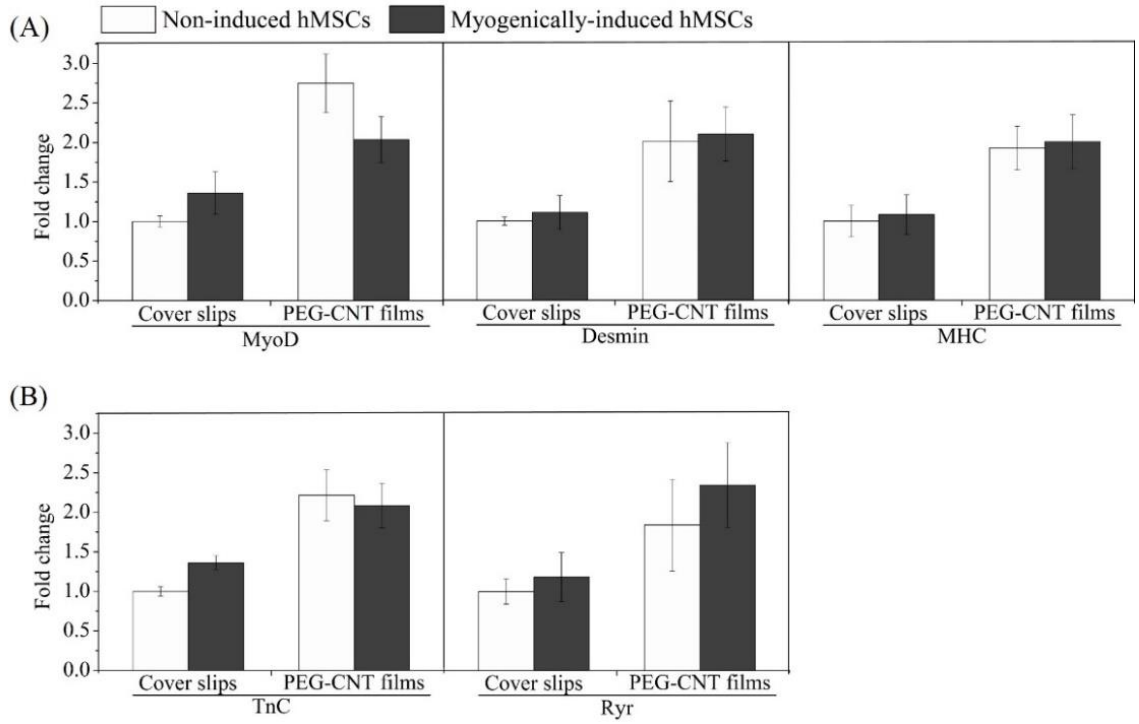

Figure 3.7 (A) Up-regulation of myogenic genes in non-induced hMSCs on PEG-CNT films, n=5. Two-way ANOVA showed substrate term $P<0.001$ for MyoD, desmin and MHC, induction term $P>0.05$ for MyoD, desmin and MHC, two-way interaction term $P<0.001$ for MyoD while $P>0.05$ for desmin and MHC; (B) up-regulation of SKMC-specific genes in non-induced hMSCs on PEG-CNT films, n=5. Two-way ANOVA showed substrate term $P<0.001$ for TnC and Ryr, induction term $P>0.05$ for TnC and Ryr, two-way interaction term $P<0.05$ for TnC and $P>0.05$ for Ryr. The *P*-values less than 0.05 denotes statistical significance.

Since the hMSCs can differentiate into various lineages beyond myocytes, markers for adipogenic, chondrogenic and osteogenic lineages were also investigated to assess whether this preferential myogenic differentiation of hMSCs was specific. In terms of osteogenesis (Figure 3.8A), comparing to the negative control, significant decrease of collagen type I (Col-I) expression was observed in PEG-CNT film groups, whereas myogenic induction did not change this expression. For osteocalcin (OCN) expression, there was no significant impact exerted by either substrate or induction. In addition, PEG-CNT films significantly up-regulated osteopontin (OPN) levels in hMSCs while myogenic induction significantly suppressed OPN expression. On the contrary, a significant suppression of alkaline phosphatase (ALP) was observed in PEG-CNT film groups, whereas a significant up-regulation of ALP was seen with myogenic induction. In terms of chondrogenesis (Figure 3.8B), results from a two-way ANOVA showed that PEG-CNT film, myogenic induction and their interaction played roles in the significant down-regulation of SRY (sex determining region Y)-box 9 (Sox9) compared to the negative control. PEG-CNT films also exerted significant influence on the depressed aggrecan expression, whereas no significant difference was found between non-induced and myogenically-induced hMSCs. Within all treated groups, the hMSCs expressed similar levels of collagen type II (Col-II) to the negative control group without any statistically significant difference. Finally for adipogenesis (Figure 3.8C), both PEG-CNT film and myogenic induction had significant influence to the decreased adipocyte protein 2 (AP2) expression in treated hMSCs compared to the negative control group. Furthermore, there was no significant difference between any two

groups in adiponectin expression. Moreover, two-way ANOVA proved significant effects of PEG-CNT film, myogenic induction and interaction between the two variables to the expression of lipoprotein lipase (LPL). Notably, myogenically-induced hMSCs significantly increased LPL levels to more than 200-fold and 40-fold on cover slips and PEG-CNT films, respectively, whereas non-induced hMSCs on PEG-CNT films decreased LPL expression compared to the negative control.

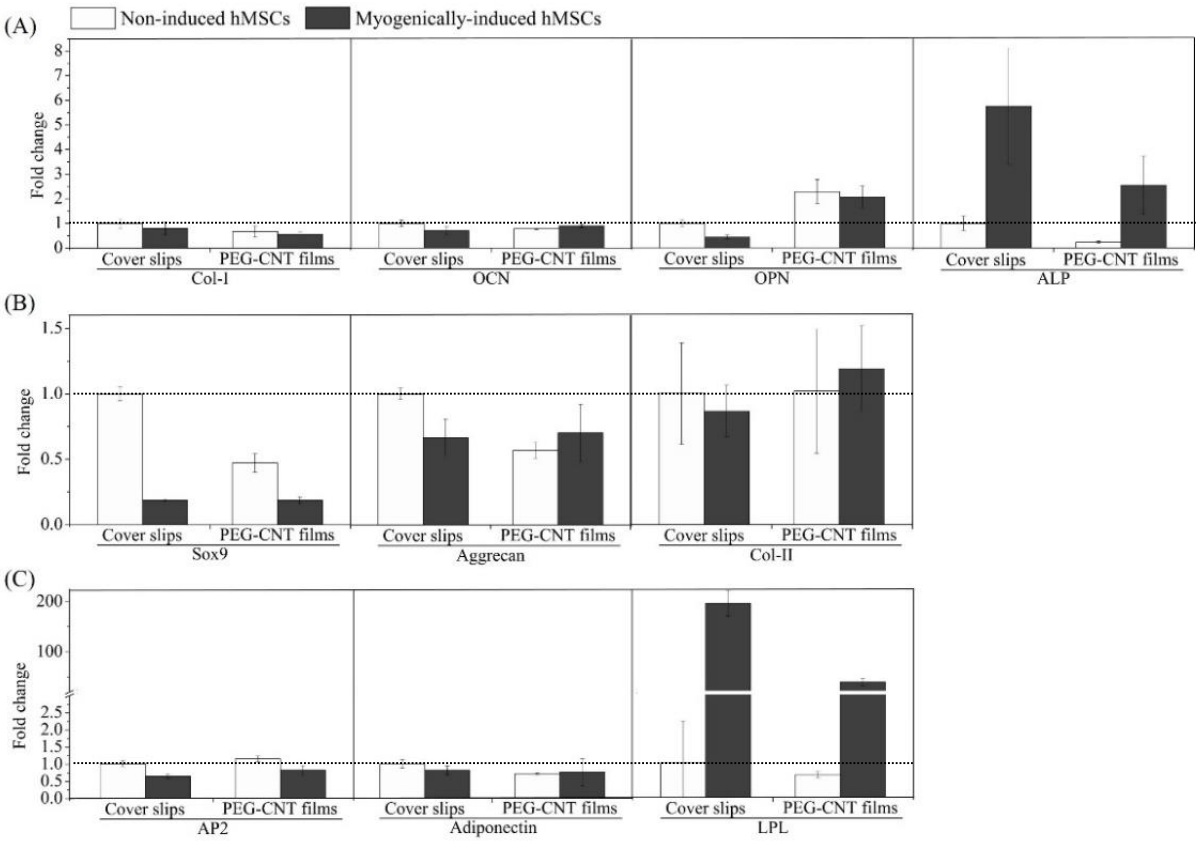

Figure 3.8 (A) Osteogenic gene expression, n=5. The two-way ANOVA showed substrate term $P<0.01$, induction term $P>0.05$, two-way interaction term $P>0.05$ for Col-I; substrate term $P>0.05$, induction term $P>0.05$, two-way interaction term $P<0.01$ for OCN; substrate term $P<0.001$, induction term $P<0.05$, two-way interaction term $P>0.05$ for OPN; substrate term $P<0.01$, induction term $P<0.001$, two-way interaction term $P>0.05$ for ALP; (B) chondrogenic gene expression, n=5. The two-way ANOVA showed substrate term $P<0.001$, induction term $P<0.001$, two-way interaction term $P<0.001$ for Sox 9; substrate term $P<0.01$, induction term $P>0.05$, two-way interaction term $P<0.01$ for aggrecan; substrate term $P>0.05$, induction term $P>0.05$, two-way interaction term $P>0.05$ for Col-II; (C) adipogenic gene expression, n=5. The two-way ANOVA showed substrate term $P<0.01$, induction term $P<0.001$, two-way interaction term $P>0.05$ for AP2; substrate term $P>0.05$, induction term $P>0.05$, two-way interaction term $P>0.05$ for adiponectin; substrate term $P<0.001$, induction term $P<0.001$, two-way interaction term $P<0.001$ for LPL. The P-values less than 0.05 denotes statistical significance.

To summarize, PEG-CNT films contributed to the significant up-regulation of myogenic markers of MyoD, desmin, MHC, TnC, Ryr and osteogenic marker of OPN, as well as significant down-regulation of hMSC-feature marker of CD90, osteogenic

markers of Col-I and ALP, chondrogenic markers of Sox9 and aggrecan, and adipogenic markers of AP2 and LPL. Overall, PEG-CNT films coaxed hMSCs-towards the phenotype of SKMCs (Figure 3.9 and Table 3.3). However, myogenic induction on the other hand led to significant increase of osteogenic marker of ALP and adipogenic marker of LPL, and significant suppression of hMSC-feature marker of CD73, CD90, CD105, osteogenic marker of OPN, chondrogenic marker of Sox9 and adipogenic marker of AP2.

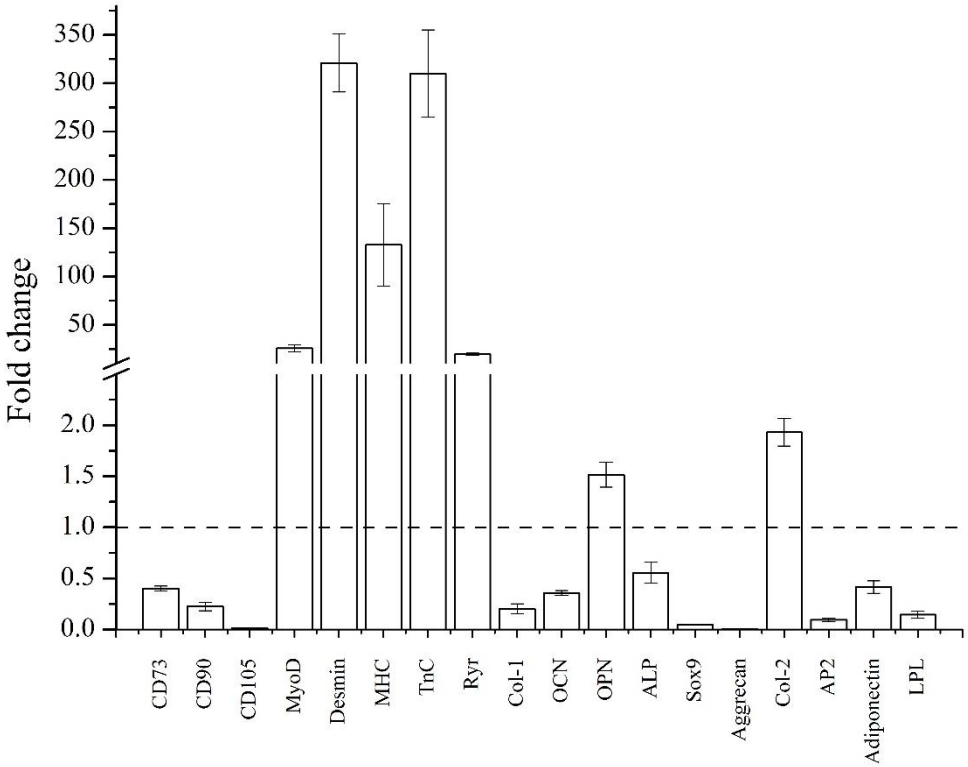

Figure 3.9 Fold change of hMSC-feature, myogenic, SKMC-specific, osteogenic, chondrogenic and adipogenic genes in SKMCs with $2^{-\Delta\Delta CT}$, n=5.

Table 3.3 *P*-value from two-way ANOVA of fold change for two variables of substrate and induction on cover slips and PEG-CNT films

	variables		
Genes	Substrate	Induction	Substrate*Induction
CD73	0.312	2.308×10^{-8}*	0.002*
CD90	0.043*	2.120×10^{-4}*	0.937
CD105	0.314	1.233×10^{-6}*	0.373
MyoD	2.980×10^{-8}*	0.167	4.530×10^{-4}*
Desmin	3.615×10^{-6}*	0.503	0.949
MHC	9.919×10^{-7}*	0.502	0.994
TnC	3.279×10^{-8}*	0.259	0.024*
Ryr	9.118×10^{-5}*	0.092	0.413
Col-I	0.006*	0.096	0.609
OCN	0.807	0.088	0.001*
OPN	5.995×10^{-8}*	0.023*	0.276
ALP	0.004*	2.069×10^{-5}*	0.056
Sox9	1.086×10^{-9}*	1.595×10^{-14}*	1.086×10^{-9}*
Aggrecan	0.005*	0.113	0.002*
Col-II	0.302	0.911	0.361
AP2	0.002*	5.549×10^{-7}*	0.734
Adiponectin	0.090	0.495	0.225
LPL	4.712×10^{-10}*	1.387×10^{-12} *	5.022×10^{-10}*

*indicated significant difference if $P<0.05$

To decipher the mechanism underlying the improved myogenic differentiation of hMSCs on PEG-CNT films, the influence of graphene sheets (coated on cover slips) to skeletal myogenic differentiation of hMSCs was examined. When the hMSCs were grown on graphene sheets and induced to myogenic differentiation, the graphene sheets alone failed to elevate any myogenic marker, while myogenic induction only up-regulated the expression of MyoD (Figure 3.10).

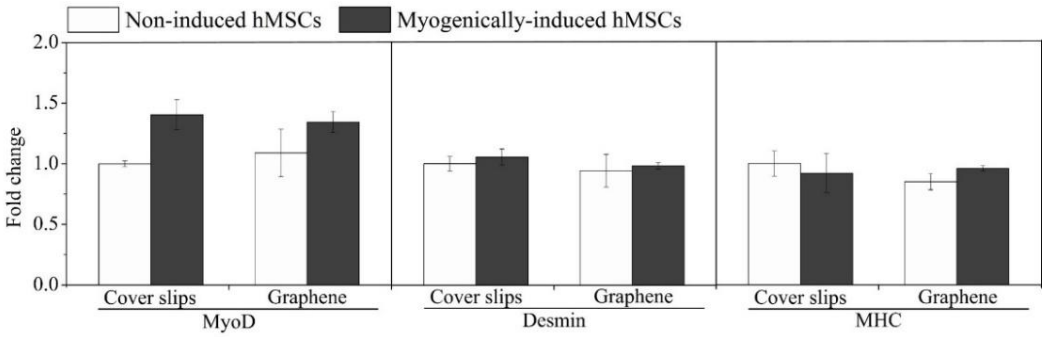

Figure 3.10 Fold change of myogenic genes on cover slips and graphene sheets with $2^{-\Delta\Delta CT}$, n=3. Two-way ANOVA analysis showed substrate term $P>0.05$ for MyoD, desmin and MHC, induction term $P<0.05$ for MyoD and $P>0.05$ for desmin and MHC, two-way interaction term $P>0.05$ for MyoD, desmin and MHC. The *P*-values less than 0.05 denotes statistical significance.

3.3.5 Protein expression analysis by western blot

Lastly, we evaluated if the increase in myogenic mRNA transcript levels was significant enough to drive to specific myogenic lineage protein expression. Comparing to the negative control, the expression of MyoD and desmin was marginally higher in the myogenically-induced hMSCs cultured on cover slips (Figure 3.11). For MHC expression in hMSCs on cover slips, there was no difference between the non-induced and myogenically-induced hMSCs. However, MyoD, desmin and MHC were more strongly detected in the hMSCs cultured on PEG-CNT films with/without myogenic induction. In all, the western blot analysis (Figure 3.11) well confirmed the above RT-PCR observations.

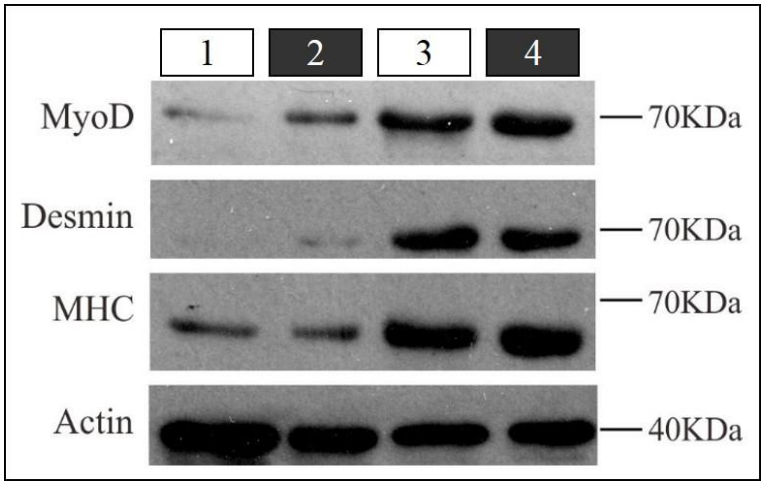

Figure 3.11 Western blot of myogenic protein and actin expression in non-induced hMSCs on cover slips (lane 1), myogenically-induced hMSCs on cover slips (lane 2), non-induced hMSCs on PEG-CNT films (lane 3) and myogenically-induced hMSCs on PEG-CNT films (lane 4). Actin was used as a loading control.

3.4 Discussion

In this study, we prepared and characterized PEG-CNT films, and then explored the ability of PEG-CNT films to modulate skeletal myogenic differentiation of hMSCs. Central to our findings, the spontaneous skeletal myogenic differentiation of hMSCs plated on PEG-CNT films represents an unprecedented observation and opportunity to promote the regeneration of injured skeletal muscle.

As a starting point for this study, advancement in film preparation was performed. In the former study by A/P Giorgia Pastorin's lab, PEG-CNT films were prepared by spraying PEG-CNTs water suspension with an airbrush onto pre-heated cover slips (67). Comparing to this method, the newly developed drop-drying method is more attractive because it is simple, cost-effective and scalable. Furthermore, the drop-drying method allows the control of film thickness by PEG-CNT concentration and suspension volume, thus minimizing batch-to-batch variability.

It was postulated that nanoscale surface roughness, which resembled the nanoarchitecture of the natural ECM, increased the opportunity for protein adsorption on scaffolds, facilitating stem cell attachment and differentiation (53, 153). Figure 3.3 A and B showed that PEG-CNT films displayed a homogeneous surface with nanoscale roughness and an orderly fashion of PEG-CNTs. This regularity may be facilitated by hydrophilic PEG, which is linked to CNTs and wraps around the CNTs, reducing aggregation and finally favoring the ordered arrangement of PEG-CNTs into films. Besides the regular arrangement, the hydrophilic PEG block may provide PEG-CNTs with improved hydrophilicity (Figure 3.3 C) which could greatly enhance favorable cellular response including adhesion and differentiation (154, 155).

It is widely accepted that the indentation depth should not exceed 10% of the sample thickness in order to obtain a true load–depth response of the tested material when it is supported by a hard substrate (cover slips in this study) (156). It is desirable to choose a depth range around 10% of film thickness to acquire mechanical strength for thin films. Since the estimated thickness of PEG-CNT films was around 5 μm (Figure 3.4A), the average Young's modulus and hardness of PEG-CNT films and cover slips were reported in a depth range of 400-500 nm (Figure 3.4 B and C). A commonly known value for the Young's modulus of a single multi-walled CNT is 1 TPa (90, 157), with a large variation from 0.40 to 4.15 TPa as reported by Treacy *et al.* (158). However, this was reported for the measurement in an axial direction. The PEG-CNTs in film was observed in a radial direction in this study (Figure 3.3 A and B). Previous studies of Young's modulus of single CNT in the radial direction showed much lower values,

between 0.3 to 4 GPa (159). In our case, the average Young's modulus of PEG-CNT films was 557.3±70.0 MPa, which correlated with the Young's modulus of single CNT in the radial direction and further indicated the horizontal alignment of PEG-CNTs. Furthermore, since the PEG-CNT films are composed of a network of PEG-CNTs, the mechanical strength of the film might have been influenced by the weak inter-tube contacts such as van der Waals and electrostatic interactions (160).

For cell culture experiments, we examined the possibility of alternative controls such as PEG-only substrates and oxidized CNT films besides uncoated cover slips. However, PEG-only matrix was deemed unsuitable since (1) the amount of PEG complexed in PEG-CNTs was very low (0.8%, mol/mol, PEG/CNTs) and such a control would be vastly different from PEG-CNTs to accurately represent the PEG effect in PEG-CNTs (67); (2) PEG alone, being highly water soluble, would instantaneously dissolve in culture medium; (3) it was reported that PEG alone typically exhibit minimal or no intrinsic biological activity in tissue engineering, because of the lack of mechanical support and non-adhesive nature of PEG chains which cannot significantly absorb proteins or cells (67, 161, 162). On the other hand, oxidized CNT films have been excluded from cell culture due to their instability and rapid breaking during cell culturing, which is in accordance with the previous report from A/P Giorgia Pastorin's group (67). In contrast, the PEG-CNT films can keep its integrity and remained intact on cover slips after 21days of incubation. For these reasons, a cover slip-only control is the next best control, without having to introduce any other extraneous factors that can confound such comparison.

Cell growth and differentiation are generally alternative processes that affect stem cell phenotype. As stem cells differentiate, their rate of growth usually decreases (163, 164). Hence, our observation of relatively lower cell number with myogenic induction and slow cell growth on PEG-CNT films (Figure 3.5 B) may be due to the myogenic differentiation of hMSCs and thus suppressed the growth of hMSCs. This was also confirmed by the lack of overt cell death based on fluorescent live/dead staining (Figure 3.5A).

A discriminating phenotype of hMSCs is the presence of CD73, CD90 and CD105 surface molecules, as stated by the mesenchymal and tissue stem cell committee of the international society for cellular therapy (ISCT) (165, 166). As shown in Figure 3.6, myogenic induction significantly down-regulated these CD genes in hMSCs, as compared to negative control. The suppressed hMSC-feature gene expression indicated that the myogenically-induced hMSCs were prone to differentiate. In contrast, PEG-CNT films alone only significantly decreased CD90 level in the non-induced hMSCs, in which there was spontaneous skeletal myogenesis. It is possible that the culturing time of 21 days is not long enough to detect significant changes on CD genes. It was found that CD markers (such as CD73) in human adipose-derived stem cells remained stable in long-term culture (until passage 20) with growth medium (167).

Myogenic regulatory factors (MRFs) are the master regulators of skeletal myogenesis. As a member in MRFs, MyoD is required for the determination of skeletal myogenic lineages at the early stage (168, 169). Desmin, a muscle-specific intermediate filament protein, also represents one of the earliest myogenic markers (170, 171). Although it

presents early in the development of myocytes, it is only expressed at low levels, and increases as the cell nears terminal differentiation. Contrary to this, MHC is expressed in myogenic precursors undergoing terminal differentiation (139). Therefore, the unanimous increased expression of MyoD, desmin and MHC in differentiated hMSCs charted the progressive myogenic lineage development of hMSCs by both RT-PCR and western blot studies (Figure 3.7A and 3.11). Moreover, TnC expresses exclusively in skeletal muscle and Ryr is primarily expressed in skeletal muscle (172). Therefore, up-regulated expression of TnC and Ryr in the differentiated hMSCs indicated that the hMSC-derived myoblasts may be committed towards SKMC development. The highlight of our experimental outcomes is the observation that the expression of myogenic and SKMC-specific markers significantly increased by the presence of PEG-CNT films while myogenic induction alone failed to do so (Figure 3.7 and 3.11). This suggests that PEG-CNT films alone, without the presence of myogenic inducers like DXM and hydrocortisone, could trigger the myogenesis of hMSCs (at the transcript and protein expression levels). This is a great achievement because myogenesis was reportedly difficult to be induced in hMSCs (173). Additionally, there is no consensus achieved so far for the optimal skeletal myogenic medium of hMSCs (15). Therefore, DXM and hydrocortisone were chosen as myogenic inducers in this study because of the simplicity, cheap price and wide usage (127, 139). However, there is no well recognized way of controlling the optimal concentrations of these inducers for efficient differentiation with reduced or no side effects. Hence, a notable advantage of spontaneous myogenesis on PEG-CNT films is the removal of potentially noxious

DXM and hydrocortisone in the induction protocol.

Besides, we considered the specificity of hMSC differentiation potential on PEG-CNT films. Osteogenic, chondrogenic and adipogenic marker investigation was therefore performed to rule out concurrent differentiation into different lineages. The justification of the selection of osteogenic, chondrogenic and adipogenic markers characterized in this study was shown in Table 3.4. Generally speaking, PEG-CNT films coaxed hMSC-derived myoblasts similar to SKMCs in terms of non-enhancement or even a significant decrease of adipogenic, chondrogenic and osteogenic markers, as well as significant up-regulation of OPN (Figure 3.8 and 3.9). Myogenic induction also resulted in non-enhancement or pronounced decrease of most adipogenic, chondrogenic and osteogenic markers. However, comparing to the negative control, there were statistically significantly increased levels of ALP and suprisingly high expression of LPL in the myogenically-induced hMSCs (Figure 3.8A and C). Hence, this study confirmed the possibility of removing myogenic inducers while still achieving the selectivity of skeletal myogenesis of hMSCs plated on PEG-CNT films alone. In short, the spontaneous myogenesis of hMSCs on PEG-CNT films may be a promising technique for skeletal muscle engineering.

Table 3.4 Justification of the selection of osteogenic, chondrogenic and adipogenic markers characterized in this study

	Markers	Remark
Osteogenic	Col-I	The organic phase in bone is mainly composed of Col-I (174).
	OCN	OCN is secreted solely by osteoblasts and implicated in bone mineralization and calcium ion homeostasis (175). It has been considered as a valid marker for fully-differentiated osteoblasts (176).
	OPN	OPN is an extracellular structural protein and an organic component of bone. OPN expression in bone occurs by osteoblasts, osteocyctes (bone-forming cells) and osteoclasts (bone-resorbing cells) (177).
	ALP	ALP and Col-I are evaluated as early markers of osteogenesis (178).
Chondrogenic	Sox9	Sox9 is expressed in pre-cartilaginous condensing mesenchyme and maturing cartilage (179). Sox9 can bind directly to an enhancer in the Col-II gene and upregulate the Col-II expression (180).
	Aggrecan and Col-II	Aggrecan and Col-II are integral part of the ECM in cartilagenous tissues to withstand compression in cartilage (181).
Adipogenic	AP2	AP2 is a carrier protein for fatty acids that is primarily expressed in adipocytes and macrophages (182).
	Adiponectin	Adiponectin is exclusively expressed in differentiated adipocytes and plays an important role in regulating energy metabolism mainly by increasing insulin sensitivity (183).
	LPL	Synthesis of LPL is found to be dominant in adipose tissue. The LPL gene is transcriptionally activated at the early phase of adipocyte development (184). During adipocyte differentiation, there is a gradual increase of LPL mRNA that reaches a plateau level when the cell has matured into an adipocyte (185).

In another study that we have performed as a comparator, graphene (a flat instead of cylindrical material with identical molecular construct with CNTs), when coated as a matrix, alone cannot trigger the myogenic differentiation of hMSCs (Figure 3.10). This result means that the building block that is common between graphene and PEG-CNTs is not the only determinant for the myogenesis of hMSCs. Instead, it was postulated

that the characteristics of PEG-CNT films, in terms of high hydrophilicity, the structure as nanotubes and orderly arrangement of PEG-CNTs, might facilitate the skeletal myogenesis of hMSCs without myogenic induction. A thorough study can be carried out in future to know the mechanism underlying the spontaneous myogenic differentiation of hMSCs on PEG-CNT films.

It has been acknowledged that hMSCs have high sensitivity to the substrate "stiffness", which directs the commitment towards different cell lineages (147). Softer matrices that mimic brain are neurogenic, stiffer matrices that mimic muscle are myogenic, and comparatively rigid matrices that mimic collagenous bone prove osteogenic. This may explain why hMSCs on the relatively softer PEG-CNT films (average Young's modulus of 557.3±70.0 MPa) promoted skeletal myogenesis while the hMSCs the stiffer cover slips (average Young's modulus of 71.1±1.2 GPa) failed to do so. It is worth mentioning that the highest up-regulation of myogenic markers in the hMSCs plated on PEG-CNT films did not exceed 4-fold, which is much lower than that in SKMCs (Figure 3.9). The weak myogenesis may be the result of different rigidity between PEG-CNT films and normal muscle (Young's modulus of 12 KPa) (186). Hence, PEG-CNT scaffolds with skeletal muscle mimicked stiffness could be a future direction for a specific and ultimate skeletal myogenesis of hMSCs.

3.5 Chapter conclusion

We report the fabrication and characterization of PEG-CNT films to support the growth and spontaneous skeletal myogenic differentiation of hMSCs. The PEG-CNT films, with high stiffness, presented nanoscale topography with orderly arrangement of PEG-CNTs and superior hydrophilicity on the surface. It is interesting and groundbreaking to observe that the PEG-CNT films alone triggered skeletal myogenic differentiation of non-induced hMSCs, which was substantiated by cell viability, RT-PCR and western blot analyses (Figure 3.12). Furthermore, the absence of enhanced adipogenic, chondrogenic and osteogenic markers ruled out concurrent differentiation and indicated the PEG-CNT films helped hMSCs specifically differentiate into myoblasts. This is the first report to show that PEG-CNTs can be utilized to induce the skeletal myogenesis of hMSCs. Our findings in this study suggest that the combination of hMSCs as a cell source and PEG-CNTs as a scaffold material could represent a potential strategy for skeletal muscle engineering.

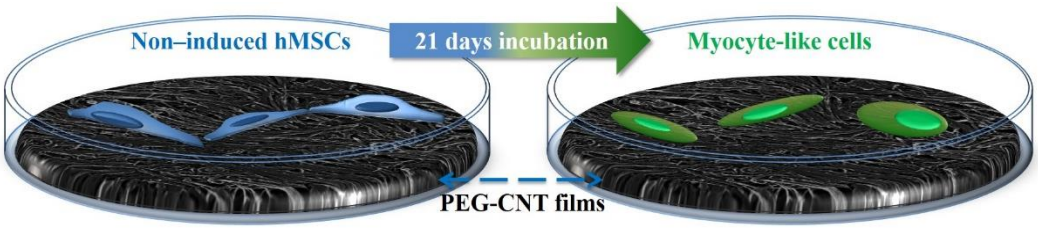

Figure 3.12 A conclusion figure for Chapter 3: PEG-CNT films alone triggered skeletal myogenic differentiation of hMSCs.

CHAPTER 4. Development and application of polyethylene glycol linked multi-walled carbon nanotubes coated hydrogels for myogenic differentiation of human mesenchymal stem cells

4.1 Introduction

The preceding Chapters alluded to the decisive role of the physical properties of scaffolds for subsequent growth, proliferation and differentiation of stem cells. In this Chapter, we will focus on the scaffold mechanical influence to the stem cells' biological cues such as differentiation. For the combined application of nanomaterial scaffolds and stem cells in tissue engineering, it was demonstrated that the scaffold stiffness is a highly adjustable parameter that may control stem cell differentiation *via* regulation of distinct cytoskeletal organization and subsequent intracellular signaling events that transfer the substrate stiffness features to cell in order to modulate cell differentiation. In another words, stem cells have been found to "sense" small fluctuations in nanomatrix rigidity (187, 188). To investigate the influence of such interaction of stem cells and nanomaterials, mechanically distinct scaffolds with identical structure and surface chemistry were produced, i.e., the substrates' surface characteristics were kept constant. The stiffer core-shell of poly-(ether sulfone)-polycaprolactone (PES-PCL) nanofibers with tensile strength of 30.6 MPa was compared against pure PCL nanofibers with tensile strength of 7.1 MPa. Differentiation results from murine embryonic mesenchymal progenitor cells on the matrixes indicated that the lower modulus PCL nanofibers facilitated chondrogenesis while the stiffer core-shell PES-PCL nanofibers enhanced osteogenesis (188). In another work, three electrospun

nanofibrous silk protein mats with different stiffness of 4.8±0.4 GPa, 6.1±0.4 GPa and 7.8±0.5 GPa were formed by varying the spinning distance. The impact of matrix rigidity features on chondrogenic differentiation of human mesenchymal stem cells (hMSCs) was clarified (187). After 4 weeks of culture, cells cultured on softer matrix (4.8±0.4 GPa) produced significantly more chondrogenesis regulating transcripts such as glycosaminoglycan, collagen type II (Col-II), SRY (sex determining region Y)-box 9 (Sox9) and aggrecan. The authors postulated that on a relatively relaxed matrix (where nanofibers are loosely deposited), hMSCs could easily migrate and assume rounded and aggregated morphologies, enhancing chondrogenesis. Whereas, the stiffer matrices (6.1±0.4 GPa and 7.8±0.5 GPa) strongly upregulated RhoA expression and showed stress fibers. This might be explained in that the stiffer nanostructure mats generated mechanical stimulations to hMSCs and activated RhoA signaling that acts through RhoA/ROCK pathway, which might inhibit chondrogenesis (189). This study confirmed again that the softer underlying matrix is more favorable for chondrogenesis. Based on the discussed studies, suitable stiffness of scaffold could be manipulated to favor specific differentiation lineages, such as relatively stiffer for osteogenesis and less stiff for chondrogenesis. A recent study also applied stiffness controlled scaffolds for successful muscle engineering. In the study, a silk fibroin nanofiber scaffold (SS-11.8) with compressive modulus of 16.7 KPa, similar to that of native muscle, initiated the myogenic differentiation of rat MSCs (190). After culturing on scaffolds in maintenance medium for 28 days, rat MSCs exhibited preferred myogenic differentiation on the SS-11.8 with significantly stronger expression of myoblast

differentiation protein-1 (MyoD) gene and protein in comparison to another silk fibroin nanofiber scaffold (SS-6.3, 6.2 KPa).

Therefore, the current consensus is that the matrix stiffness should closely match that of the gross native tissue to elicit physiological cell responses. These known effects therefore compel us to examine stiffness as a mechanical influence for myogenic differentiation of hMSCs. Up till now, we know that polyethylene glycol linked multi-walled carbon nanotube (PEG-CNT) films have enormously higher rigidity as compared to normal human muscle (Chapter 3, section 3.3, page 35), but not much has been done to modify this property. This gap creates an avenue for further exploration and optimization, and thus we consider poly-acrylamide hydrogel (PA) as a material with tunable stiffness to be used as a base to mimic the normal human muscle, whose stiffness (Young's modulus) is around 12 KPa (186). PEG-CNTs can be subsequently coated on the muscle stiffness-mimicked PA to develop a novel scaffold, namely CNT-PA-M. With this scaffold development and characterization, **this study aimed to explore the influence of CNT-PA-M to modulate the myogenic differentiation of hMSCs, with an expectation of enhanced differentiation into myocytes *in vitro*.**

4.2 Material and methods

4.2.1 Preparation of hydrogels

A feasible approach to the preparation of PA from base solutions of 40% acrylamide (Bio-Rad, USA) and 2% bis-acrylamide (Bio-Rad, USA) has been published before (191). The final concentration of acrylamide and bis-acrylamide was 10% and 0.1%,

respectively to ensure the stiffness of PA close to 12 KPa (191). After mixing the solutions in water, hydrogels were fabricated by crosslinking with tetramethylethylenediamine (TEMED, 0.1%) and ammonia persulfate (APS, 1%) between two round cover slips. After gelation, the hydrogel surfaces were rinsed with water to remove any un-polymerized monomer.

PEG-CNTs were synthesized following the procedure mentioned in Chapter 3 (section 3.2.1, page 22). Random adsorption of PEG-CNTs on PA was achieved by immersing the hydrogels in 50 μg/ml PEG-CNT water suspension for 3 hours. The obtained CNT-PA-M was rinsed with water and remained hydrated at 4 ^{o}C until use.

As a control, collagen type I (Col-I) coated muscle stiffness mimicked PA (Col-PA-M) was prepared by covalently attaching Col-I molecules onto the PA surface (191, 192). According to the product instruction, a thin layer of 0.5 mg/ml sulfosuccinimidyl 6-((4-azido-2-nitrophenyl) amino) hexanoate (sulfo-SANPAH, ProteoChem, USA) solution, which activated PA with an end of NHS ester that can react with Col-I, was placed on top of the hydrogels. Another PA without sulfo-SANPAH treatment was also used in the following steps as a comparison to ensure successful linkage of Col-I. The hydrogels were then exposed to ultraviolet light (OmniCure S2000, Excelitas Technologies, USA) for 10 minutes to crosslink the sulfo-SANPAH on hydrogel surfaces. The treated hydrogels were washed with 50 mM HEPES and soaked in a solution of 0.1 mg/ml Col-I derived from calf skin (EPC Elastin Products Company, USA) overnight at 4 ^{o}C. They were finally rinsed with water and kept in hydration at 4 ^{o}C until use.

All the reagents used were sterile and the hydrogels were prepared in a biological safety cabinet to prevent contamination during cell culturing. Right before cell seeding, the hydrogels were placed in the biological safety cabinet under UV for sterilization.

4.2.2 Characterization of hydrogels

The presence of Col-I cross-linked on the Col-PA-M surfaces was verified by immunostaining with rabbit polyclonal Col-I antibody (1:500, Abcam, UK) in 2% bovine serum albumin (BSA) for 1 hour at room temperature. The hydrogel was then washed three times with PBS and incubated with goat anti-rabbit Alexa Fluor 488 secondary antibody (1:500, Invitrogen, USA) for 1 hour at room temperature. After washing with PBS, the stained Col-PA-M was imaged using a confocal microscope (Fluoview, FV10i, Olympus, Japan).

The surfaces of wet hydrogels with different coatings were observed with a phase contrast microscope (BX51, Olympus, Japan) and photos were taken by Olympus DP72 camera (Olympus, Japan). To view with higher magnification, the hydrogels were lyophilized, coated with gold and imaged with scanning electron microscope (SEM, JSM-6701F, JEOL, Japan). The stiffness of these hydrogels in wet state was quantified using an atomic force microscope (AFM, NanoWizard II, JPK instruments AG, Germany), which is a nanoindentation method of calculating elasticity. This technique was described extensively in an earlier publication (193).

4.2.3 hMSC culture condition

The maintenance and myogenic differentiation of hMSCs were carried out with the same conditions as described in Chapter 3 (section 3.2.3, page 25). In this study, we included 6 experimental groups: (1) non-induced hMSCs plated on cover slips as a negative control; (2) myogenically-induced hMSCs plated on cover slips; (3) non-induced hMSCs plated on Col-PA-M; (4) myogenically-induced hMSCs plated on Col-PA-M; (5) non-induced hMSCs plated on CNT-PA-M; (6) myogenically-induced hMSCs plated on CNA-PA-M.

4.2.4 Cell viability test

An alamarBlue assay for cell viability was carried out at day 1, 7, 14, 21 to monitor the cell growth rate. Briefly, 10% alamarBlue (Invitrogen, USA) diluted in culture medium was added to cells and incubated for 1 hour at 37 ^{o}C. The medium was subsequently collected and the fluorescence was measured at an excitation wavelength of 565 nm and emission wavelength of 595 nm using a plate reader (EnSpire Multimode Plate Reader, Perkin Elmer, USA). Cells were washed three times with PBS and returned to fresh medium for further incubation. The fluorescent value of each sample at day 1 was defined as the control to normalize the respective sample data as fold change at other days. Results represented 3 independent biological replicates. Cell morphology at different time points was examined by a phase contrast microscope (CKX41, Olympus, Japan) and photos were taken (Olympus DP26 camera).

4.2.5 Immunostaining

At the end of 21 days differentiation protocol, cells were washed with PBS and fixed with 4% paraformaldehyde solution for 10 minutes at room temperature. Cell membranes were then permeabilized with 0.1% Triton X-100 for 10 minutes at room temperature. Non-specific sites of the samples were blocked using 2% BSA for 30 minutes and cells were incubated overnight at 4 ^{o}C with one of the following primary antibodies in 2% BSA: anti-MyoD (1:200, mouse monoclonal, Abcam, UK), anti-desmin (1:150, rabbit monoclonal, Abcam, UK) or anti-myosine heavy chain (MHC, 1:500, mouse monoclonal, Santa Cruz, USA). The next day, the cells were washed three times with PBS and incubated with corresponding secondary antibody (anti-mouse IgG-FITC or anti-rabbit IgG-FITC, 1:500, Invitrogen, USA) for 1 hour at room temperature in the dark. After washing three times with PBS, the cells were incubated with 4, 6-diamidino-2-phenylindole (DAPI, 1:1000, Invitrogen, USA) to stain the nuclei. After washing five times with PBS, the stained cells were visualized and imaged using the confocal microscope.

4.3 Results

4.3.1 Characterization of hydrogels

Shown from morphological characterization (Figure 4.1A), both of the stiffness-customized hydrogels (i.e., Col-PA-M and CNT-PA-M) were transparent, thereby allowing cell and scaffold structure to be observed directly and clearly by optical microscope. In addition, optical microscope (Figure 4.1A) and SEM images (Figure

4.1B) indicated the precipitation of randomly agglomerated PEG-CNTs on the CNT-PA-M surface. Comparing to the plain PA which had clear surface, red pigmentation on the surface of Col-PA-M was observed, suggesting the presence of sulfo-SANPAH linkage (Figure 4.1A). Immunostaining with Col-I verified the successful outcome of Col-I linkage on Col-PA-M with sulfo-SANPAH treatment (Figure 4.1C).

In this study, the hydrogels were customized to mimic the stiffness of the normal human muscle for enhancing myogenic differentiation of hMSCs. Therefore, scaffold stiffness was tested by AFM nanoindentation and the results revealed that Col-PA-M and CNT-PA-M had Young's modulus of 8.72±0.49 KPa and 9.30±0.25 KPa, respectively (Figure 4.1D). Therefore, both hydrogels achieved desired stiffness which is close to that of human muscle (12 KPa) (186).

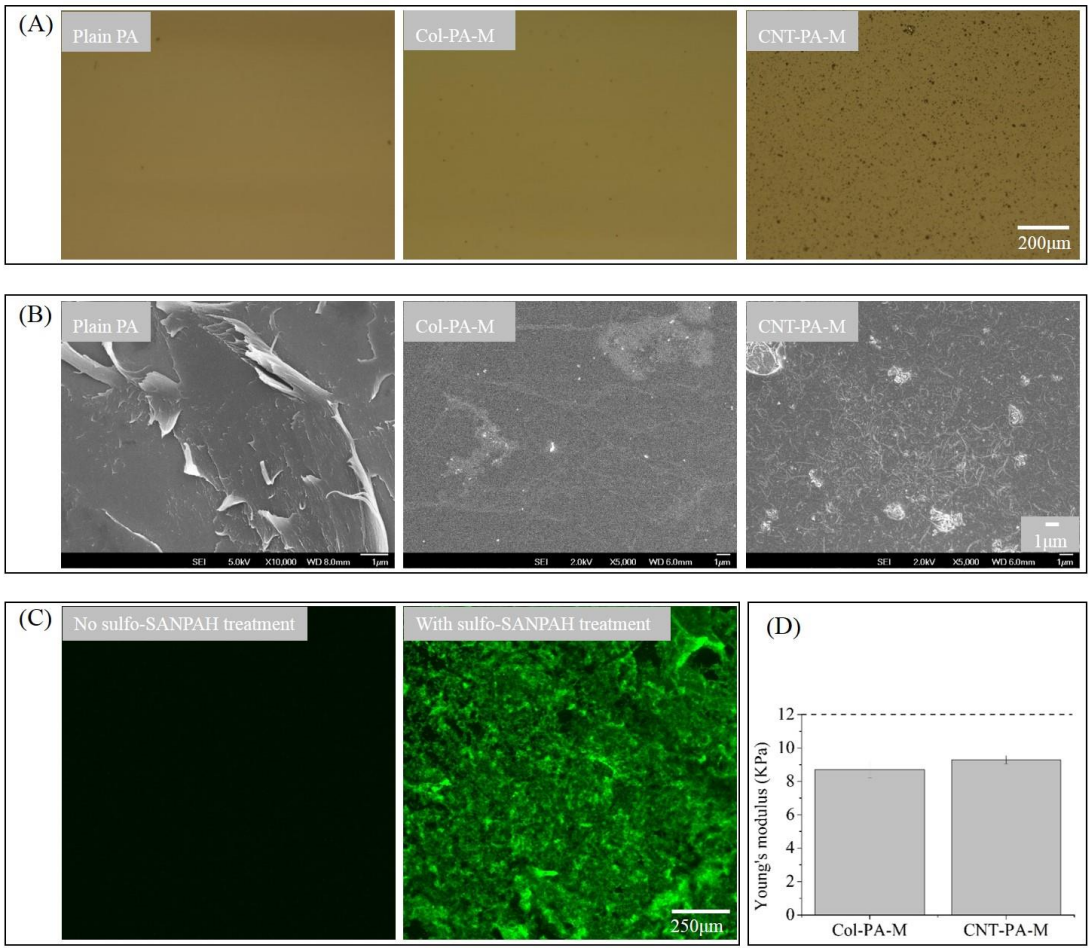

Figure 4.1 Characterization of hydrogels. (A) Surface morphology of different hydrogels taken by microscope with bright field; (B) surface morphology of hydrogels observed by SEM; (C) fluorescent staining of Col-I on PA without (left)/with (right) the treatment of sulfo-SANPAH and subsequently incubated with Col-I to prepare Col-PA-M; (D) stiffness (Young's modulus) of hydrogels tested by AFM nanoindentation. The dotted horizontal line at Young's modulus of 12 KPa is the stiffness of human muscle.

4.3.2 Cell morphology and viability on hydrogel

Figure 4.2 shows typical cell attachment and growth on cover slips, Col-PA-M and CNT-PA-M without/with myogenic induction. Elongated hMSCs were observed to be deposited on all scaffolds from day 1. The hMSCs on cover slips and Col-PA-M appeared more spread-out and flattened while cells on CNT-PA-M exhibited a more spindle-like shape. On cover slips and Col-PA-M, hMSCs (non-induced/induced) grow

significantly and formed a continuous monolayer on the scaffolds from day 7 onwards. In contrast, hMSCs on CNT-PA-M did not grow robustly, but their viability were well maintained. Over 21 days culturing, all hMSC groups grew as morphologically homogenous populations. The non-induced cells preserved the stretched morphology typical of hMSCs, whereas myogenic induction yielded polygonal shape for hMSCs, distinct from the spindle shape of human SKMCs.

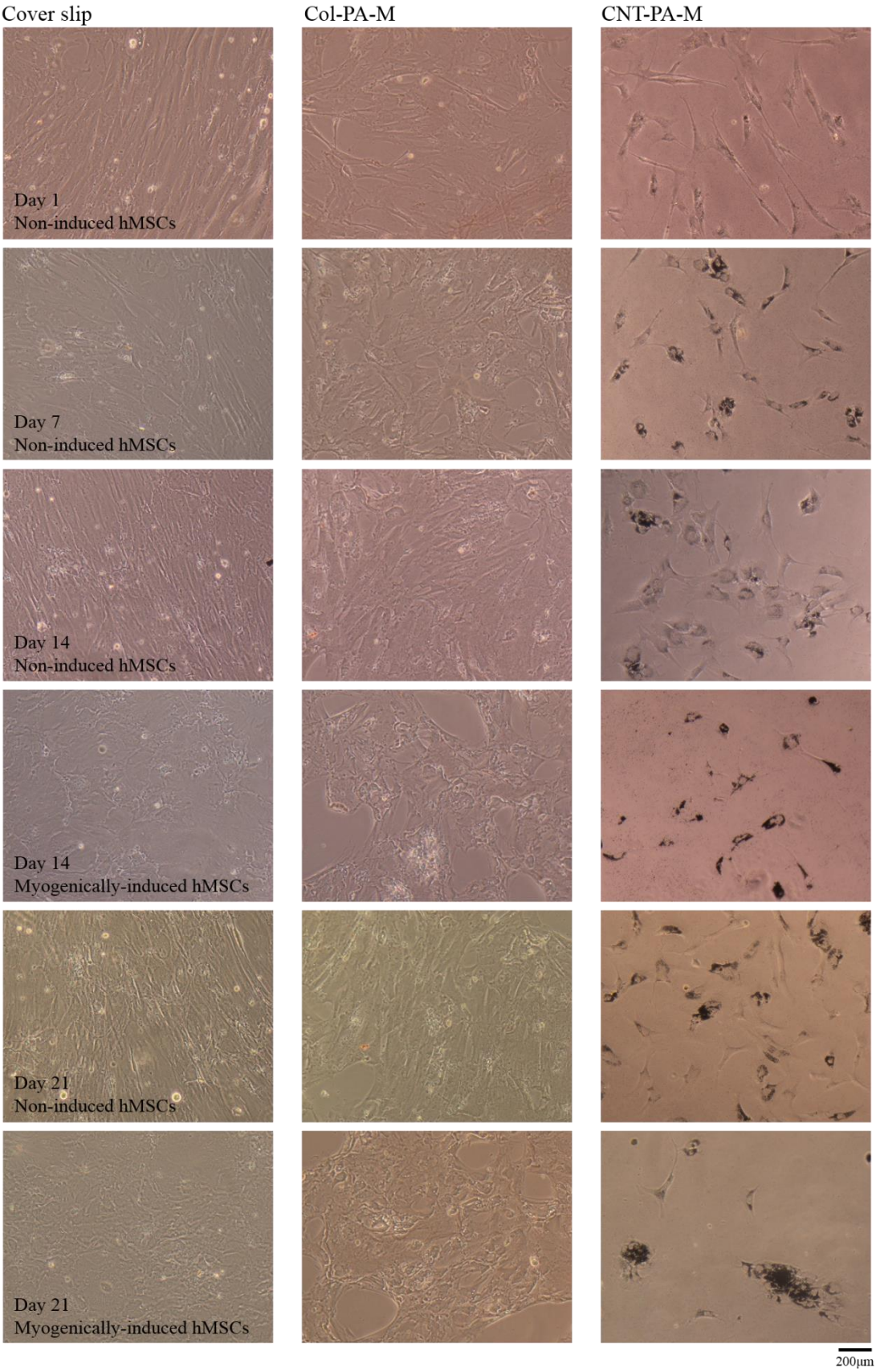

Figure 4.2 Cell morphology of hMSCs without/with myogenic induction on different substrates across 21 days.

Further quantifications of cell viability were performed on day 1, 7, 14 and 21 using an alamarBlue assay, which revealed that cell numbers on these scaffolds increased up to 21 days with a plateau. As indicated in Figure 4.3, larger cell numbers were achieved on the controls of cover slips and Col-PA-M as compared to CNT-PA-M, consistent with earlier qualitative results (Figure 4.2). In other words, cover slips and Col-PA-M supported the growth of hMSCs while CNT-PA-M sustained the cell viability. With myogenic induction, the cell viability in all cases registered a decline, which can be easily observed on day 21.

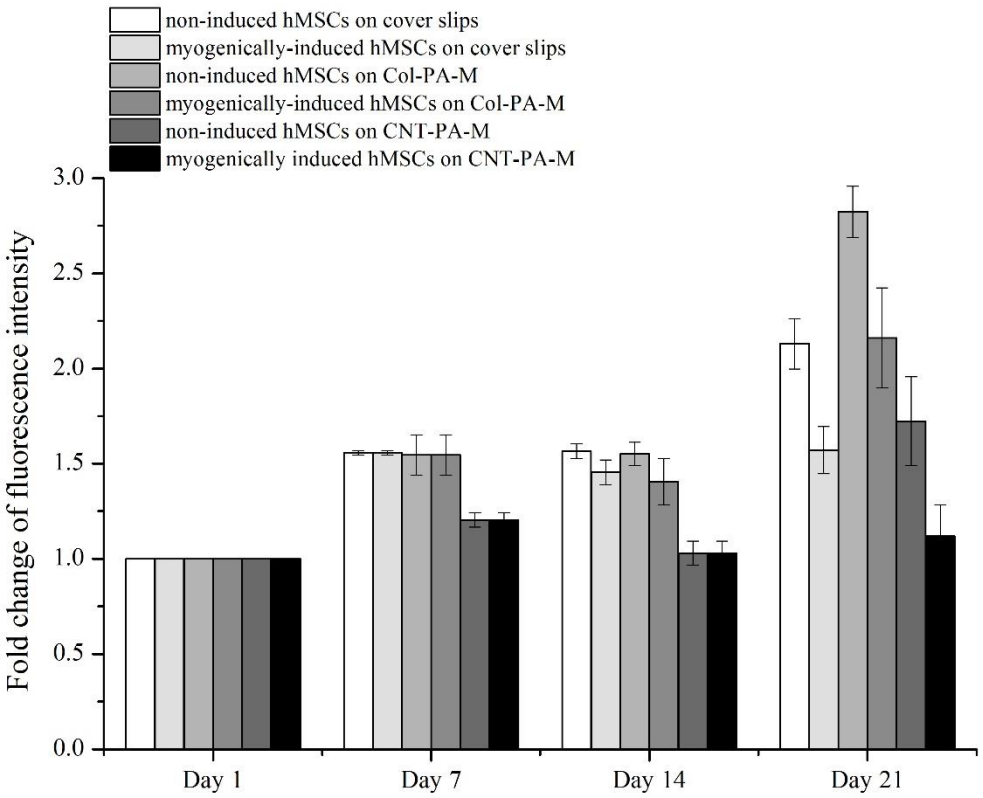

Figure 4.3 Viability of non-induced and myogenically-induced hMSCs on various substrates across 21 days as measured by alamarBlue assay, n=3.

4.3.3 Immunostaining

In order to clarify the effects of CNT-PA-M on the differentiation of hMSCs, expression of MyoD, desmin and MHC proteins was studied at the end of 21 days incubation *via* immunofluorescence staining as a quick analytical method. Compared to cover slips, there was slightly higher fluorescence intensity of MyoD and MHC on hydrogels (Col-PA-M and CNT-PA-M), regardless of the presence or absence of myogenic induction. (Figure 4.4A and C). Moreover, stronger expression of desmin appeared on hydrogels than on cover slips, without any clear difference between the myogenically-induced or non-induced hMSCs (Figure 4.4B).

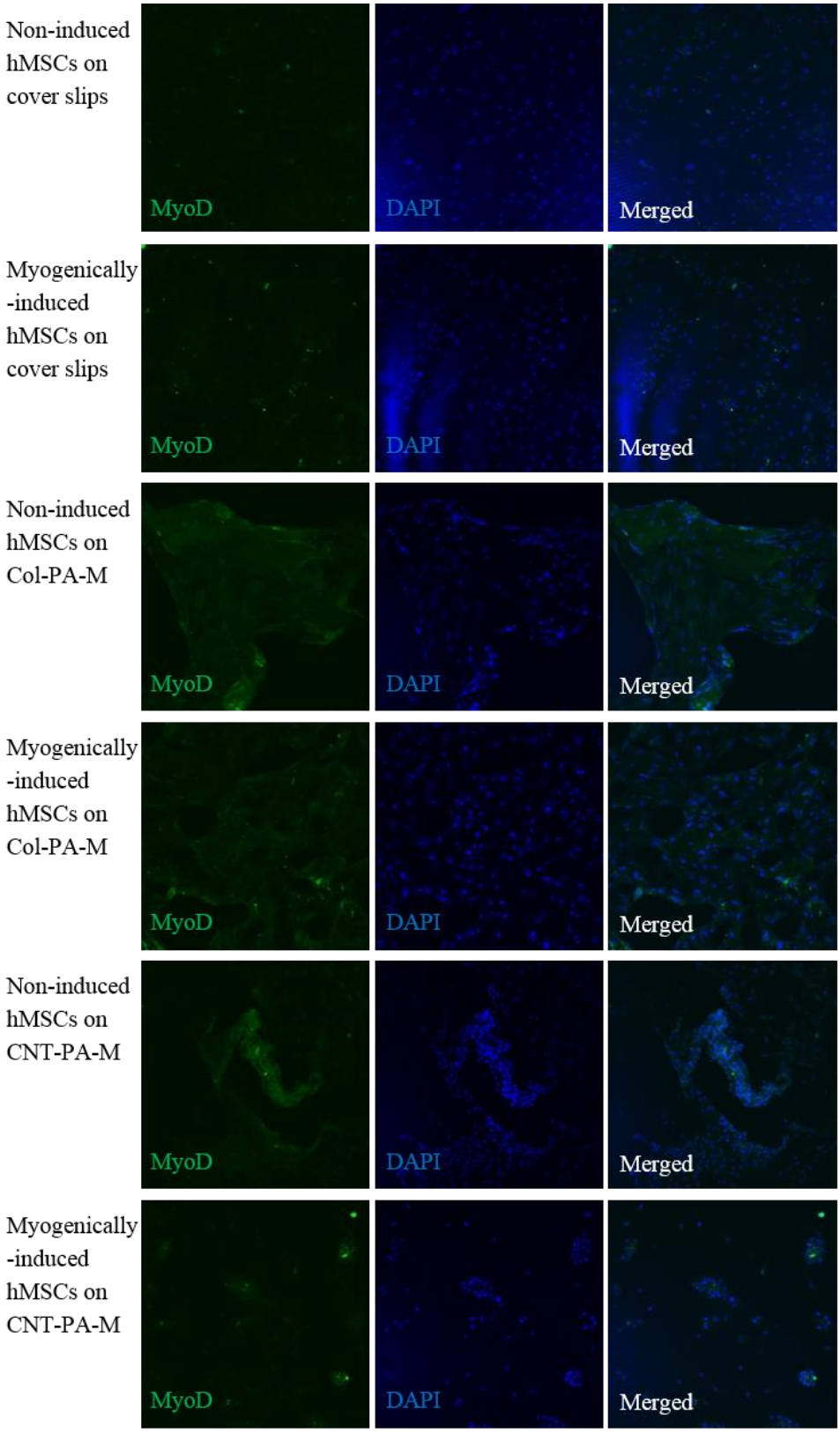
Non-induced hMSCs on cover slips
MyoD
DAPI
Merged
Myogenically -induced hMSCs on cover slips
MyoD
DAPI
Merged
Non-induced hMSCs on Col-PA-M
MyoD
DAPI
Merged
Myogenically -induced hMSCs on Col-PA-M
MyoD
DAPI
Merged
Non-induced hMSCs on CNT-PA-M
MyoD
DAPI
Merged
Myogenically -induced hMSCs on CNT-PA-M
MyoD
DAPI
Merged
250μm

(A)

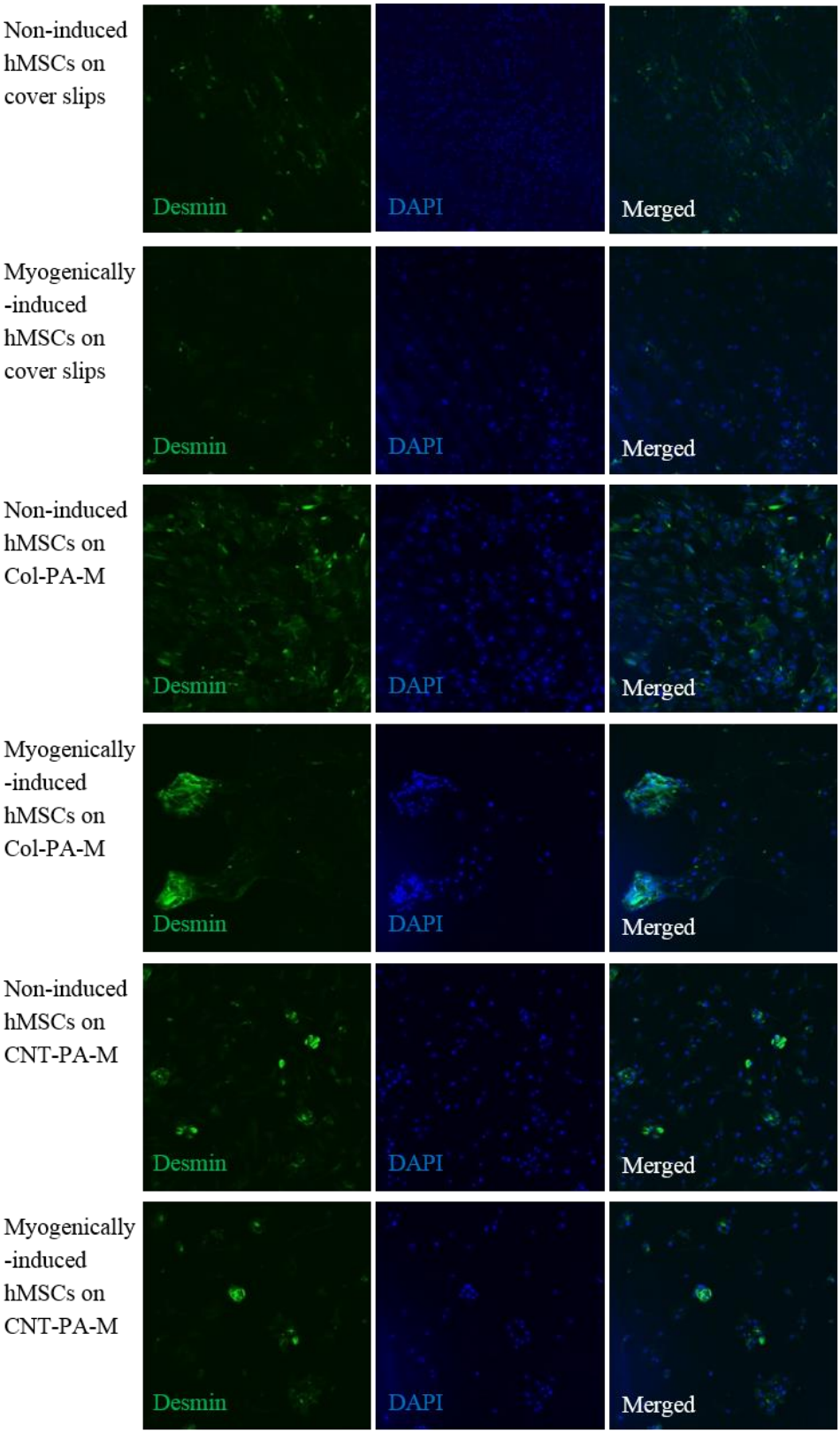
Non-induced hMSCs on cover slips
Desmin
DAPI
Merged
Myogenically -induced hMSCs on cover slips
Desmin
DAPI
Merged
Non-induced hMSCs on Col-PA-M
Desmin
DAPI
Merged
Myogenically -induced hMSCs on Col-PA-M
Desmin
DAPI
Merged
Non-induced hMSCs on CNT-PA-M
Desmin
DAPI
Merged
Myogenically -induced hMSCs on CNT-PA-M
Desmin
DAPI
Merged
(B)
250μm

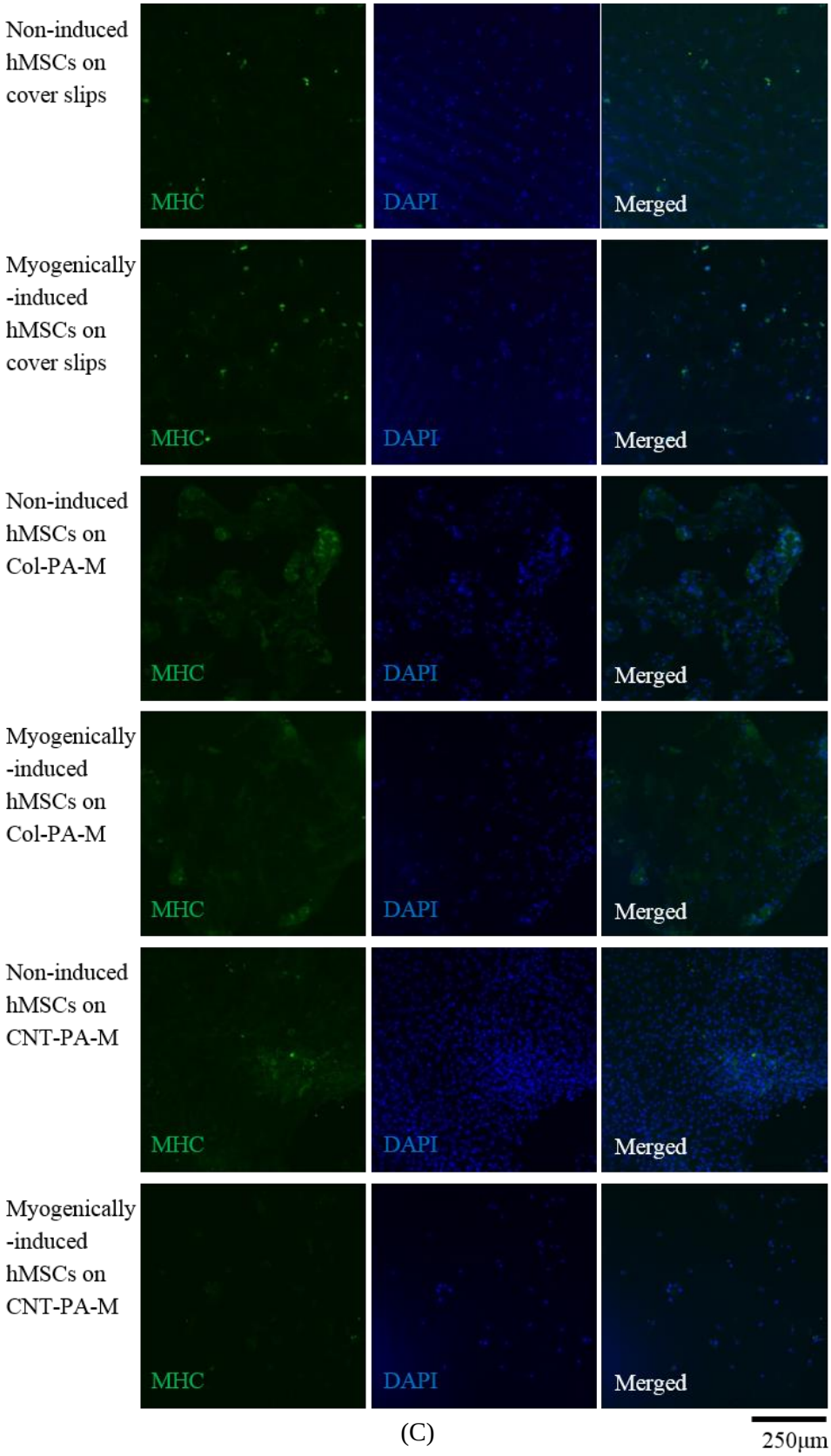

Figure 4.4 Immunostaining of non-induced and myogenically-induced hMSCs on different scaffolds at day 21. The cells were stained for (A) MyoD (green), (B) desmin (green), (C) MHC (green) and DAPI (blue), respectively.

4.4 Discussion

The aim of this study was to investigate the influence of the improved CNT-PA-M to the myogenic differentiation of hMSCs. First of all, matrixes of CNT-PA-M and Col-PA-M (as a control) were successfully prepared with a customized stiffness mimicking that of human muscle. Both of Col-PA-M and CNT-PA-M were transparent (Figure 4.1A), thereby allowing cell and scaffold structure to be observed directly and clearly by optical microscope. This initial characteristic already spells an advantage of these hydrogels over PEG-CNT films which are opaque and can compromise cell and scaffold visualization. The sample optical microscope and SEM images of CNT-PA-M (Figure 4.1A and B) were taken after several washes post PEG-CNT incubation, thus the strong bonding of PEG-CNTs on PA surface would be a prerequisite for cell adhesion to support long-term cell culturing. This is proven by cell morphology study (Figure 4.2) that PEG-CNT coating on CNT-PA-M can still be seen after 21 days incubation. Moreover, the slightly higher stiffness of CNT-PA-M compared to Col-PA-M (Figure 4.1D) could be attributed to the thin layer of PEG-CNTs attached on the hydrogel surface.

The perturbation of cell morphology through changing surface mechanics can lead to tremendous biological implications. Several studies have noted that changes in cell shape regulated biological processes in cells, such as differentiation. For example, culturing in a chondrogenic differentiation medium with transforming growth factor β3 (TGF β3) for 1 week, hMSCs spreading on large fibronectin islands (10,000 μm^2) and un-patterned fibronectin-coated flat regions showed a greater expression level of

calponin (a smooth muscle cell marker), whereas hMSCs which were prevented from spreading when grown on small fibronectin islands (1024 μm^2) showed an up-regulation of Col-II, a chondrogenic marker (194). Changes in cell shape *via* rearrangements in the architecture and mechanics of the cytoskeleton, can mechanically induce focal adhesion, physically distort the nucleus, and even directly impact receptor-mediated signaling to alter cell differentiation (194, 195). Hence taking all these aspects together, multiple independent or inter-dependent mechanisms may transduce changes in cell shape to drive stem cell fate. As shown from Figure 4.2, myogenically-induced hMSCs adopted a new morphology with polygonal shape, yet maintaining cell viability. Therefore, the change in cell shape and cytoskeleton may correlate with the induction of hMSCs into muscle cells, which unfortunately was not observed in this study. However, it was also found that skeletal myogenic precursor cells extended into elongated spindles, similar to SKMCs, to execute their muscular functions (194). This finding may explain why non-induced hMSCs on Col-PA-M and CNT-PA-M, which retained the spindle-like shape, could also trigger the myogenesis of hMSCs (based on MyoD, desmin, MHC expression). More research is required to investigate how the change in cell shape influences the myogenesis of hMSCs. Since the shape of non-induced hMSCs is closer to SKMC shape compared to the myogenically-induced hMSCs, Col-PA-M and CNT-PA-M could represent easier and more controllable substrates to manipulate myogenesis of hMSCs. The decreased cell number of hMSCs on CNT-PA-M and myogenically-induced hMSCs may be a result of the transition from the growth phase to the differentiation phase, as we have

discussed in Chapter 3 (section 3.4, page 48).

From the immunostaining (Figure 4.4), the stronger expression of myogenic proteins appeared on hydrogel scaffolds than on the negative control (non-induced hMSCs on cover slips), confirming the myogenic differentiation of hMSCs. No matter myogenic induction medium treated or not, hMSCs on hydrogel scaffolds obtained similar expression of MyoD, desmin and MHC. These results suggest the possibility of that tailoring matrix stiffness alone could intrinsically induce the differentiation of hMSCs to muscle cells. In future study, it would be a promising tool to fabricate PEG-CNTs or Col-I coated PA with controlled stiffness to match different tissues for diverse stem cell differentiation.

In this study, myogenic induction medium failed to induce or enhance the myogenesis of hMSCs, which is a similar finding with that in Chapter 3. To improve myogenic differentiation of hMSCs, more robust myogenic induction medium (e.g., addition of SKMC specific growth factors) can be investigated in future. Furthermore, PEG-CNT coating had similar ability with Col-I coating in the spontaneous myogenesis of hMSC on hydrogels, indicating that PEG-CNTs worked as well as the widely used ECM protein, Col-I.

On this note, the myogenic differentiation of hMSCs on PEG-CNT films was also studied with immunostaining in this research, but no result is displayed here due to a lack of signal for any myogenic protein. Moreover, the nuclei in hMSCs on PEG-CNT films stained with DAPI (fluorescence excitation/emission: 358/461 nm) cannot be detected, which may be due to the interference of PEG-CNTs. It has been reported that

CNTs exhibit strong optical absorption of wavelength below 380 nm due to its semiconducting excitonic energy levels (196). This overwhelming absorption under 380 nm by CNT may suppress the fluorescence from DAPI at 358 nm excitation. Hence, YoYo-1 with fluorescence excitation/emission of 491/509 nm (Invitrogen, USA) was tested to locate the cell nuclei. Although the YoYo-1 staining can be observed in hMSCs grown on PEG-CNT films, it was not specific for nuclei and cell plasma was also stained. It was assumed that the PEG-CNTs had strong absorption of YoYo-1 dye and retained a large amount of the dye in the nanotubes, making it difficult to wash the dye out of the PEG-CNTs and leading to over-labeling of the cells. Hence, the images of hMSCs on PEG-CNT films were not shown.

To further challenge the capability of PEG-CNT-based scaffolds in directing hMSCs' lineages, trans-differentiation of hMSCs into hepatocytes, cardiomyocytes or neurons can be investigated on PEG-CNT-based scaffolds in future.

4.5 Chapter conclusion

In this study, muscle stiffness mimicked Col-PA-M and CNT-PA-M were prepared and evaluated with their biological effects on viability and myogenic differentiation of hMSCs. The hydrogels of Col-PA-M and CNT-PA-M well supported the growth of hMSCs and induced spontaneous myogenesis of hMSCs (Figure 4.5). This mechanical influence offers new opportunities to fine-tune existing scaffolds in support of different types of stem cell differentiation. In the following Chapter, we will exploit the versatility of this approach in liver engineering.

Figure 4.5 A conclusion figure for Chapter 4: CNT-PA-M induced spontaneous myogenic differentiation of hMSCs.

CHAPTER 5. Enhanced hepatic differentiation of human amniotic epithelial cells on polyethylene glycol linked multi-walled carbon nanotubes coated hydrogels

5.1 Introduction

Liver performs a wide range of functions in metabolism and digestion, including detoxification, protein synthesis and bile production. As the main metabolic organ, the liver is exposed to large amounts of xenobiotics which makes liver very vulnerable (197). In addition, viral infections, genetic disorders or alcoholic injuries can cause liver failure, leading to acute or chronic liver diseases. Thus, human hepatocytes that are suitable for *in vivo* liver regeneration (the treatment of acute liver failures and end-stage liver diseases), for construction of bio-artificial liver devices, or for *in vitro* testing of xenobiotics (e.g., drugs and pathogens) in the pharmaceutical industry, have been in great demand. However, such supplies are scarce due to the worldwide shortage of donor organs. Moreover, the application of fresh primary human hepatocytes as an attempt to enlarge this pool is severely limited by poor proliferation capacity and difficulty in maintaining metabolic functions when cultured *in vitro* (198). Therefore, it is both rational and necessary to develop a strategy that can circumvent donor liver scarcity for alternative cell sources, and yet be able to fully recapitulate hepatocyte phenotype and functions. In this respect, stem cell-derived hepatocytes believed to be a possible method that allows sustainable source of hepatocytes, have being pursued.

Human amniotic epithelial cells (hAECs), with pluripotency and self-renewal capabilities, can be readily isolated from human amniotic membrane and maintained *in*

vitro (45, 199-202). Advantages of hAECs over other stem cell sources (e.g., human embryonic stem cells, hESCs and human mesenchymal stem cells, hMSCs) include abundant availability, non-invasive collection methods and ethically neutral since the placenta is usually discarded as bio-waste after parturition. More importantly, hAECs are not tumorigenic upon transplantation in comparison with hESCs (202) and are not known to induce immune reaction (203), thus allowing potential *in vivo* application. It has been reported that isolated hAECs resembled hepatic progenitor cell behaviors, such as albumin (ALB) secretion (204, 205) and expression of a subset of hepatocyte-related markers including cytokeratin-18 (CK18), α-fetoprotein (AFP) and α1-anti-trypsin (α1AT) (204, 206). All these properties make hAECs a promising cell source for liver engineering. Being fetal in origin, hAECs are highly plastic and have been differentiated into hepatocytes to different extents with a cocktail of growth factors, cytokines and hormones (44, 45, 207). When subjected to such differentiation medium, hAECs exhibited morphologic and phenotypic characteristics of hepatocytes, performed key hepatic functions in terms of ALB secretion, urea synthesis, indocyanine green (ICG) uptake and elimination, low-density lipoprotein uptake and inducible cytochrome P450 (CYP) activities. Yet, besides differentiation medium, culturing conditions could also be innovated to facilitate hepatic differentiation of hAECs. For example, co-culturing with mouse hepatocytes was shown to improve expression of hepatocytic markers (e.g., ALB and CYP) and metabolically active and inducible CYP3A enzyme functions in the hAEC-derived hepatocytes (207). Nonetheless, it is difficult and inconvenient to co-culture hAECs with mouse

hepatocytes for hepatic differentiation (207) and this combination also limits human implantation as a subsequent application. In another study, hAECs was encapsulated into barium alginate microspheres for hepatic differentiation along with enhanced hepatic functions in terms of urea output and CYP3A4 activity (44). While encouraging results were obtained, all of these studies shared a problem that the efficiency of hepatic differentiation remained low, and that the hepatically-differentiated hAECs were more fetal-like rather than mature adult hepatocytes. Consequently, a robust and efficient protocol for the differentiation of hAECs into functionally mature hepatocytes remains elusive.

In addition to the use of hepatic differentiation medium, molecular scaffold for cell seeding is required for stem cell differentiation into hepatocytes *ex vivo*. As we discussed in Chapter 1, an ideal scaffold should mimic the structure and biological function of the *in vivo* liver microenvironment, the extracellular matrix (ECM). Carbon nanotubes (CNTs), with controlled nanoscale topography, may represent a promising material for the creation of liver ECM mimics (208). Compared to the cover slip control, aligned CNT (multi-walled) sheets and CNT yarns were proved to enhance liver-specific functions of primary rat hepatocytes, including ALB production and CYP1A2 induction (208). Albeit optimistic results were obtained, this study only investigated CNTs' effects to maintain rat hepatocytes. So far, there was no research investigating the influence of CNTs on hepatic differentiation of stem cells, which is a more complicated process than just cell maintenance. Furthermore, pristine CNTs which are extremely hydrophobic with restricted application in tissue engineering was employed

in this earlier study (208). We therefore envisage that polyethylene glycol linked multi-walled carbon nanotubes (PEG-CTNs) with increased hydrophilicity can be employed for the hepatic differentiation of hAECs (67, 122). This also represents the first attempt to exploit the versatility of CNTs in the differentiation of adult stem cells besides those of mesenchymal origin.

Other than the compatibility of the nanoscale structure to support cell growth and differentiation, scaffold stiffness can exert significant influence in determining stem cell fate (147), which has been demonstrated in Chapter 4 (section 4.1, page 54). The current consensus is that the matrix stiffness should closely match that of the gross native tissue to elicit physiological cell responses. As a result, the employment of poly-acrylamide hydrogel (PA) as a material with tunable stiffness was considered as a base to mimic the normal human liver, whose stiffness (Young's modulus) is below 6 KPa (209, 210). PEG-CNTs were then coated on the liver stiffness-mimicked PA to develop PEG-CNTs coated PA (CNT-PA-L). **With that, we positioned this study to explore the influence of CNT-PA-L to modulate the hepatic differentiation of hAECs, with the expectation of enhanced differentiation into functional hepatocyte-like cells (HLCs) *in vitro*.**

5.2 Materials and methods

5.2.1 Preparation of hydrogels

The PA was prepared with the method described in Chapter 4 (section 4.2.1, page 56). The final concentration of acrylamide and bis-acrylamide was 5% and 0.15%,

respectively to ensure the stiffness of PA lower than 6 KPa (191). The CNT-PA-L and collagen-I (Col-I) coated liver stiffness mimicked PA (Col-PA-L) were fabricated following the procedure mentioned in Chapter 4 (section 4.2.1, page 57).

5.2.2 Characterization of hydrogels

The surfaces and stiffness of hydrogels with different coatings were characterized as described in the previous chapter (Chapter 4, section 4.2.2, page 58).

5.2.3 Cell culture

hAECs were isolated from amniotic membrane as previously described (45, 199). They were maintained at 80,000 cells/cm^2 in growth medium composed of high glucose-Dulbecco's Modified Eagles medium (Hyclone, USA), 20 ng/ml epidermal growth factor (BD Bioscience, USA), ITS premix (1:1000 dilution, BD Bioscience, USA), 10 mM HEPES (Gibco, USA), 1 mM sodium pyruvate (Gibco, USA), Glutamax (1X, Gibco, USA) and 0.2 mM ascorbic acid (Sigma-Aldrich, USA). HepG2 cells (a hepatoblastoma cell line) were cultured in high glucose-Dulbecco's Modified Eagles medium (Sigma-Aldrich, USA) with 10% fetal bovine serum (PAA Technologies, Austria). Sub-culturing was performed when hAECs and HepG2 cells reached 80-90% confluence with 0.25% trypsin–EDTA (Invitrogen, USA). Cryopreserved differentiated HepaRG cells (a human hepatic progenitor cell line, Life Technologies, USA) were thawed using HepaRG General Purpose medium and seeded into 96 well plates at a density of 100 000 cells/well. Medium was changed to HepaRG Tox media the next

day and refreshed every 3 days. Cells were ready for use after 7 days of maintenance. All cells were maintained at 37 ℃, 5% CO_2 air atmosphere.

5.2.4 Hepatic differentiation of hAECs in vitro

To induce hepatic differentiation of hAECs (80,000 cells/cm^2), defined medium were used at different stages during 18 days incubation. The hepatic induction was performed with a 4-step protocol as described previously (45): (1) growth medium supplemented with B-27 (Biotool, USA) and 100 ng/ml Activin A (PeproTech, USA) from day 1 to day 5; (2) growth medium supplemented with B-27, 20 ng/ml bone morphogenetic protein-4 (BMP-4, Gibco, USA) and 10 ng/ml fibroblast growth factor-2 (FGF-2, BD Bioscience, USA) from day 6 to day 10; (3) growth medium supplemented with B-27 and 20 ng/ml hepatocyte growth factor (HGF, PeproTech, USA) from day 11 to day 15; (4) Hepatocyte culture medium (HCM, Lonza, Switzerland) supplemented with 20 ng/ml Oncostatin M (R&D systems, USA) and 100 μM Sodium taurocholate (Sigma-Aldrich, USA) from day 16 to day 18.

The experimental samples were: (1) hAECs on collagen (Invitrogen, USA) coated cover slips in growth medium as a negative control, (2) HLCs (hAECs subjected to hepatic induction) on collagen coated cover slips, (3) HLCs on Col-PA-L, (4) HLCs on CNT-PA-L, (5) HepG2 and (6) HepaRG cells on cover slips as positive controls.

5.2.5 Cell viability test

An alamarBlue assay for cell viability was carried out at the indicated time points (day 3, 5, 8, 10, 13, 15, 18) to monitor the cell growth rate. The procedures of alamarBlue assay and cell morphology observation were shown in Chapter 4 (section 4.2.4, page 59). The fluorescent value of each sample at day 3 was defined as control to normalize the respective sample data as fold change at other days. Results represented 3 independent biological replicates.

5.2.6 Real-time polymerase chain reaction (RT-PCR)

After incubation for 18 days, hAECs and HLCs were processed for total RNA isolation, cDNA synthesis and quantitative RT-PCR study as mentioned in Chapter 3 (Section 3.2.5, page 27). The primers were either designed using web-based Primer 3 software (http://frodo.wi.mit.edu/), cited from PrimerBank (http://pga.mgh.harvard.edu/primer bank/) or taken from other reported works. The primer information was listed in Table 5.1. The cycle thermal profile comprised an enzyme activation at 50 ℃ for 2 minutes, followed by an initial denaturation at 95 ℃ for 10 minutes, 40 cycles of 95 ℃ for 15 s and 60 ℃ for 1 minute. Expression changes of various genes were analyzed using Livak ($2^{-\Delta\Delta CT}$) method (148). Each gene was first normalized to GAPDH to obtain ΔCT and subsequently normalized to the negative control of non-induced hAECs on cover slips. Results represented 3 independent biological replicates.

Table 5.1 Primer sequences of target and reference genes in RT-PCR analysis

	Gene name	Gene symbol	Gene ID	Forward primer (5'->3')	Reverse primer (5'->3')	Product size (bp)	Reference
Hepatic markers	Alpha-Fetoprotein	AFP	NM_001134.1	AGC TTG GTG GTG GAT GAA AC	TCT GCA ATG ACA GCC TCA AG	182	(211)
	Albumin	ALB	NM_000477.5	TGG CAC AAT GAA GTG GGT AA	CTG AGC AAA GGC AAT CAA CA	166	Primer 3
	Alpha-1-antitrypsin	α1AT	M11465.1	GGG AAA CTA CAG CAC CTG GA	CCC CAT TGC TGA AGA CCT TA	175	Primer 3
	Hepatocyte nuclear factor-4-alpha	HNF4α	NM_175914	CAC GGG CAA ACA CTA CGG T	TTG ACC TTC GAG TGC TGA TCC	227	Primer bank
	Cytokeratin-18	CK18	X12881.1	AAG GCC TAC AAG CCC AGA TT	CAC TGT GGT GCT CTC CTC AA	179	Primer 3
	glucose-6-phosphatase	G6P	NM_000151	GTG TCC GTG ATC GCA GAC C	GAC GAG GTT GAG CCA GTC TC	126	Primer bank
Phase I enzymes	Cytochrome P450 3A4	CYP3A4	NM_017460.5	TGT GCC TGA GAA CAC CAG AG	CAT TGG ATG AAG CCC ATC TT	75	Primer 3
	Cytochrome P450 2C9	CYP2C9	NM_000771	CCT CTG GGG CAT TAT CCA TC	ATA TTT GCA CAG TGA AAC ATA GGA	137	(211)
Pluripotent genes	Nodal	Nodal	NM_018055.4	GAA GGG CTC AGT GGA GTC TG	TGC ACT TGT GCT TTT CCT TG	129	Primer 3
	Nanog	Nanog	NM_024865.2	GAT TTG TGG GCC TGA AGA AA	AAG TGG GTT GTT TGC CTT TG	155	Primer 3
	Octamer-binding transcription factor 4	OCT4	NM_001173531.1	GTA CTC CTC GGT CCC TTT CC	CAA AAA CCC TGG CAC AAA CT	168	Primer 3
Reference gene	Glyceraldehyde-3-phosphate dehydrogenase	GAPDH	NM_002046.4	ATG TTC GTC ATG GGT GTG AA	TGT GGT CAT GAG TCC TTC CA	144	Primer 3

5.2.7 Immunostaining

At the end of the 18 days differentiation protocol, cells were processed for immunostaining with the methods described in Chapter 4 (section 4.2.5, page 59). The used primary antibodies are anti-human octamer-binding transcription factor 4 (OCT4, 1:200, mouse monoclonal IgG, Santa Cruz, USA), anti-human AFP (1:200, goat polyclonal IgG, Santa Cruz, USA), anti-human ALB (1:200, goat polyclonal IgG, Santa Cruz, USA) or anti-human hepatocyte nuclear factor-4-alpha (HNF4α, 1:200, goat polyclonal IgG, Santa Cruz, USA). The secondary antibodies are donkey anti-goat IgG-FITC (1:200, Santa Cruz, USA) or rabbit anti-mouse IgG3-FITC (1:200, Santa Cruz, USA). Pictures were taken and processed by ImageJ software (National Institutes of Health, USA) to quantify the average fluorescence intensity per area on OCT4, AFP, ALB and HNF4α stained images. Quantification was performed on at least 30 randomly selected areas with cells.

5.2.8 Hepatic function test

5.2.8.1 Secretion of ALB

Cell culture media were collected at every medium change (day 3, 5, 8, 10, 13, 15, 18), and spun at 10,000 rpm for 3 minutes to remove cell debris. Supernatants were stored at -20 ^{o}C until the day of assay. ALB production was assayed using a quantitative enzyme linked immunosorbent assay (ELISA) kit (Cygnus, USA) according to the manufacturer's recommendations. The ALB concentration was normalized to cell viability quantified by alamarBlue intensity. Results represented 3 independent

biological replicates.

5.2.8.2 Cellular uptake and clearance of ICG

ICG (MP Biomedicals, France) was freshly dissolved in culture medium to 1 mg/ml and added to cells. After incubation for 1 hour at 37 ^{o}C in incubator, cells were rinsed three times with PBS and returned to fresh culture medium without ICG. The cellular uptake of ICG was immediately examined by a phase contrast microscope (CKX41, Olympus, Japan) and photos were taken by a DP26 camera (Olympus, Japan). At 6 hours post incubation, a repeat imaging was performed to examine the clearance of ICG (212).

5.2.8.3 Functional metabolism assay of CYP3A4

Functional metabolism assay was carried out with a P450-Glo Luciferin-IPA kit (Promega, USA) according to manufacturer's instructions. Cells were seeded on 96-black-walled, clear bottom plates and processed for hepatic differentiation. After 18 days incubation, previous culture medium was removed and replaced with 60 µl of 3 µM Luciferin-IPA dissolved in culture medium. Control without cells was also performed for background luminescence correction. The plate was incubated for 1 hour. Thereafter, an aliquot of 50 µl medium was transferred to a white opaque polystyrene plate containing 50 µl of Luminescence Detection Reagent (LDR) in each well. The white plate was incubated for 20 minutes at room temperature and luminescence was read using a plate reader (Tecan, Switzerland). The cells were washed with PBS and alamarBlue assay was performed to test cell viability. The net luminescence signal due to CYP3A4 activity was calculated by subtracting the respective signal from control

wells without cells from the signal generated from wells with cells. The net luminescence signal was then normalized against the respective fluorescence signal from the alamarBlue assay. Results represented 3 independent biological replicates.

5.2.8.4 Induction of CYP3A4

Cells were seeded on 96-black-walled, clear bottom plates and processed for hepatic differentiation. At the end of 18 days incubation, the medium was changed to fresh culture medium containing 25 μM rifampicin in 0.1% DMSO or containing the vehicle of 0.1% DMSO (solvent control). The medium with rifampicin was refreshed every 24 hours for 48 hours. Thereafter, rifampicin medium and solvent control medium were removed and cells were rinsed with PBS, followed by P450-Glo Luciferin-IPA and alamarBlue assays. The induction fold of CYP3A4 activity was determined by dividing normalized net luminescence of a treated group with that of the corresponding solvent control group. Results represented 3 independent biological replicates.

5.2.9 Statistical analysis

Quantitative data were represented as mean ± standard deviation (SD) with 3 independent biological replicates. Statistical differences among various groups (n>2) were analyzed using SPSS with one-way ANOVA followed by Tukey post hoc test. Otherwise, a two-tailed unpaired student's *t* test with SPSS was used. Significant difference was set as $P<0.05$ and represented as *=$P<0.05$, #=$P<0.01$, &=$P<0.001$.

5.3 Results

This study explored the effects of CNT-PA-L on the hepatic differentiation of hAECs and we demonstrated that CNT-PA-L could enhance the differentiation of hAECs into functional HLCs.

5.3.1 Characterization of hydrogels

We set out to perform morphological characterization of the stiffness-customized hydrogels. Similar to the results in Chapter 4 (section 4.3.1, page 60), optical microscope (Figure 5.1A) and SEM images (Figure 5.1B) showed the precipitation of randomly agglomerated PEG-CNTs on the CNT-PA-L surface, resulting in nanostructured surface. In addition, the successful outcome of Col-I linkage on Col-PA-L was verified by immunostaining with Col-I (Figure 5.1C).

In this study, the hydrogels were tailored to mimic the stiffness of the normal human liver for effective hepatic differentiation of hAECs. AFM nanoindentation results showed that Col-PA-L and CNT-PA-L had Young's modulus of 3.39±0.56 KPa and 3.92±0.15 KPa, respectively (Figure 5.1D). The slight increase in CNT-PA-L stiffness could be attributed to the thin layer of PEG-CNT deposition. Anyway, both hydrogels achieved desired stiffness to mimic normal liver, whose stiffness should be kept lower than 6 KPa.

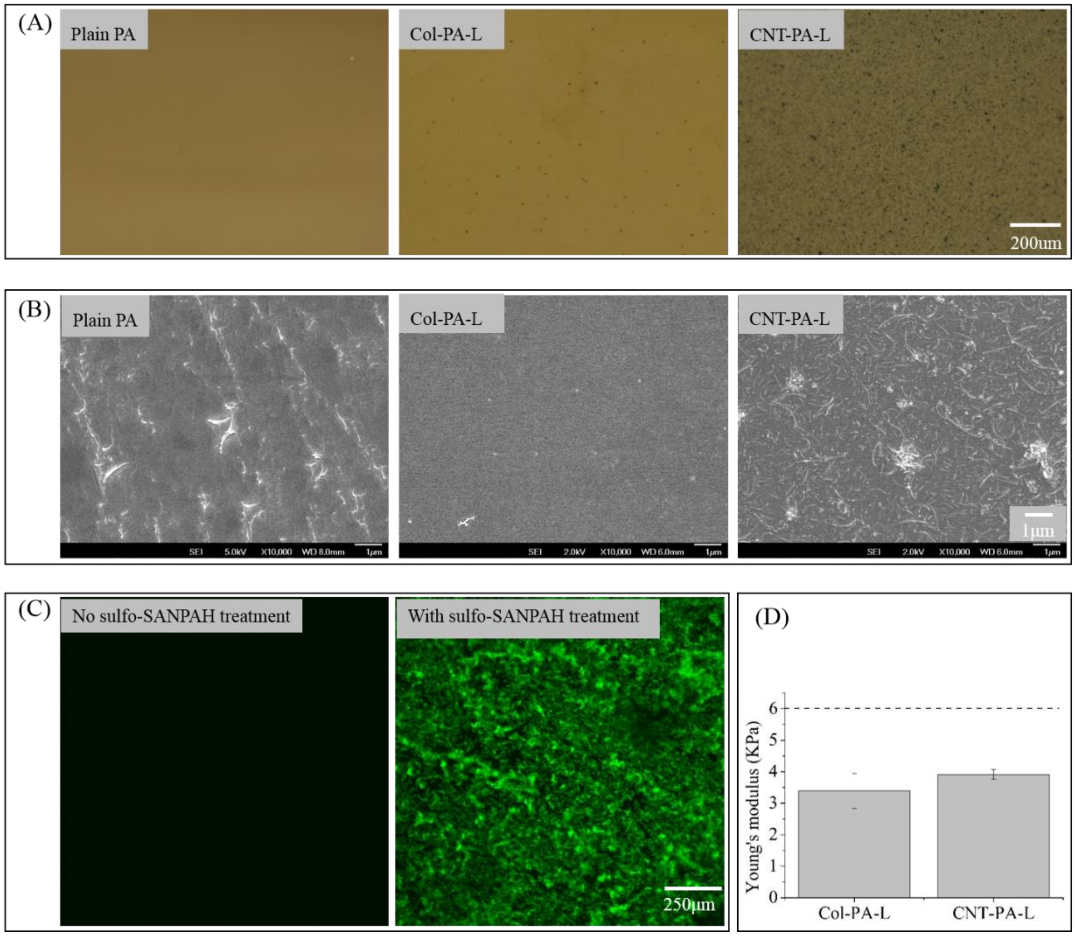

Figure 5.1 Characterization of hydrogels. (A) Surface morphology of different hydrogels taken by microscope with bright field; (B) surface morphology of hydrogels observed by SEM; (C) fluorescent staining of Col-I on PA without (left)/with (right) the treatment of sulfo-SANPAH and subsequently incubated with Col-I to prepare Col-PA-L; (D) stiffness (Young's modulus) of hydrogels tested by AFM nanoindentation. The dotted horizontal line at Young's modulus of 6 KPa, is a threshold of stiffness for a normal healthy liver.

5.3.2 Cell morphology and viability

Over the 18 days differentiation period, cells remained effectively attached on the matrix as shown in Figure 5.2. The hAECs and HLCs exhibited limited growth, regardless of the substrates (cover slips, Col-PA-L and CNT-PA-L) or culture media (growth medium and hepatic induction medium) they are incubated with. When subjected to hepatic induction, hAECs gradually acquired a polygonal and granular

morphology (similar to normal hepatocytes) from the fibroblastic bipolar morphology in a time-dependent manner.

Using alamarBlue assay as a real-time indication of cell viability (Figure 5.3), hAECs and HLCs on various surface coating demonstrated slow growth and the cell number reached plateau around day 10, followed by a slight decrease. All the samples maintained comparable cell growth until day 13. Statistically significant difference was obtained (1) on day 15, when HLCs on cover slips had higher cell growth than the other three samples ($P<0.01$) and (2) on day 18 when HLCs on cover slips displayed higher cell growth than both the negative control ($P<0.001$) and HLCs on CNT-PA-L ($P<0.01$).

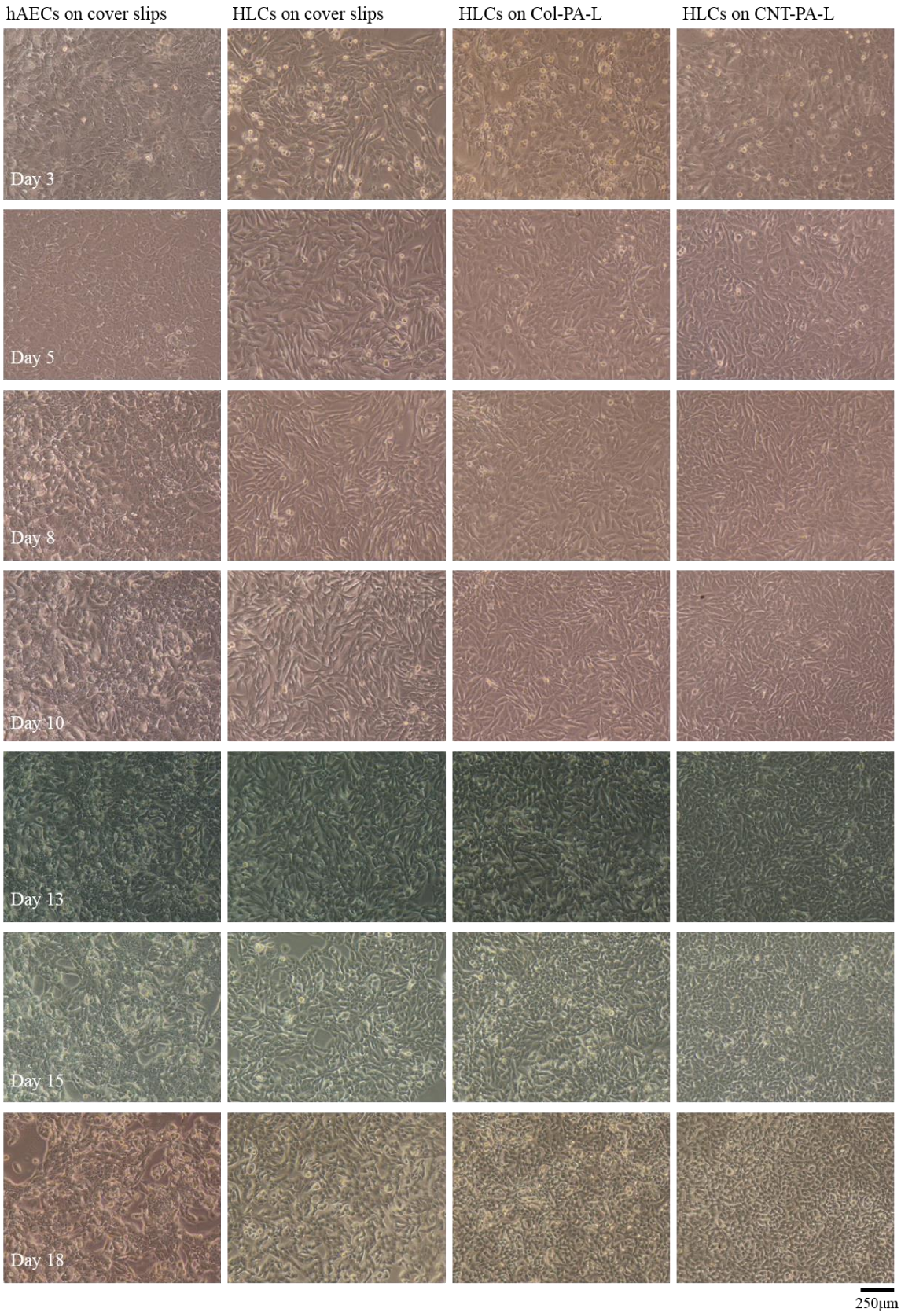

Figure 5.2 Cell morphology of hAECs and HLCs on different substrates across 18 days.

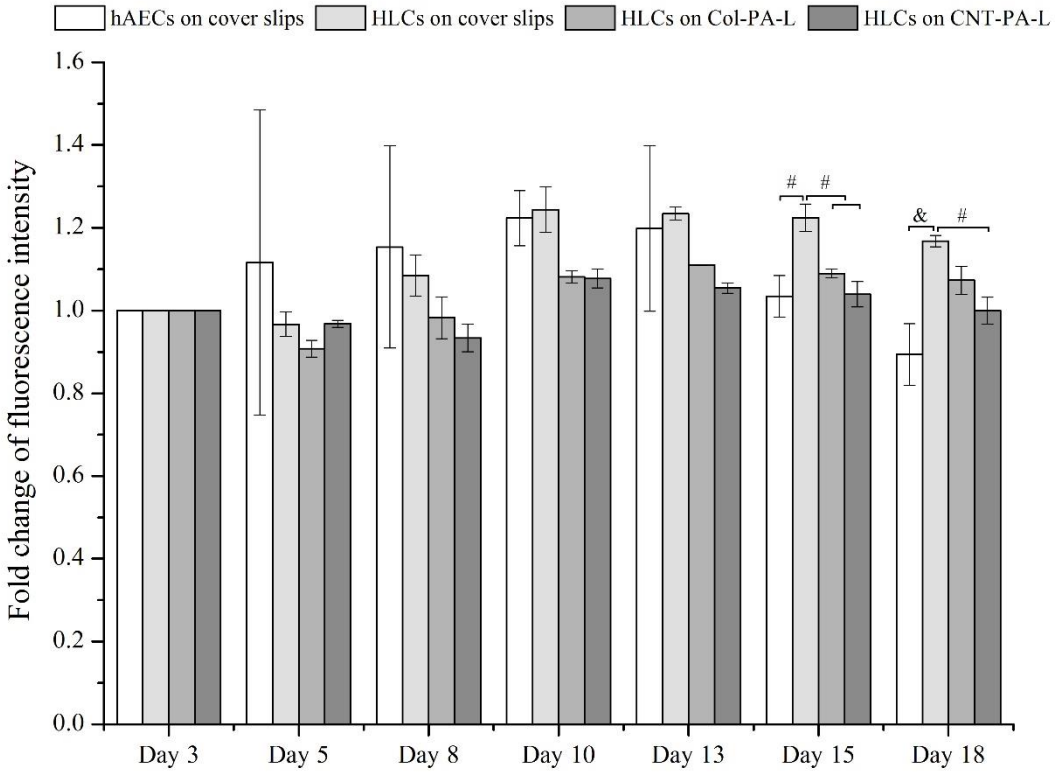

Figure 5.3 Viability of hAECs and HLCs on various substrates across 18 days as measured by alamarBlue assay, n=3. One-way ANOVA was used for statistical analysis, #=P<0.01, &=P<0.001.

5.3.3 RT-PCR

In order to assess the commitment of the treated hAECs towards hepatogenesis, transcript levels of genes representative of stem cell pluripotency, liver development and hepatic functions were measured using RT-PCR at the end of the 18 days differentiation protocol. As shown in Figure 5.4, transcriptional levels of Nodal, Nanog and OCT4 in all HLCs groups were significantly decreased compared to the negative control (non-induced hAECs on cover slips) (P<0.05). This observation was comparable to the positive controls of HepG2 and HepaRG cells as hepatocytic lineages.

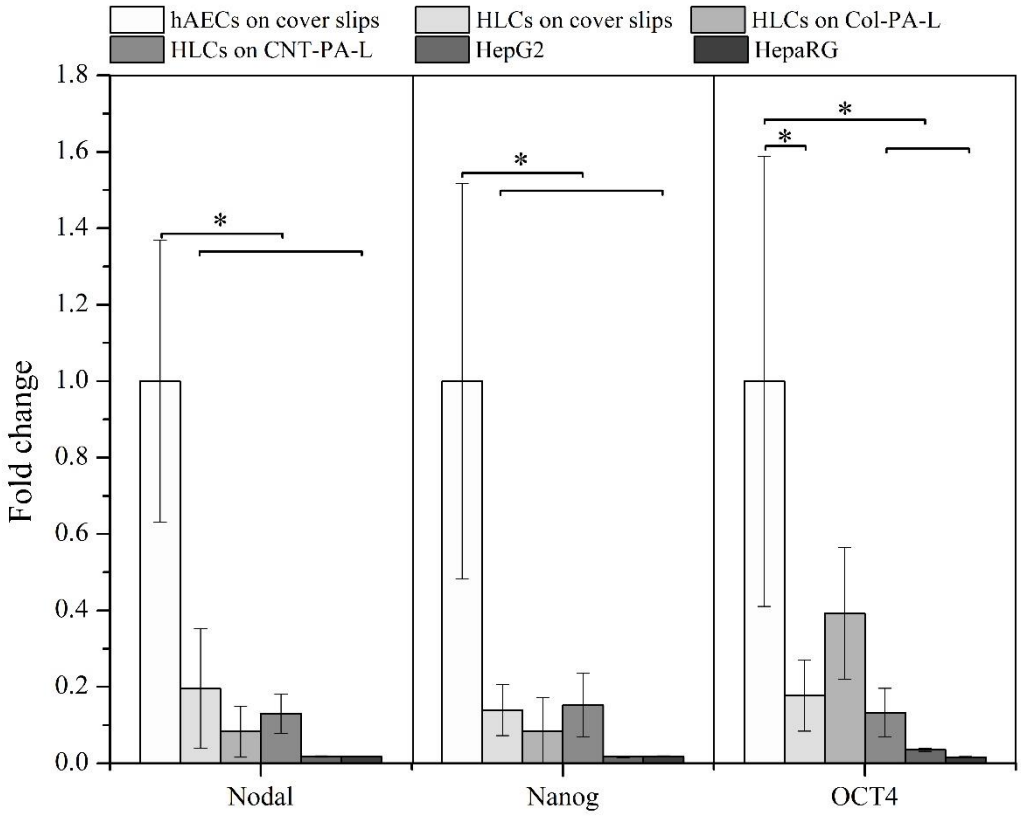

Figure 5.4 Expression of pluripotent markers by hAECs, HLCs on different scaffolds, HepG2 and HepaRG cells by RT-PCR analysis, n=3. One-way ANOVA was used for statistical analysis, *=P<0.05.

In terms of hepatocytic phenotype, compared to the negative control, the level of AFP expression was slightly higher in the HLCs on cover slips and Col-PA-L while the level was 20-fold higher in the HLCs on CNT-PA-L albeit no statistically significant difference was observed (Figure 5.5A). HepG2 cells expressed thousand-fold higher level of AFP, which was significantly higher than any other sample, including HepaRG (P<0.001). As for ALB (Figure 5.5B), hepatic induction condition failed to up-regulate its expression in HLCs on cover slips, but significantly improved ALB expression by 3-fold on Col-PA-L (P<0.01) compared with the negative control. Moreover, the

expression of ALB in HLCs on CNT-PA-L was significantly elevated by 50-fold as compared to negative control and by 45-fold as compared to Col-PA-L (P<0.01). The expressed ALB levels in HepG2 and HepaRG cells were much higher than that in the hAEC-derived hepatocytes (P<0.05). Likewise, Figure 5.5C and D showed that the levels of HNF4α and α1AT marginally increased in HLCs on cover slips and Col-PA-L. This level of induction was more pronounced in the case of CNT-PA-L as the scaffold in spite of non-significant difference compared to the negative control. Notably, the HNF4α level on CNT-PA-L was comparable with that of HepaRG cells. The mRNA expression level of glucose-6-phosphatase (G6P) was slightly up-regulated in HLCs on cover slips without any statistically significant difference to the negative control, whereas Col-PA-L boosted G6P expression in HLCs with significantly higher level in comparison with the negative control (Figure 5.5E). Compare to Col-PA-L, CNT-PA-L significantly up-regulated G6P expression in HLCs (P<0.05), and the level was even significantly higher than that in HepG2 and HepaRG cells (P<0.05). Specifically, the HLCs on CNT-PA-L displayed 250-fold higher level of G6P than HepG2 and HepaRG cells. Again, the HLCs on CNT-PA-L exhibited the significantly higher level of CK18 than the rest samples, including the positive controls (P<0.01, Figure 5.5F). Similarly, HLCs on CNT-PA-L gained significantly higher production levels of hepatic enzyme markers of CYP3A4 and CYP2C9 when compared to all the other samples (P<0.05, Figure 5.5G and H). These levels were even hundred times higher than that in HepG2 and HepaRG cells. HLCs on Col-PA-L revealed the second highest expression level of CYP3A4 and CYP2C9, which was significantly higher than that in the negative control

(P<0.05). Again, the expression of CYP3A4 and CYP2C9 in HLCs on cover slips was slightly increased without any statistically significant difference compared to negative control.

To sum up, RT-PCR results revealed an unequivocally higher expression levels of AFP, ALB, α1AT and HNF4α in HLCs on CNT-PA-L compared to negative control and HLCs on cover slips and Col-PA-L, although the levels were lower than that in HepG2 or HepaRG cells. Moreover, the expression levels of other classical hepatocyte biomarkers such as CK18, G6P, CYP3A4 and CYP2C9 in HLCs on CNT-PA-L were the highest among all groups, including the positive controls (Figure 5.5).

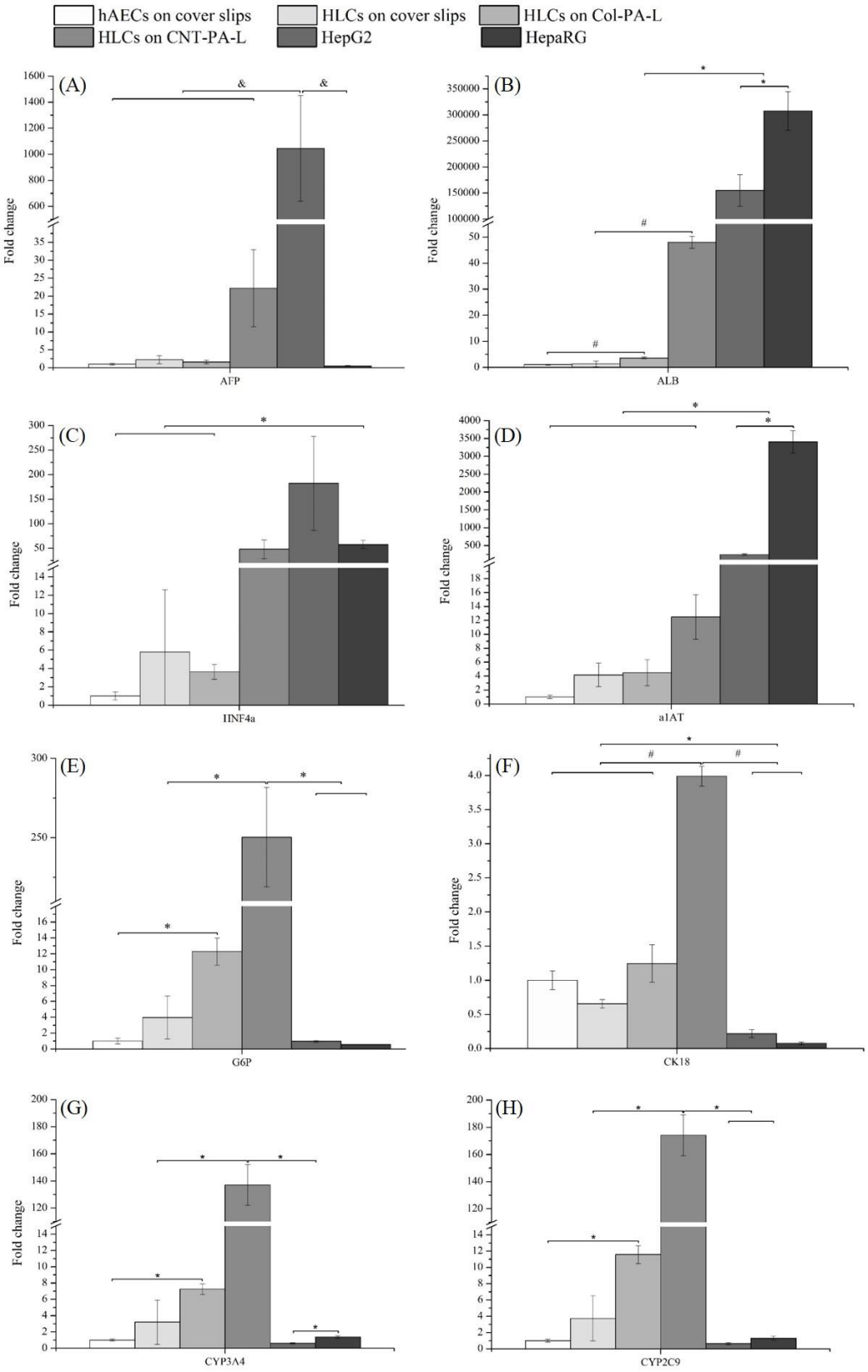

Figure 5.5 Expression of hepatic markers including (A) AFP, (B) ALB, (C) HNF4α, (D) α1AT, (E) G6P, (F) CK18, (G) CYP3A4 and (H) CYP2C9 in hAECs, HLCs on different substrates, HepG2 and HepaRG cells by RT-PCR analysis, n=3. One-way ANOVA was used for statistical analysis, *=P<0.05, #=P<0.01, &=P<0.001.

5.3.4 Immunostaining

The extent of hepatic differentiation of HLCs as observed from transcript analysis was further corroborated by immunofluorescence imaging of pluripotent and hepatic markers. DAPI staining indicate the presence of nuclei to help in enumeration of cells, while HepG2 cells were included as a positive control.

Overall, weak OCT4 protein staining was seen in all samples. This result indicated pronounced loss of pluripotency in hAECs and HLCs, which was similar to HepG2 cells (Figure 5.6A). Shown from Figure 5.6B, minimal AFP staining was observed in the hAECs and HLCs on cover slips. In contrast, there was a small fraction of HLCs positively stained on Col-PA-L, which was comparable with the staining in HepG2 cells. As compared to the rest samples, a larger fraction of HLCs on CNT-PA-L was positive for AFP staining. Figure 5.6C illustrated strongly positive expression of ALB in HLCs on CNT-PA-L while the ALB staining in the rest samples, including HepG2 cells, was negligible. Additionally, hAECs and HLCs on cover slips showed weakly positive staining of HNF4α protein. Relatively more HNF4α positive cells were obtained in HLCs on Col-PA-L and CNT-PA-L, while HepG2 cells possessed strongest staining of HNF4α protein which was localized to the nuclei (Figure 5.6D). The semi-quantitative average fluorescence intensity of various proteins per cell area was shown in supplementary data Figure 5.6E. In all, the immunostaining substantiated the results from RT-PCR.

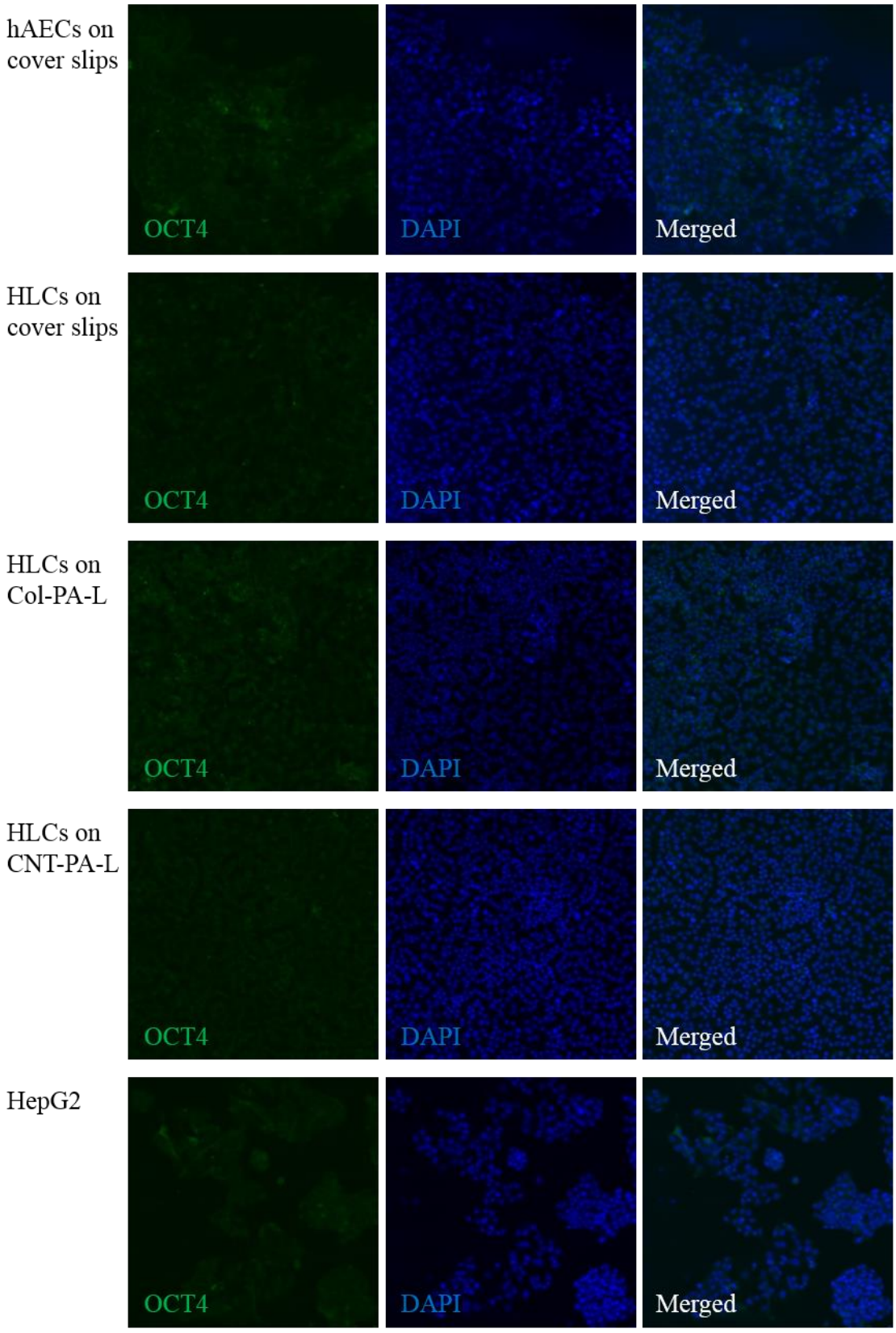
hAECs on cover slips
OCT4
DAPI
Merged
HLCs on cover slips
OCT4
DAPI
Merged
HLCs on Col-PA-L
OCT4
DAPI
Merged
HLCs on CNT-PA-L
OCT4
DAPI
Merged
HepG2
OCT4
DAPI
Merged
250μm

(A)

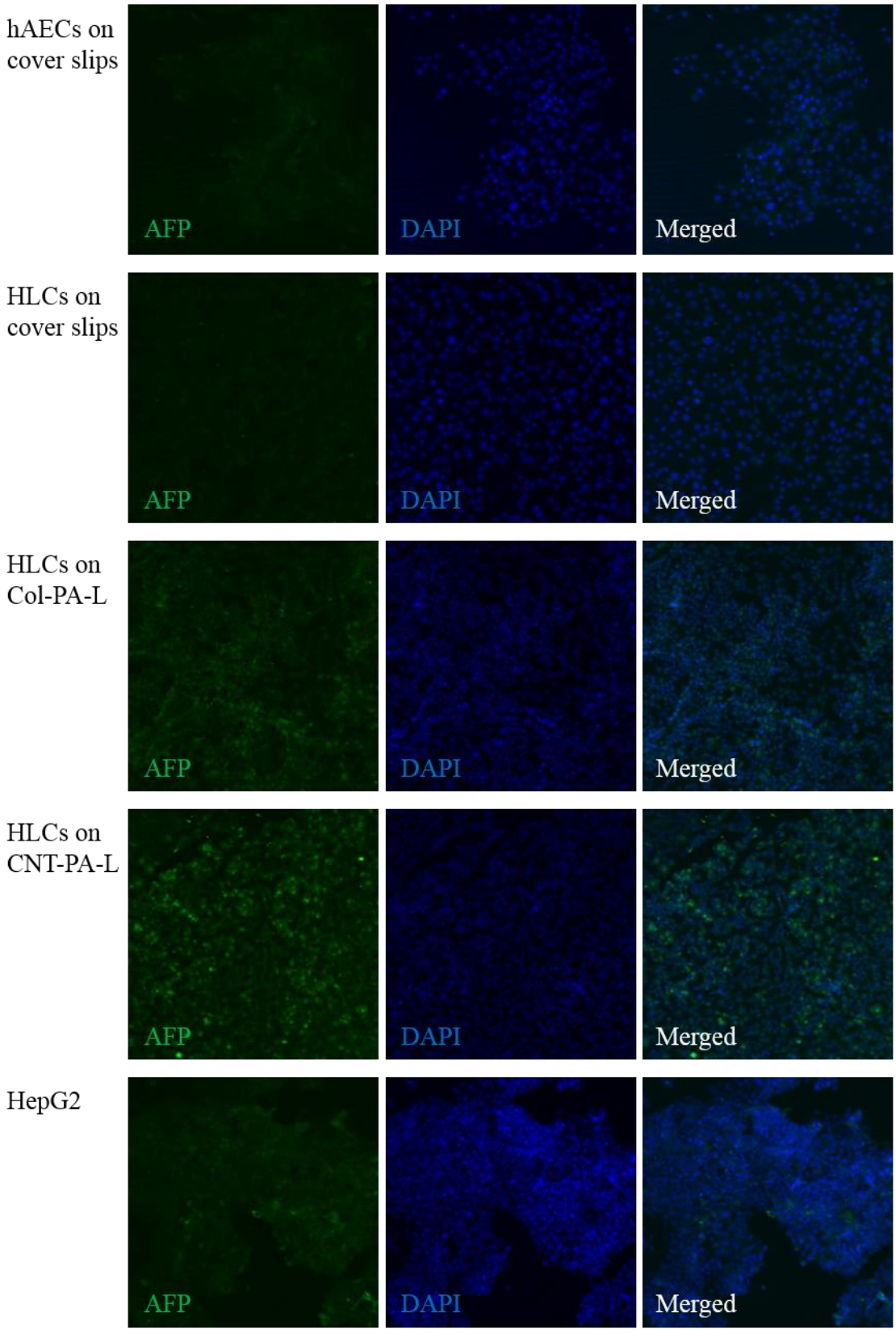
hAECs on cover slips
AFP
DAPI
Merged
HLCs on cover slips
AFP
DAPI
Merged
HLCs on Col-PA-L
AFP
DAPI
Merged
HLCs on CNT-PA-L
AFP
DAPI
Merged
HepG2
AFP
DAPI
Merged
250μm

(B)

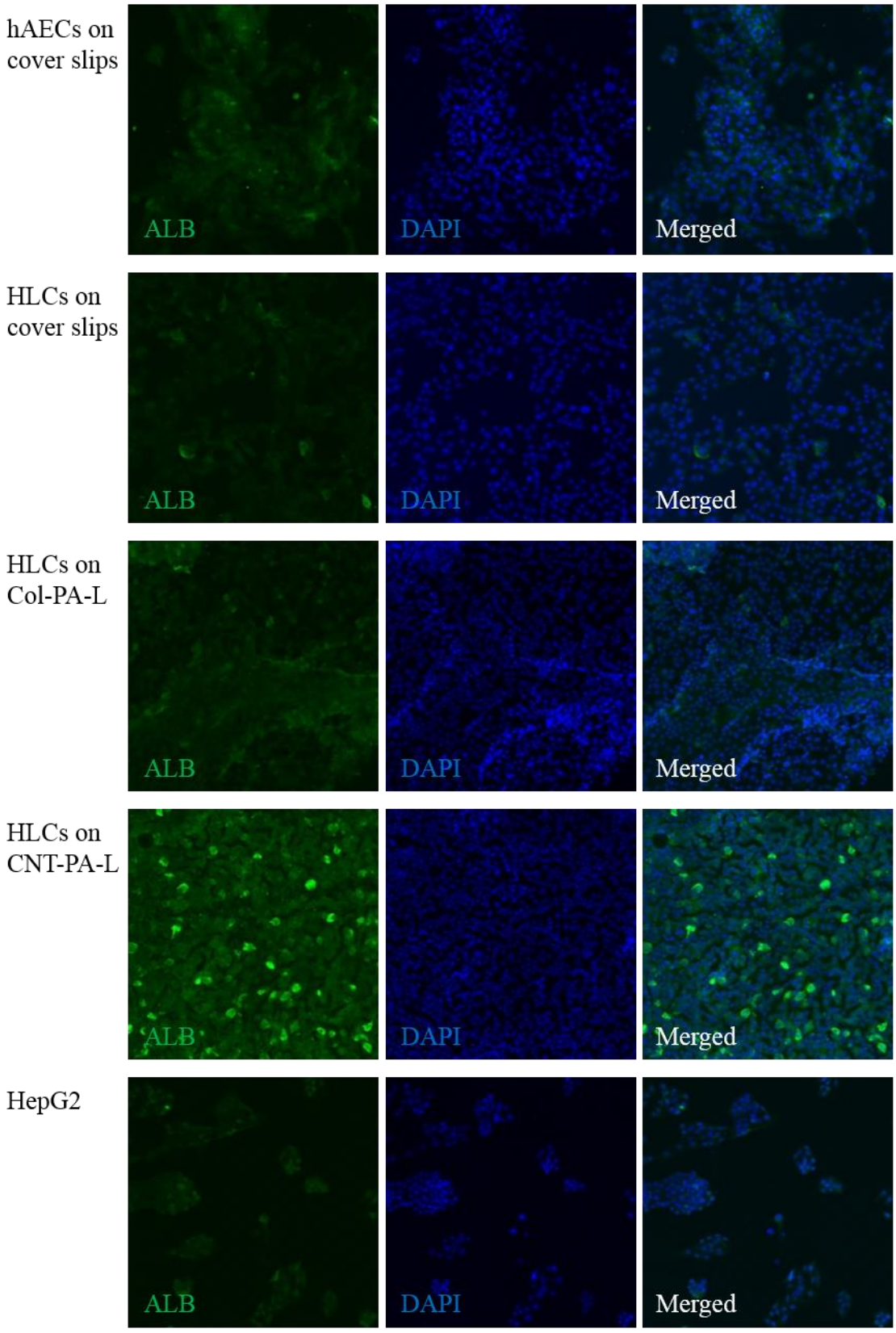
hAECs on cover slips
ALB
DAPI
Merged
HLCs on cover slips
ALB
DAPI
Merged
HLCs on Col-PA-L
ALB
DAPI
Merged
HLCs on CNT-PA-L
ALB
DAPI
Merged
HepG2
ALB
DAPI
Merged
250μm

(C)

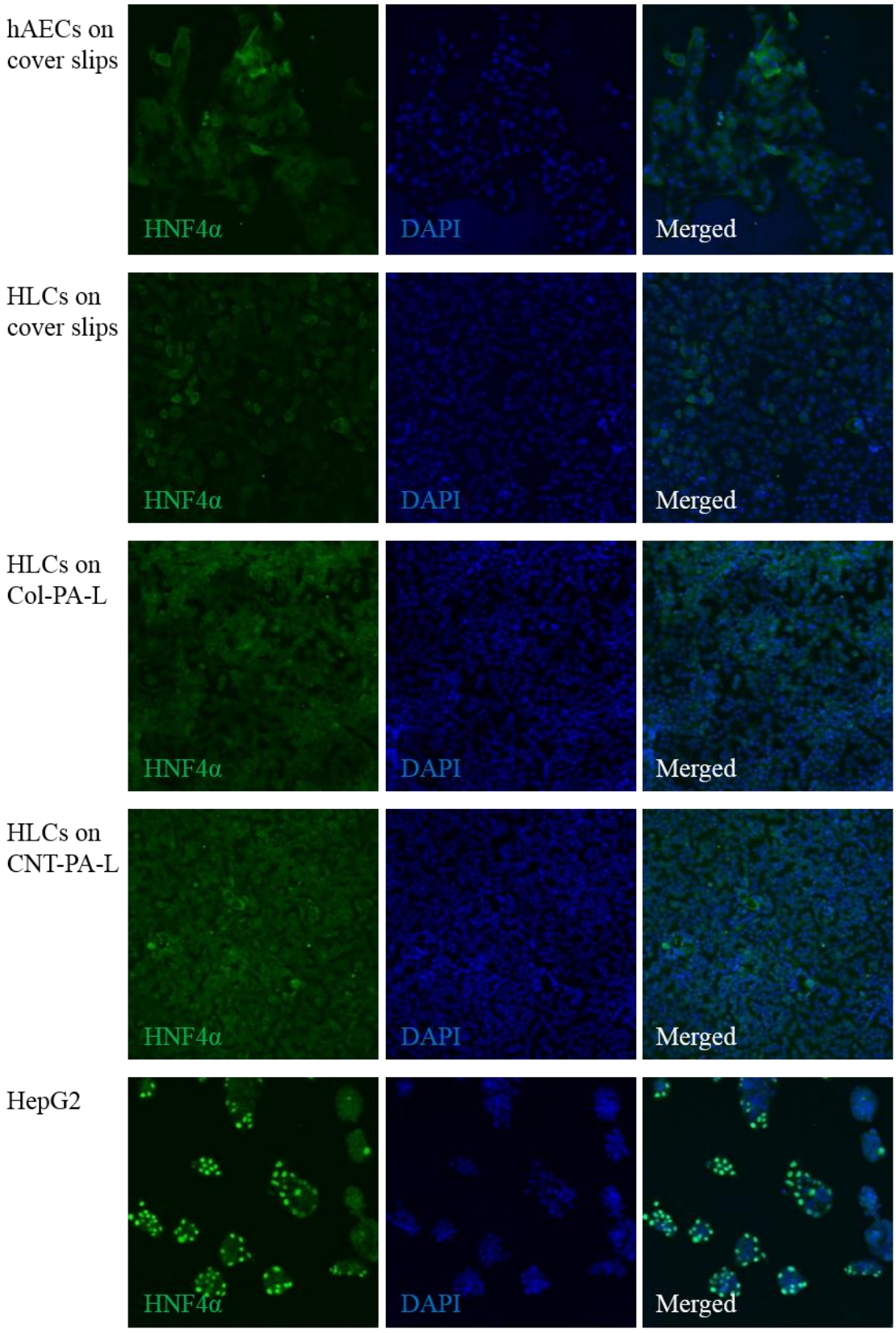
hAECs on cover slips
HLCs on cover slips
HLCs on Col-PA-L
HLCs on CNT-PA-L
HepG2
HNF4α
DAPI
Merged
250μm

(D)

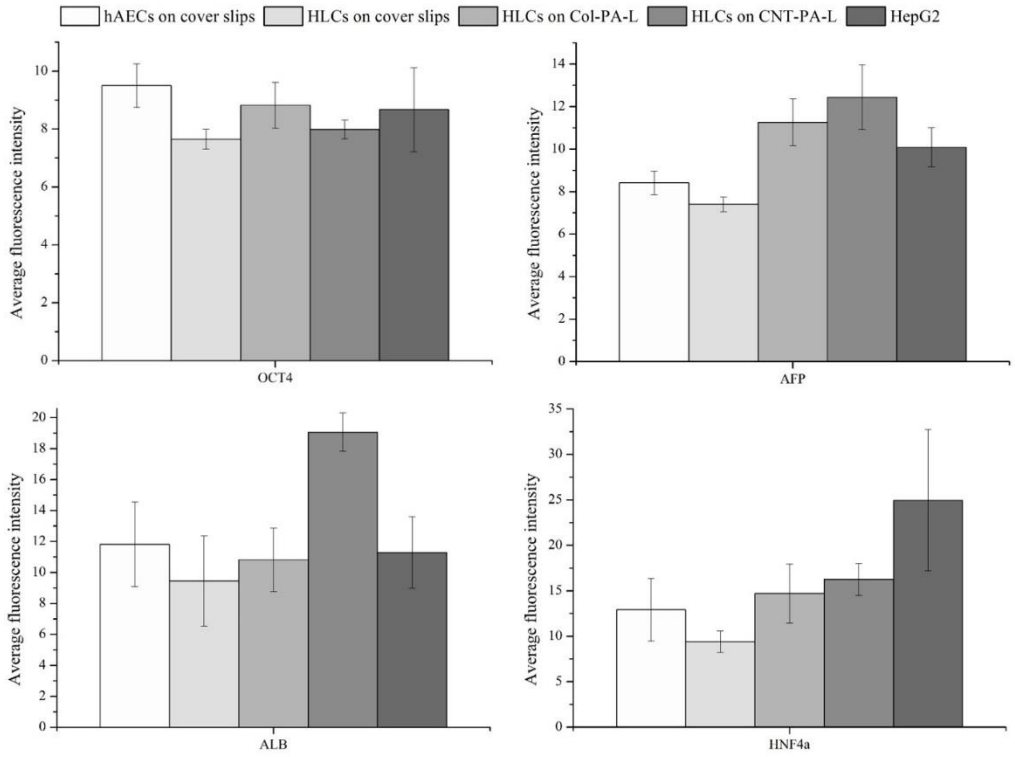

(E)

Figure 5.6 Immunostaining of hAECs, HLCs on various substrates and HepG2 cells at day 18 with (A) OCT4 (green), (B) AFP (green), (C) ALB (green), (D) HNF4α (green) and DAPI (blue), as well as (E) semi-quantitative average fluorescence intensity per cell area.

5.3.5 Hepatic function studies

5.3.5.1 ALB secretion

To analyze classical hepatic function, the secretion of ALB from treated cells into culture medium was examined by ELISA. As shown from Figure 5.7, human specific ALB produced by HLCs on Col-PA-L and CNT-PA-L was detected in cell culture supernatant from day 3 onwards, whereas the cells grown on cover slips only showed ALB production from day 5. No secreted ALB was detected in the negative control (non-induced hAECs on cover slips) throughout the 18 days incubation (data not shown), indicating that ALB secretion was only acquired in the presence of hepatic

induction medium. For the rest of the samples, a progressive increase in ALB production was observed in all HLCs, confirming the commitment towards hepatocytic lineage. Generally speaking, there was no statistically significant difference between HLCs on various scaffolds, except on day 8 when HLCs grown on hydrogels released significantly larger amount of ALB than that on cover slips (P<0.05). The peak concentration of ALB from HLCs on cover slips, Col-PA-L and CNT-PA-L normalized by cell viability (alamarBlue intensity) were 3.99±0.30 (10^{-5}ng/ml), 6.23±0.67 (10^{-5}ng/ml) and 5.74±0.90 (10^{-5}ng/ml), respectively on day 18. The corresponding level of this activity in HepG2 cells was significantly higher than hAEC-derived hepatocytes (P<0.001) and reached 40.78±1.48 (10^{-5}ng/ml).

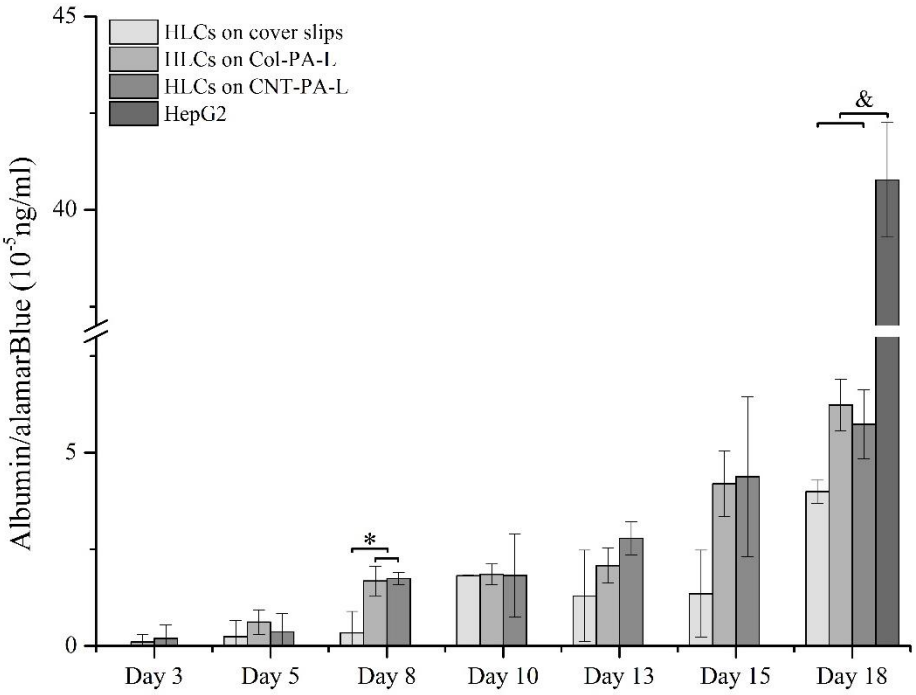

Figure 5.7 ALB secretion by HLCs on different scaffolds and HepG2 cells during the course of 18 days differentiation, n=3. One-way ANOVA was used for statistical analysis, *=P<0.05, &=P<0.001.

5.3.5.2 ICG uptake and clearance

The vital liver cell function of eliminating diverse compounds from the circulation involves an intricate balance of hepatocellular uptake, conjugation, and subsequent release of the compounds (213). ICG, used clinically for hepatic function test, is a non-toxic organic anion that is exclusively taken into mature hepatocytes through an active uptake mechanism and subsequently released with time (214, 215). Hence, ICG uptake and elimination was used to identify differentiated hepatocytes *in vitro*.

At the end of 18 days culturing, ICG-positive cells were detected in every sample after 1 hour incubation with ICG (Figure 5.8). Comparing to the negative control which was only stained with a small amount of ICG, the capacity of ICG uptake in the HLCs on cover slips, Col-PA-L and CNT-PA-L was notably higher. HLCs on CNT-PA-L most effectively took up ICG with the largest amount of cells stained intensely in green color. This uptake ability of HLCs on CNT-PA-L was higher than that observed in HepG2 cells.

After incubation with ICG free culture medium for another 6 hours, all HLCs and HepG2 cells eliminated most of the dye from the cytoplasm. On the contrary, the negative control retained ICG intracellularly, indicating their initial uptake of ICG was *via* non-specific mechanisms and they lacked the molecular machinery to mediate its efflux. Therefore, only the HLCs on cover slips, Col-PA-L and CNT-PA-L as well as HepG2 cells demonstrated the capacity of mature hepatocytes with regard to uptake and excretion of ICG with time. Again, these results confirm the enhanced hepatic function in HLCs provided by CNT-PA-L as a scaffold.

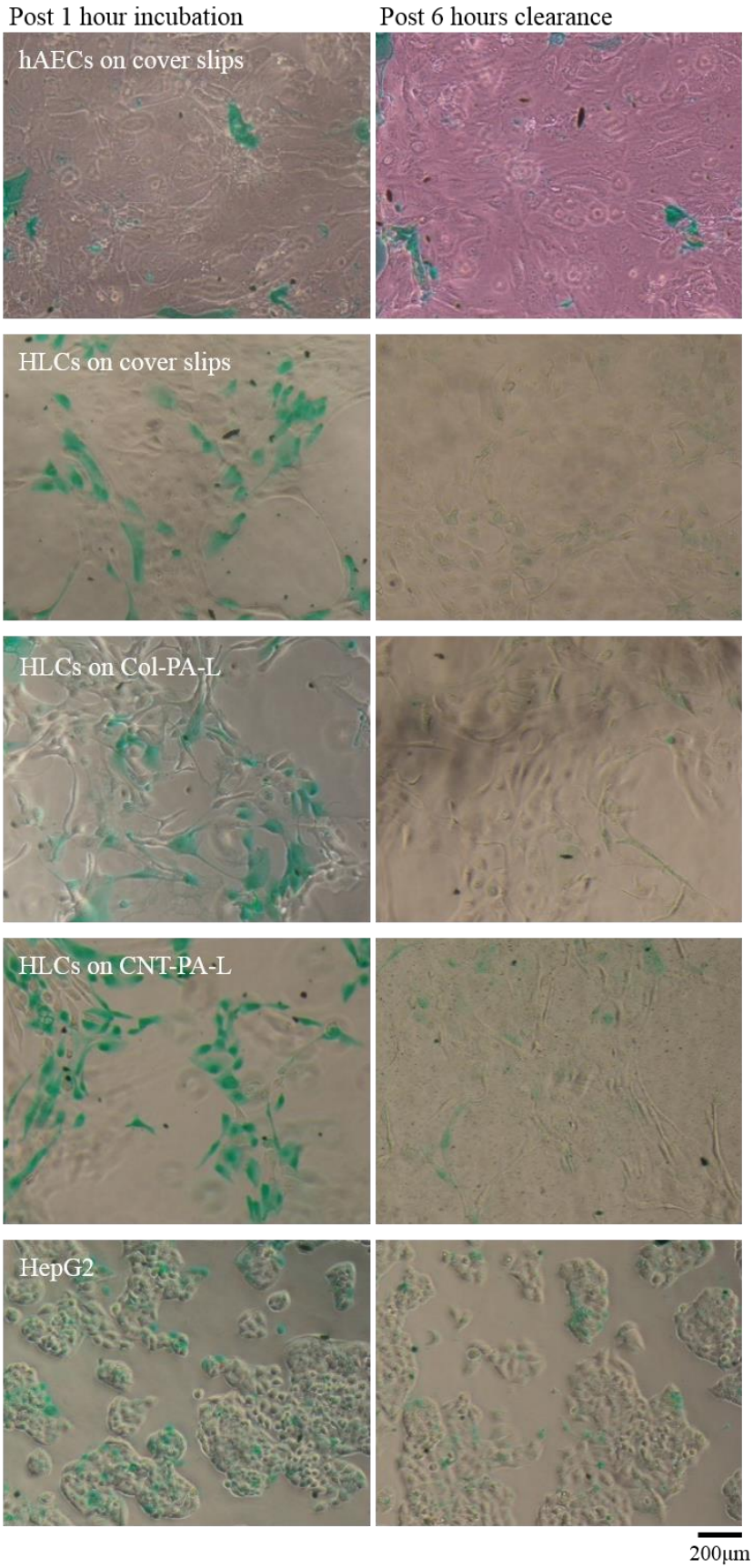

Figure 5.8 ICG uptake and clearance by hAECs, HLCs on different scaffolds and HepG2 cells.

5.3.5.3 CYP3A4 activity

Given a likely application of *ex vivo* cultured hepatocytes as diagnostic tools for evaluating drug toxicity, the key hepatic enzyme, CYP3A4, was monitored. We assayed the metabolism of Luciferin-IPA as a prototypical substrate for the enzyme. No functional CYP3A4 activity was detected in the negative control (hAECs on cover slips). The order of CYP3A4 activity found in the remaining samples was: HLCs on cover slips < HLCs on Col-PA-L < HLCs on CNT-PA-L < HepG2. (Figure 5.9). As another positive control, HepaRG cells exhibited 10 times higher CYP3A4 activity than HepG2 cells (data not shown in Figure 5.9 due in the insufficient replicates).

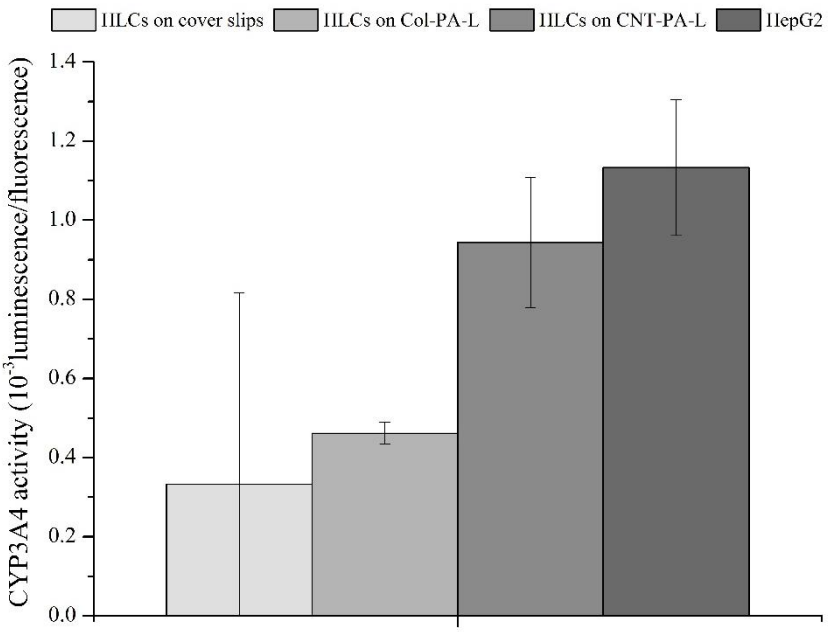

Figure 5.9 CYP3A4 activity corrected against cell viability in HLCs on different scaffolds and HepG2 cells, n=3. One-way ANOVA was used for statistical analysis.

5.3.5.4 CYP3A4 induction

The hepatic CYP3A4 is uniquely regulated by PXR transcription factor which can be induced by a variety of drugs such as rifampin, leading to accelerated metabolism (216). Therefore, the ability of CYP3A4 induction by rifampicin was monitored to assess if the HLCs obtained the key attribute of hepatocytes. In the rifampicin-treated groups, no functional CYP3A4 activity was detected in the negative control, HLCs on cover slips and on Col-PA-L. The CYP3A4 function in HLCs on CNT-PA-L was induced by rifampicin to a similar extent as that in HepG2 cells (2-fold change) without statistically significant difference (Figure 5.10). On the other hand, the CYP3A4 activity in HepaRG cells were highly induced with around 70-fold change (data not shown in Figure 5.10 due to insufficient replicates). The results of CYP3A4 and induced CYP3A4 activities (Figure 5.9 and 5.10) were in accordance with the former findings that HepaRG cells generate improved hepatic functions including major CYP enzymes involved in drug metabolism compared to HepG2, which is a hepatoblastoma cell line and does not carry high level of metabolic capacity (217).

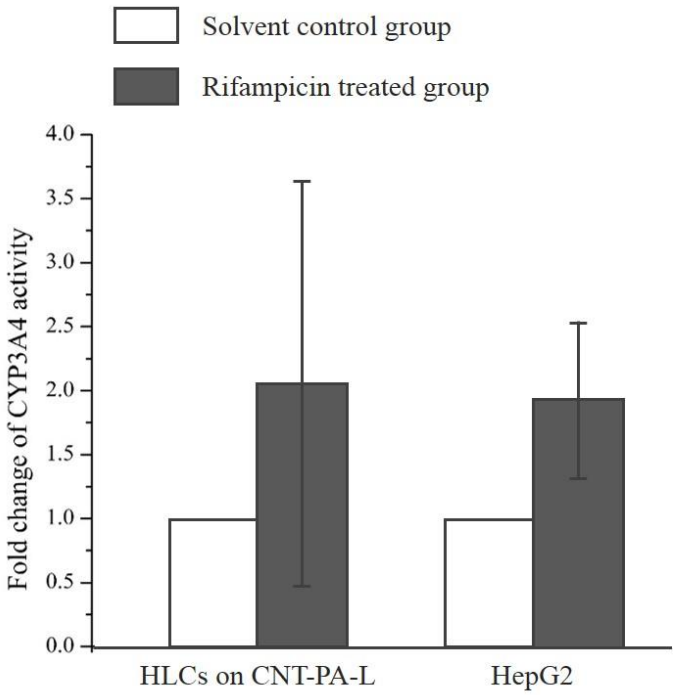

Figure 5.10 Induction of CYP3A4 enzyme activity by rifampicin in HLCs on CNT-PA-L and HepG2 cells, n=3. The two-tailed unpaired student's *t* test was used for statistical analysis.

Together, this study firstly confirmed the successful preparation of CNT-PA-L matrix with a customized stiffness mimicking that of a normal liver. Secondly, when treated with hepatic differentiation medium, hAECs on cover slips partially differentiated into HLCs by losing their stem cell phenotype and acquiring a hepatocytic phenotype in terms of cell morphology, mRNA signature, protein expression and functional characteristics. Thirdly, compared to cover slips, Col-PA-L enhanced the hepatic differentiation of hAECs with better performance in up-regulating hepatic genes and protein expression as well as hepatic function. Lastly, CNT-PA-L were superior to existing matrix (cover slips and Col-PA) in coaxing hAECs towards mature hepatocytes, shown by higher expression of several hepatic markers, higher ICG uptake and comparable CYP3A4 enzymatic function and CYP3A4 induction activity in

comparison with HepG2 cells. Table 5.2 summarized the observation of the characteristics of hAECs, HLCs on various substrates, HepG2 and HepaRG cells.

Table 5.2 Summary of characteristics of hAECs, HLCs on various substrates, HepG2 and HepaRG cells.

	Characteristics	hAECs on cover slips	HLCs on cover slips	HLCs on Col-PA	HLCs on CNT-PA	HepG2	HepaRG
Pluripotent genes	Nodal	Control	↓	↓	↓	↓↓	↓↓
	Nanog	Control	↓	↓	↓	↓↓	↓↓
	OCT4	Control	↓	↓	↓	↓↓	↓↓
Pluripotent protein	OCT4	Control	~	~	~	~	NA
Hepatic genes	AFP	Control	↑	↑	↑↑	↑↑↑↑	↓
	ALB	Control	~	↑	↑↑	↑↑↑↑	↑↑↑↑
	HNF4α	Control	↑	↑	↑↑	↑↑↑	↑↑
	α1AT	Control	↑	↑	↑	↑↑↑	↑↑↑↑
	G6P	Control	↑	↑↑	↑↑↑	~	↓
	CK18	Control	↓	~	↑	↓	↓↓
	CYP3A4	Control	↑	↑	↑↑↑	↓	↑
	CYP2C9	Control	↑	↑↑	↑↑↑	↓	↑
Hepatic proteins	AFP	Control	~	↑	↑↑	↑	NA
	ALB	Control	~	~	↓	~	NA
	HNF4α	Control	↓	↑	↑	↑↑	NA
Hepatic functions	ALB secretion	NA	↑	↑↑	↑↑	↑↑↑	NA
	ICG uptake	Control	↑	↑	↑↑	↑	NA
	CYP3A4 activity	NA	↑	↑	↑	↑	↑↑
	CYP3A4 induction	NA	NA	NA	↑	↑	↑↑

↓=decreased, ↑=increased, ~=no change, NA=not applicable

5.4 Discussion

In this study, we explored CNT-PA-L influence on hepatic differentiation of hAECs, with the aim to maximize the potential of this readily available stem cell type. Critical to our hypothesis was that (1) PA could tailor the matrix stiffness close to that of a normal human liver; (2) PEG-CNTs as a coating material resulted in a nanostructure surface, which mimicked the native ECM in liver. When put together, the crux of our

findings was that CNT-PA-L worked as a remarkable scaffold that not only preserved the viability of the hAECs adhered to its surface, but also further enhanced the differentiation of hAECs to functional HLCs compared to cover slips and Col-PA-L.

Viability of all the cells was found to be good with progressive but limited growth observed over the 18 days incubation (Figure 5.3). While hAECs on cover slips initially exhibited great growth potential (until day 10), HLCs (which were incubated in hepatic medium on cover slips) had significantly higher cell growth than hAECs on day 15 ($P<0.01$) and day 18 ($P<0.001$). It is plausible that the stimulants for higher viability with prolonged incubation were likely the growth factors contained within the hepatic medium. It was reported that the hepatic inducing medium consisting of HGF and FGF promoted both growth and hepatic differentiation of adipose-derived stem cells (218). However, the focal point of interest is the differential effect of matrix, where cell viability on CNT-PA-L was the lowest among the three platforms on day 15 and day 18 ($P<0.01$ compared to HLCs on cover slips). In the absence of overt cytotoxicity as a cause of reduced viability (Figure 5.2), we speculate this to be an outcome of a trade-off between cell differentiation and growth, a phenomenon extensively reported and widely accepted (163, 164). In other words, the stimuli provided by the CNT-PA-L had committed the HLCs towards differentiation at the expense of some growth. This will be a point of evaluation for the subsequent experiments.

Accordingly, transcript profiling and immunostaining were conducted to gain insights into the spectrum of stem cell and liver signature markers at the end of the differentiation protocol. hAECs were reported to express OCT4 and Nanog, genes

known to be required for self-renewal and pluripotency (202, 219). The reduced expression of these genes characterized loss of pluripotency and early differentiation of HLCs (Figure 5.4 and 5.6, Table 5.2).

The hepatic markers evaluated in this study represented an attempt to capture the distinctive clinical functions of the liver, and also to identify the different stages during liver development. To facilitate this discussion and substantiate our hypothesis, a summary of the justification of the chosen markers is provided in the Table 5.3. Collectively, the increased expression of ALB, HNF4α, α1AT and CK18 supported that the HLCs subjected to different matrices were committed to hepatocyte differentiation. The elevation of AFP indicated a fetal liver characteristic, whereas the up-regulation of G6P, CYP3A4 and CYP2C9 suggested that the HLCs were more like mature hepatocytes.

Importantly, at both transcript and protein levels, CNT-PA-L demonstrated superior expression of all hepatic markers in HLCs compared with other matrices such as cover slips and Col-PA-L (Figure 5.5 and 5.6, Table 5.2). Moreover, CNT-PA-L coaxed these HLCs towards higher hepatic functions such as secretion of ALB, uptake and clearance of ICG, CYP3A4 and inducible CYP3A4 activities (Table 5.2). These demonstrable hepatic functions corroborated the findings obtained from transcript and protein up-regulation. Comparatively, the presence of Col-I in the matrix only supported hepatic differentiation of hAECs to limited extents with partial acquisition of hepatic markers and functions although Col-PA-L displayed better performance in the aspects of hepatic gene and protein expression as well as CYP3A4 activity than cover slips. Therefore,

the presence of PEG-CNTs enhanced the hepatic differentiation of hAECs vs. other well established matrices.

Table 5.3 Justification of the selection of gene and protein markers characterized in this study

Markers	Remarks
AFP	AFP, thought to be the fetal form of serum ALB, is a major plasma protein produced by the fetal liver. AFP possesses transport function by binding heavy metals, fatty acids, various organic drugs and other agents (220). It is also proposed that AFP is involved in the control of proliferation, embryonic differentiation, regulation of osmotic pressure, protection of developing fetus from maternal immune system (220, 221). After birth the AFP level decrease rapidly and thus AFP is used as a fetal liver marker. AFP expression in adults is often associated with hepatoma or teratoma (222), explaining why HepG2 cells expressed thousand-fold higher level of AFP compared to the negative control (Figure 5.8).
ALB	ALB, the most abundant blood plasma protein, is initially expressed in early fetal liver cells and reach the maximal level in functional adult hepatocytes (223, 224). It is essential for maintaining the osmotic pressure of blood and also acts as a plasma carrier and transport proteins. The extent of albumin biosynthesis reflects the intrinsic function of the liver.
HNF4α	HNF4α was demonstrated crucial for specification of human hepatic progenitor cells from pluripotent stem cells by establishing the expression of a network of transcriptional factors that controls the onset of hepatocyte cell fate (225, 226).
α1AT	α1AT, produced predominantly by hepatocytes, is a serum protease inhibitor. Its major physiological function is inhibition of the destructive neutrophil proteases elastase, cathepsin G, and proteinase (204, 227, 228).
CK18	The putative functions of cytokeratin in hepatocytes include cellular structure and integrity support, uptake and secretion of dyes and protein (229). The cytokeratin intermediate filament cytoskeleton of normal adult hepatocytes is composed of only CK8 and CK18 (229, 230). CK18 is weakly expressed in human hepatoblasts from the 4^{th} week of gestation and continues to be expressed until mature hepatocytes (231).
G6P	In liver, G6P catalyzes the terminal step of glycogenolysis and gluconeogenesis for the production of glucose to release into blood (232). Hepatic G6P appears in late gestation and increases rapidly after birth (233), thus it is a marker of hepatic mature differentiation.

Table 5.3 Justification of the selection of gene and protein markers characterized in this study (continued)

CYP3A4	CYP enzymes are essential for the metabolism of many medicines and endogenous compounds. CYP3A4 is the most abundant of all CYP enzymes in the liver and it is known to be involved in the metabolism of nearly 50% of all the drugs currently prescribed. CYP3A4 contributes to bile acid detoxification, the termination of action of steroid hormones, and elimination of phytochemicals in food and the majority of medicines (234, 235). Expression of this enzyme seems to be a key predictor of drug responsiveness and toxicity (236). CYP3A4 activity is absent in newborns but reaches adult levels at around one year of age (237). Therefore, it is a mature marker in hepatic development.
CYP2C9	CYP2C9 is primarily expressed in the liver, and the expression level is the second highest among CYP isoforms (238). It has been estimated that CYP2C9 is responsible for the metabolic clearance of up to 15-20% of all drugs undergoing phase I metabolism (239). Similar to CYP3A4, the level of CYP2C9 activity is very low during fetal development and increases dramatically during the first year of life after birth (240-242).

Central to our innovation is the customization of the stiffness of the PEG-CNT matrix. PA as a basement allowed us to manipulate the stiffness of the thin PEG-CNT layer without confounding cell signaling *via* direct cellular contact. The reported Young's modulus of human healthy liver was below 6 KPa (209, 210), whereas a dysfunctional liver can stiffen to 20 KPa or higher as fibrosis and cirrhosis develop (243). Increased stiffness of the ECM could be both a passive pathological process and an initiating factor for the development of liver carcinoma (244). It has been shown that the matrix stiffness can broadly impact the *in vitro* behaviors of hepatocytes. For example, compared to stiffer heparin gels (Young's modulus, 116 KPa), the softer heparin gels (11 KPa) promoted better maintenance of the hepatic phenotype in primary rat hepatocytes with higher ALB secretion and stronger immunostaining of ALB and E-cadherin (245). For these reasons, by setting the stiffness lower than 6 KPa, Col-PA-L and CNT-PA-L approximated the mechanical property of the normal liver and were

observed to enhance the hepatic differentiation of hAECs compared to cover slips.

Collagen is the most widely used ECM protein for cell culture in facilitating cell attachment, growth, differentiation, migration, and tissue morphogenesis. Col-I coated matrix (Col-PA-L), therefore, was used in this study to compare the effect of PEG-CNT coating in hAEC differentiation in to HLCs. Throughout all the investigation (acquisition of hepatic markers and function), CNT-PA-L were superior to Col-PA-L in coaxing hAECs towards mature hepatocytes (Table 5.2). This set of results followed a range of studies regarding nanomaterial-based scaffolds which have been already shown to boost the hepatic differentiation of various stem cells. For instance, when compare to substrata including Col-I, Matrigel, gelatin and fibronectin, all of which are commonly used to resemble the complex ECM, the hepatic differentiation of murine embryonic stem cells (mESCs) grown on a commercial nanofiber matrices were more dedicated into hepatic differentiation (246). Additionally, comparing to plain culture plate, a nanofiber scaffold composed of poly-L-lactic acid (PLLA) and collagen was shown to enhance hepatic differentiation of hMSCs (247) while a poly-amide nanofiber scaffold enhanced the hepatic differentiation of mMSCs (248) and hESCs (249). The enhanced hepatic differentiation was symbolized by up-regulation of hepatic markers (e.g., ALB, HNF4α and AFP) and increased hepatic functions like ALB secretion, ICG uptake and metabolic activity of the CYP enzymes. These observations imply that compared to Col-PA-L, CNT-PA-L possess the PEG-CNTs on surface and gain the potency to mimic the nanostructure in basement membrane substratum of the liver cells (46, 49), thus better facilitating the hAECs to differentiate into HLCs. Therefore, both

liver stiffness-mimicking PA and PEG-CNT coating in CNT-PA-L can synergistically instruct the enhanced differentiation of the hAECs into functional HLCs.

Previous reports described insufficient *in vitro* hepatic differentiation of hAECs, where the generated HLCs were more fetal-like rather than functional adult hepatocytes. For example, the HLCs from hAECs on culture plates possessed low transcript levels of hepatic markers, as the increase in hepatic genes was not higher than 5-fold compared to hAECs (45). Additionally, the HLCs from hAECs cultured on porcine liver-derived ECM metabolized drugs in a manner similar to fetal human hepatocytes (207). The encapsulated HLCs from hAECs in barium alginate microspheres were found to be functionally close to HepG2 cells in terms of induced CYP3A4 activity and urea synthesis (44). However, conditioned medium from HepG2 cells with potential problems in clinical application, was used in this study for hepatic differentiation of hAECs. Comparing to these reports, HLCs on CNT-PA-L in our study were more mature HLCs with high expression of hepatic genes and proteins, as well as adequately hepatic functions although they preserved fetal-liver property like AFP expression. Specifically, the transcript levels of G6P, CK18, CYP3A4 and CYP2C9, protein expression of AFP and ALB, as well as ICG uptake in HLCs on CNT-PA-L were even higher than that in the positive control (i.e., HepG2 or HepaRG cells). Moreover, CYP3A4 activity and fold change of CYP3A4 activity with rifampicin induction in the HLCs on CNT-PA-L were comparable to that of HepG2 cells. Taken together, these observations revealed that the CNT-PA-L is a conducive matrix to enhance the extent of hepatic differentiation of hAECs into functional HLCs. As far as we know, this is

the first reported study of *in vitro* stem cell-derived hepatocytes on CNT-based scaffolds.

At this stage, there remains additional characterization to ascertain if such differentiated HLCs are really capable of reproducing functions that are comparable with normal adult hepatocytes for the specific application intended. Critical hepatocytic functions such as clotting factor biosynthesis, metabolism of ammonia and bilirubin, as well as handling of xenobiotics by more Phase I and II enzymes should be established as part of the evaluation of cell maturity (34). Therefore, the functional assessment of the HLCs on CNT-PA-L would be an immediate interest for future studies.

5.5 Chapter conclusion

In this study, liver-stiffness mimicked Col-PA-L and CNT-PA-L was developed and well supported hAEC attachment, growth and hepatic differentiation. Functional HLCs derived from hAECs lost their stem cell characteristics and switched to increased expression of hepatocyte specific markers, transcription factors and functional enzymes. Moreover, HLCs demonstrated the functional capabilities of hepatocytes such as ALB secretion, uptake and clearance of ICG, CYP3A4 function and inducible CYP3A4 activities. HLCs on CNT-PA-L showed enhanced hepatic induction and were more like the functional hepatocytes compared with that on cover slips and Col-PA-L (Figure 5.11). The use of functional hepatocytes derived from hAECs may circumvent the scarcity of liver donors and offer a promising source of hepatocytes for cell therapy and tissue engineering in future. More importantly for the interest of this thesis, this work enabled us to push the limits of PEG-CNTs as a versatile material to support the maintenance and differentiation of stem cells beyond those of mesenchymal origin.

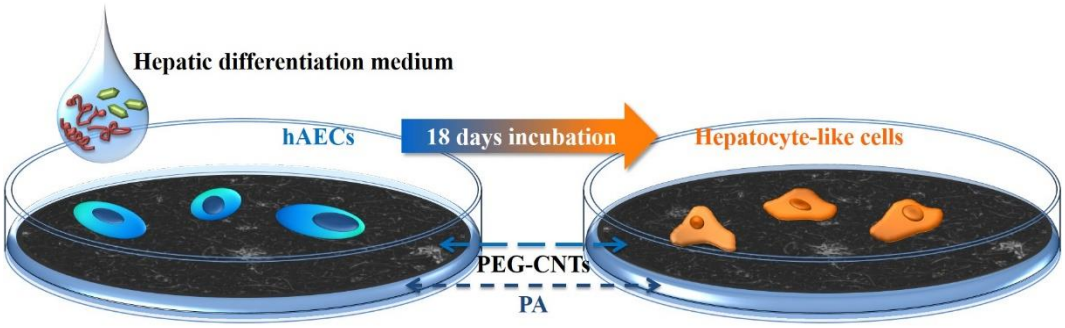

Figure 5.11 A conclusion figure for Chapter 5: CNT-PA-L enhanced the hepatic differentiation of hAECs.

CHAPTER 6. Conclusion and future perspectives

6.1 Overall conclusion

In Chapter 1, the combination of carbon nanotube (CNT)-based scaffolds and stem cells was discussed as a versatile strategy in tissue engineering. Subsequently, Chapter 2 indicated that aim of this thesis was to evaluate the versatility of polyethylene glycol-linked multi-walled carbon nanotubes (PEG-CNTs) as a coating material in enhancing the course of stem cell differentiation towards dedicated lineages under suitable conditions, specifically in skeletal muscle engineering and liver engineering.

In Chapter 3, we reported the fabrication and characterization of PEG-CNT films to support the growth and spontaneous skeletal myogenic differentiation of human mesenchymal stem cells (hMSCs). The PEG-CNT films (coated on cover slips) of around 5 μm thickness were successfully prepared with nanorange surface roughness, orderly arrangement of PEG-CNTs, high hydrophilicity and high mechanical strength. Cell viability staining and quantification demonstrated that PEG-CNT films well supported cellular adhesion and growth of hMSCs. The highlight of this study was that PEG-CNT films alone could direct the skeletal myogenic differentiation of hMSCs in the absence of myogenic inducing factors. Quantitative real-time polymerase chain reaction (RT-PCR) showed that the non-induced hMSCs plated on PEG-CNT films, compared to the negative control, presented higher levels of myogenic markers including early commitment markers of myoblast differentiation protein-1 (MyoD) and desmin, late phase marker of myosin heavy chain (MHC), as well as higher level of the skeletal muscle-specific marker, fast skeletal troponin-C (TnC) and ryanodine receptor

1 (Ryr). Moreover, the levels of these myogenic markers were higher than myogenically-induced hMSCs plated on cover slips and comparable with myogenically-induced hMSCs plated on PEG-CNT films. Corresponding protein analysis by immunoblot assays corroborated the RT-PCR results by detection of stronger expression of myogenic proteins in terms of MyoD, desmin and MHC in all hMSCs plated on PEG-CNT films. The commitment of non-induced hMSCs plated on PEG-CNT films to specific skeletal myocytes was further substantiated by the absence of enhanced adipogenic, chondrogenic and osteogenic markers. These findings strengthened the distinctive role of PEG-CNTs in the differentiation process that is non-replaceable by myogenic induction.

To optimize the physical characteristics of the PEG-CNT-based scaffold, we explored the role of matrix stiffness in myogenic differentiation of hMSCs in Chapter 4. Therein, we successfully designed, fabricated and characterized PEG-CNTs coated poly-acrylamide hydrogel (PA) with stiffness close to muscle (CNT-PA-M). Moreover, we demonstrated spontaneous myogenesis of hMSCs on CNT-PA-M and collagen-I coated PA with mimicked muscle stiffness (Col-PA-M). This study indicated new opportunities to fine-tune scaffolds in support of different types of stem cell differentiation.

We, therefore, presented a customized PEG-CNTs coated PA with mimicked liver stiffness (CNT-PA-L) to enhance hepatic differentiation of a different stem cell source, human amniotic epithelial cells (hAECs) in Chapter 5. The CNT-PA-L well supported the attachment and growth of hAECs. For the hepatic differentiation, hepatocyte-like

cells (HLCs) derived from hAECs lost their stem cell characteristics and switched to increased expression of hepatocyte specific markers, transcription factors and functional enzymes, demonstrated by RT-PCR and immunostaining assays. Moreover, HLCs demonstrated the functional capabilities of hepatocytes such as albumin (ALB) secretion, uptake and clearance of indocyanine green (ICG), CYP3A4 function and inducible CYP3A4 activities. Overall, we gathered evidence that HLCs on CNT-PA-L showed enhanced hepatic induction and resembled functional hepatocytes more closely than that on cover slips and collagen-1 coated PA with mimicked liver stiffness (Col-PA-L).

As we now conclude in Figure 6.1, PEG-CNTs work well as a versatile coating material that can maintain the *ex vivo* expansion of various stem cell types (e.g., hMSC or hAECs) and also coax them into differentiation with/without the influence of differentiation induction factors in our studies. Importantly, these findings offer an important tool of the combination of stem cells and PEG-CNT-based scaffolds in tissue engineering for innovative treatments of diseases and *in vitro* pharmacological and toxicological screening.

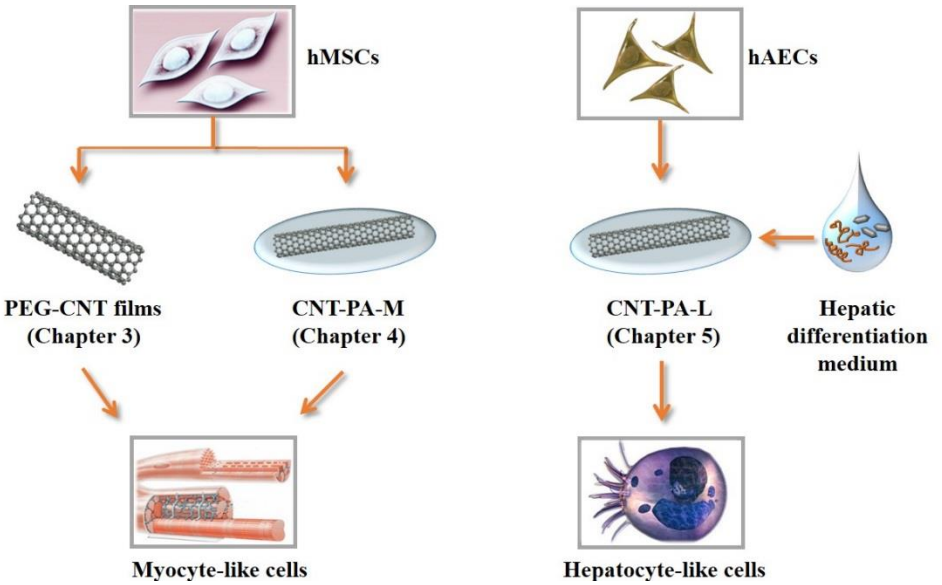

Figure 6.1 PEG-CNTs worked as a versatile coating material to coax different stem cells to differentiate into various lineages.

6.2 Future perspectives

Our current findings open new research opportunities and knowledge along a number of well-defined tangents. The specific future work was proposed in the discussion or conclusion sections of each chapter. Here we broadly discuss the future direction of PEG-CNT-based scaffold design and preparation for optimizing stem cell differentiation with promoted tissue-specific characteristics.

6.2.1 Aligned PEG-CNTs coated PA

Cells in tissues are arranged in distinct patterns. The orientation and the position of the cells with respect to each other are dictated by the tissue type (250). For instance, the skeletal muscle tissues are predominantly composed of bundles of highly oriented and dense muscle fibers, each comprising a multinucleated cell derived from myoblasts (137). In other words, skeletal muscle is composed of many muscle cells that are

aligned with one another. Meanwhile, the liver is organized into lobules which are typically hexagonal in cross section. These lobules comprise of rows of hepatocytes which orderly radiate out from a central vein.

Various studies proved that cells are affected by the topography of the surface on which they were seeded. The growth and differentiation of stem cells could also be guided by the orientation of the individual nanomaterials within the bulk matrix. Wang and colleagues demonstrated that neural progenitor cells (NPCs) could recognize the arrangement of collagen nanofibers and grew more efficiently on the aligned nanofibers than on substrates with random orientation (251). Likewise, compared with the random array of nanomaterials, the aligned poly-L-lactic acid (PLLA) nanofibers could enhance the differentiation of bone marrow stromal cells into osteocytes (252); aligned poly-caprolactone (PCL)/PLLA/nano-hydroxyapatite (HA) scaffolds increased the differentiation of human unrestricted somatic stem cells (USSCs) into bone cells (60), and the aligned CNTs exhibited enhanced proliferation and osteogenic differentiation of hMSCs (75). A possible explanation for the enhanced proliferation and differentiation of stem cells might be that ordered nanomaterials better mimic the orderly pattern of natural extracellular matrix (ECM) in which the fibers/fibrils are parallel to each other and form an arranged field to support cells (251).

To mimic the ECM arrangement in the muscle and liver, the next phase of scaffold development could involve aligned PEG-CNTs coated PA (A-CNT-PA) as a promising advancement. As a preliminary attempt at this, an electrophoretic deposition method was used for PEG-CNT alignment. We designed and fabricated an alignment setup into

a commercial optical microscope (Figure 6.2A). This design is an *in situ* observation and control on the PEG-CNT alignment. Figure 6.2B shows the real apparatus and Figure 6.2C is the design plot. This setup, easy to assemble and disassemble, is composed of two electrodes between which the distance is 1 cm, two magnets and a Teflon base. In the process of electrophoretic deposition, PEG-CNT water suspension (200 μg/ml) was loaded onto the dried glass (1 cm X 1 cm, connected to the electrodes). With the electric (alternating current, AC, 200 V, 50 Hz) and magnetic fields, the PEG-CNTs can be rotated and align along the direction of the electric field. The magnetic field introduces external Lorentz force on PEG-CNTs for vibrating and thus good dispersion of individual PEG-CNT can be achieved. Because of the structure of PEG-CNTs, the dipole moment in the direction parallel to the tube axis is significantly stronger than that in the perpendicular direction. Therefore, PEG-CNTs could be aligned along the direction of the electric field (253). After evaporation of water, aligned PEG-CNTs were deposited onto the glass as shown in Figure 6.3A.

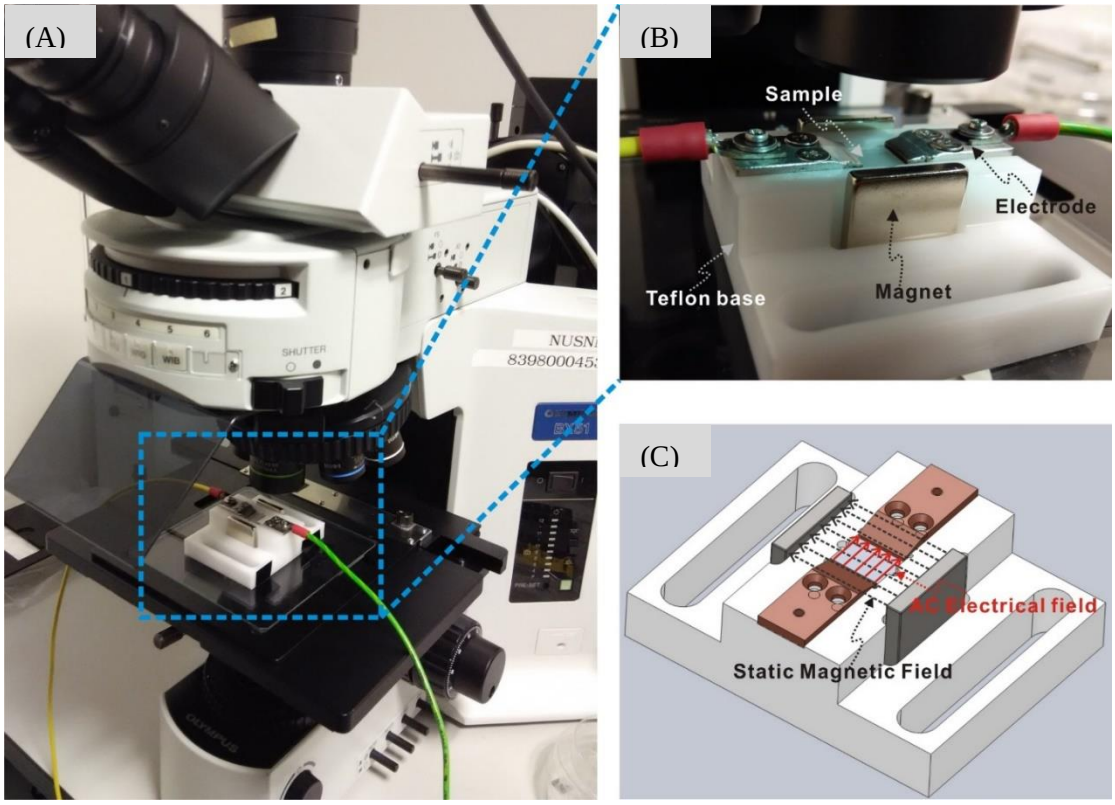

Figure 6.2 (A) A photo of the *in situ* observation setup for PEG-CNT alignment; (B) different components of the setup; (C) a design plot to show the electrical (AC) and magnetic field.

The muscle stiffness mimicked A-CNT-PA (A-CNT-PA-M) and liver stiffness mimicked A-CNT-PA (A-CNT-PA-L) were prepared according to the methods in Chapter 4 (section 4.2.1, page 56) and Chapter 5 (section 5.2, page 75), respectively, but with one of the cover slips changed into the aligned PEG-CNT deposited glass. The aligned PEG-CNTs can be easily transferred onto the PA and the stiffness difference did not affect the scaffold fabrication and surface properties (Figure 6.3B and C). SEM observation showed higher magnification images of the A-CNT-PA-M and A-CNT-PA-L (Figure 6.3 C), indicating that the alignment of PEG-CNTs only existed in microrange, not in nanoscale. Since the cell size is in microrange, cell culturing was carried out on the two scaffolds for a trial.

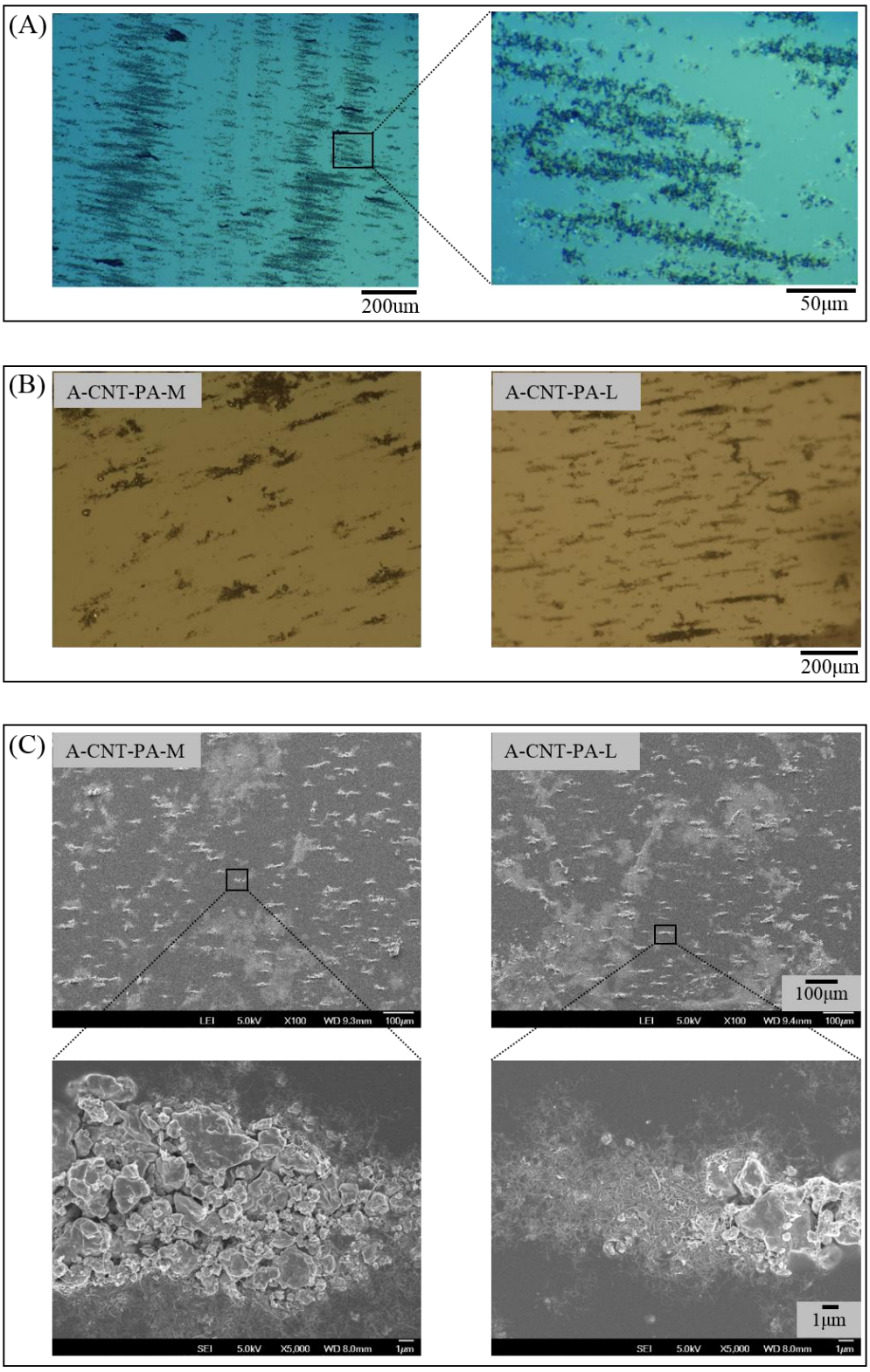

Figure 6.3 Morphology of the aligned PEG-CNTs coated surfaces. (A) Aligned PEG-CNTs coated glass; (B) optical microscope observation of A-CNT-PA-M and A-CNT-PA-L; (C) SEM images of the surfaces of A-CNT-PA-M and A-CNT-PA-L.

Non-induced hMSCs and hAECs were cultured on A-CNT-PA-M and A-CNT-PA-L in maintenance medium, respectively. The cell culturing methods were shown in Chapter 3 (section 3.2.3, page 25) and Chapter 5 (section 5.2.3, page 76), respectively. Unfortunately, neither hMSCs nor hAECs could attach onto the scaffolds (Figure 6.4). This may be because PA does not readily adsorb proteins, and thus it is essential to coat the hydrogel with PEG-CNTs to ensure efficient cell attachment (254). However, the gap between aligned PEG-CNT bundles may be too wide to support cell attachment. Therefore, denser aligned PEG-CNT bundles can be developed in future for desired cell adherence. This may be achieved by increasing the electric filed intensity or AC frequency in aligning PEG-CNTs.

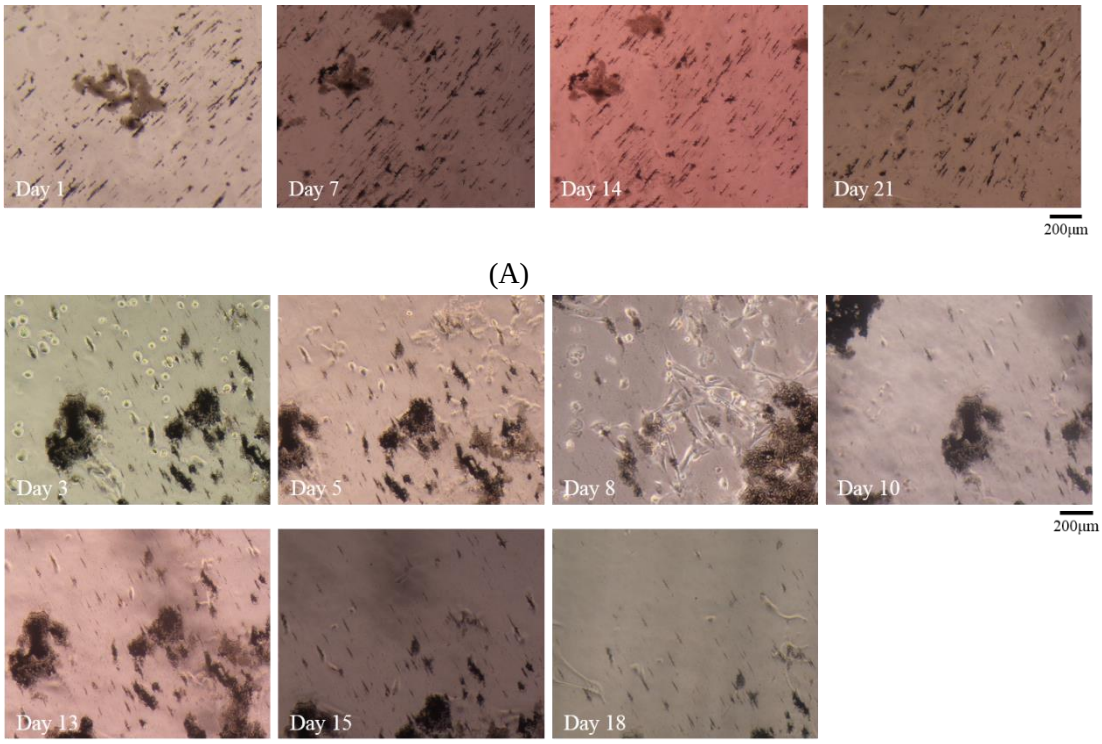

Figure 6.4 (A) hMSCs cultured on A-CNT-PA-M across 21 days; (B) hAECs cultured on A-CNT-PA-L for 18 days.

6.2.2 PEG-CNT-based 3D scaffold

Nowadays, an increasing number of researchers have questioned the validity of studying cells in two dimensional (2D) environment because all the tissues and organs, such as muscle and liver, are comprised of three dimensional (3D) arranged cells (46, 137). 2D culture surface is not physiological for cells and induced cells to lose their native characteristics and display vast difference to their *in vivo* counterparts. These drawbacks of 2D culture systems can cause alterations in cell morphology, metabolism, gene expression patterns and cellular signaling, which may compromise cellular functions (255-258). As such, 2D substrates are significantly limited in reproducing the complex cellular environment in the muscle and liver.

The benefits of 3D scaffolds in skeletal muscle engineering and liver engineering were shown in previous studies. For example, murine myoblasts (C2C12) seeded 3D collagen composite scaffolds were implanted into the defect sites in the mice skeletal muscle and the muscle healing was improved by an increased quantity of innervated and vascularized regenerated muscle fibers (128). In another study, the differentiating potential of human embryonic stem cells (hESCs) into hepatocytes on 2D collagen coated dishes and in 3D collagen scaffold culture systems was examined with exogenous growth factors to induce hepatic histogenesis (215). Although the differentiated cells in 2D and 3D culture system displayed several characteristics of hepatocytes [including expression of transthyretin, α-1-antitrypsin (α1AT), cytokeratin 8, 18, 19, tryptophan-2, 3-dioxygenase, tyrosine aminotransferase, glucose-6-phosphatase (G6P), production of alpha-fetoprotein (AFP), ALB and urea], ALB and

G6P were detected earlier and higher levels of urea and AFP were produced in 3D culture compared with 2D culture. Therefore, to further explore PEG-CNT applications in tissue engineering, a 3D scaffold with PEG-CNTs coated surface can be developed.

Beside the merits in muscle and liver engineering studied in this thesis, the combination of stem cells and PEG-CNT-based scaffolds can also be explored in other areas such as kidney, nerve, lung or skin in future. Based on the promising results obtained in this thesis, it is expected that such combination strategy will develop into an important tool in tissue engineering and benefit patients in future.

References

1. Organization WH. Human organ transplantation. Available from: http://www.who.int/transplantation/organ/en/.
2. Levey AS, Coresh J, Balk E, Kausz AT, Levin A, Steffes MW, et al. National Kidney Foundation practice guidelines for chronic kidney disease: evaluation, classification, and stratification. Annals of internal medicine. 2003;139(2):137-47.
3. Canelo MPaR. Liver Transplantation, Introduction to Organ Transplantation. 2nd ed: Imperial College Press; 2012.
4. Varun R. Kshettry VRK. Heart Transplantation, Introduction to Organ Transplantation. 2nd Edition ed: Imperial College Press; 2012. 150 p.
5. Egusa H, Sonoyama W, Nishimura M, Atsuta I, Akiyama K. Stem cells in dentistry--Part II: Clinical applications. Journal of prosthodontic research. 2012;56(4):229-48.
6. Xu ZW, Shen J. Repair of truncus arteriosus: choice of right ventricle outflow reconstruction. Journal of cardiac surgery. 2010;25(6):724-9.
7. Di Puccio F, Mattei L. Biotribology of artificial hip joints. World journal of orthopedics. 2015;6(1):77-94.
8. Chapekar MS. Tissue engineering: challenges and opportunities. Journal of biomedical materials research. 2000;53(6):617-20.
9. Boeckstyns ME. Wrist arthroplasty--a systematic review. Danish medical journal. 2014;61(5):A4834.
10. Copeland M, Kressel A, Spiera H, Hermann G, Bleiweiss IJ. Systemic inflammatory disorder related to fibrous breast capsules after silicone implant removal. Plastic and reconstructive surgery. 1993;92(6):1179-81.
11. Williams DF. On the nature of biomaterials. Biomaterials. 2009;30(30):5897-909.
12. Nerem RM. Cell-based therapies: from basic biology to replacement, repair, and regeneration. Biomaterials. 2007;28(34):5074-7.
13. Liu J, Zhou H, Weir MD, Xu HH, Chen Q, Trotman CA. Fast-degradable microbeads encapsulating human umbilical cord stem cells in alginate for muscle tissue engineering. Tissue engineering Part A. 2012;18(21-22):2303-14.
14. Ko EK, Jeong SI, Rim NG, Lee YM, Shin H, Lee BK. In vitro osteogenic differentiation of human mesenchymal stem cells and in vivo bone formation in composite nanofiber meshes. Tissue engineering Part A. 2008;14(12):2105-19.
15. Stern-Straeter J, Bonaterra GA, Juritz S, Birk R, Goessler UR, Bieback K, et al. Evaluation of the effects of different culture media on the myogenic differentiation potential of adipose tissue- or bone marrow-derived human mesenchymal stem cells. International journal of molecular medicine. 2014;33(1):160-70.
16. Zhao C, Tan A, Pastorin G, Ho HK. Nanomaterial scaffolds for stem cell proliferation and differentiation in tissue engineering. Biotechnology advances. 2013;31(5):654-68.
17. Ikada Y. Challenges in tissue engineering. Journal of the Royal Society, Interface / the Royal Society. 2006;3(10):589-601.

18. Green RM. Can we develop ethically universal embryonic stem-cell lines? Nature reviews Genetics. 2007;8(6):480-5.
19. Takahashi K, Yamanaka S. Induction of pluripotent stem cells from mouse embryonic and adult fibroblast cultures by defined factors. Cell. 2006;126(4):663-76.
20. Takahashi K, Tanabe K, Ohnuki M, Narita M, Ichisaka T, Tomoda K, et al. Induction of pluripotent stem cells from adult human fibroblasts by defined factors. Cell. 2007;131(5):861-72.
21. Yu J, Vodyanik MA, Smuga-Otto K, Antosiewicz-Bourget J, Frane JL, Tian S, et al. Induced pluripotent stem cell lines derived from human somatic cells. Science. 2007;318(5858):1917-20.
22. Knoepfler PS. Deconstructing stem cell tumorigenicity: a roadmap to safe regenerative medicine. Stem Cells. 2009;27(5):1050-6.
23. Satija NK, Singh VK, Verma YK, Gupta P, Sharma S, Afrin F, et al. Mesenchymal stem cell-based therapy: a new paradigm in regenerative medicine. Journal of cellular and molecular medicine. 2009;13(11-12):4385-402.
24. Barrilleaux B, Phinney DG, Prockop DJ, O'Connor KC. Review: ex vivo engineering of living tissues with adult stem cells. Tissue engineering. 2006;12(11):3007-19.
25. Shih DT, Lee DC, Chen SC, Tsai RY, Huang CT, Tsai CC, et al. Isolation and characterization of neurogenic mesenchymal stem cells in human scalp tissue. Stem Cells. 2005;23(7):1012-20.
26. Gage FH. Neuronal stem cells: their characterization and utilization. Neurobiology of aging. 1994;15 Suppl 2:S191.
27. Habeeb MA, Vishwakarma SK, Bardia A, Khan AA. Hepatic stem cells: A viable approach for the treatment of liver cirrhosis. World journal of stem cells. 2015;7(5):859-65.
28. Eaves CJ. Hematopoietic stem cells: concepts, definitions, and the new reality. Blood. 2015;125(17):2605-13.
29. Zhang Z, Wang X, Wang S. Isolation and characterization of mesenchymal stem cells derived from bone marrow of patients with Parkinson's disease. In vitro cellular & developmental biology Animal. 2008;44(5-6):169-77.
30. Bruno S, Camussi G. Isolation and characterization of resident mesenchymal stem cells in human glomeruli. Methods Mol Biol. 2012;879:367-80.
31. Pereira WC, Khushnooma I, Madkaikar M, Ghosh K. Reproducible methodology for the isolation of mesenchymal stem cells from human umbilical cord and its potential for cardiomyocyte generation. Journal of tissue engineering and regenerative medicine. 2008;2(7):394-9.
32. Delalat B, Pourfathollah AA, Soleimani M, Mozdarani H, Ghaemi SR, Movassaghpour AA, et al. Isolation and ex vivo expansion of human umbilical cord blood-derived CD34+ stem cells and their cotransplantation with or without mesenchymal stem cells. Hematology. 2009;14(3):125-32.
33. You S, Kublin CL, Avidan O, Miyasaki D, Zoukhri D. Isolation and propagation of mesenchymal stem cells from the lacrimal gland. Investigative ophthalmology & visual science. 2011;52(5):2087-94.

34. Dan YY. Bioengineering the artificial liver with non-hepatic cells: where are we headed? Journal of gastroenterology and hepatology. 2009;24(2):171-3.
35. Dhar M, Neilsen N, Beatty K, Eaker S, Adair H, Geiser D. Equine peripheral blood-derived mesenchymal stem cells: Isolation, identification, trilineage differentiation and effect of hyperbaric oxygen treatment. Equine veterinary journal. 2012.
36. Clarke DL, Johansson CB, Wilbertz J, Veress B, Nilsson E, Karlstrom H, et al. Generalized potential of adult neural stem cells. Science. 2000;288(5471):1660-3.
37. Oliveira JT, Almeida FM, Biancalana A, Baptista AF, Tomaz MA, Melo PA, et al. Mesenchymal stem cells in a polycaprolactone conduit enhance median-nerve regeneration, prevent decrease of creatine phosphokinase levels in muscle, and improve functional recovery in mice. Neuroscience. 2010;170(4):1295-303.
38. De Coppi P, Bartsch G, Jr., Siddiqui MM, Xu T, Santos CC, Perin L, et al. Isolation of amniotic stem cell lines with potential for therapy. Nature biotechnology. 2007;25(1):100-6.
39. Kim EY, Lee KB, Kim MK. The potential of mesenchymal stem cells derived from amniotic membrane and amniotic fluid for neuronal regenerative therapy. BMB reports. 2014;47(3):135-40.
40. Fauza D. Amniotic fluid and placental stem cells. Best practice & research Clinical obstetrics & gynaecology. 2004;18(6):877-91.
41. Petsche Connell J, Camci-Unal G, Khademhosseini A, Jacot JG. Amniotic fluid-derived stem cells for cardiovascular tissue engineering applications. Tissue engineering Part B, Reviews. 2013;19(4):368-79.
42. Shinya M, Komuro H, Saihara R, Urita Y, Kaneko M, Liu Y. Neural differentiation potential of rat amniotic epithelial cells. Fetal and pediatric pathology. 2010;29(3):133-43.
43. Jiawen S, Jianjun Z, Jiewen D, Dedong Y, Hongbo Y, Jun S, et al. Osteogenic differentiation of human amniotic epithelial cells and its application in alveolar defect restoration. Stem cells translational medicine. 2014;3(12):1504-13.
44. Vaghjiani V, Vaithilingam V, Saraswati I, Sali A, Murthi P, Kalionis B, et al. Hepatocyte-like cells derived from human amniotic epithelial cells can be encapsulated without loss of viability or function in vitro. Stem cells and development. 2014;23(8):866-76.
45. Lin JS, Zhou L, Sagayaraj A, Jumat NH, Choolani M, Chan JK, et al. Hepatic differentiation of Human Amniotic Epithelial cells and in vivo therapeutic effect on animal model of cirrhosis. Journal of gastroenterology and hepatology. 2015.
46. Gelain F, Bottai D, Vescovi A, Zhang S. Designer self-assembling peptide nanofiber scaffolds for adult mouse neural stem cell 3-dimensional cultures. PloS one. 2006;1:e119.
47. Liang D, Hsiao BS, Chu B. Functional electrospun nanofibrous scaffolds for biomedical applications. Advanced drug delivery reviews. 2007;59(14):1392-412.
48. Seyedjafari E, Soleimani M, Ghaemi N, Sarbolouki MN. Enhanced osteogenic differentiation of cord blood-derived unrestricted somatic stem cells on electrospun nanofibers. Journal of materials science Materials in medicine. 2011;22(1):165-74.

49. Abrams GA, Goodman SL, Nealey PF, Franco M, Murphy CJ. Nanoscale topography of the basement membrane underlying the corneal epithelium of the rhesus macaque. Cell and tissue research. 2000;299(1):39-46.
50. Bettinger CJ, Langer R, Borenstein JT. Engineering substrate topography at the micro- and nanoscale to control cell function. Angew Chem Int Ed Engl. 2009;48(30):5406-15.
51. Lock J, Liu H. Nanomaterials enhance osteogenic differentiation of human mesenchymal stem cells similar to a short peptide of BMP-7. International journal of nanomedicine. 2011;6:2769-77.
52. Smith LA, Liu X, Hu J, Ma PX. The enhancement of human embryonic stem cell osteogenic differentiation with nano-fibrous scaffolding. Biomaterials. 2010;31(21):5526-35.
53. Jose MV, Thomas V, Xu Y, Bellis S, Nyairo E, Dean D. Aligned bioactive multi-component nanofibrous nanocomposite scaffolds for bone tissue engineering. Macromolecular bioscience. 2010;10(4):433-44.
54. Perumcherry SR, Chennazhi KP, Nair SV, Menon D, Afeesh R. A novel method for the fabrication of fibrin-based electrospun nanofibrous scaffold for tissue-engineering applications. Tissue engineering Part C, Methods. 2011;17(11):1121-30.
55. Chen JP, Chang YS. Preparation and characterization of composite nanofibers of polycaprolactone and nanohydroxyapatite for osteogenic differentiation of mesenchymal stem cells. Colloids and surfaces B, Biointerfaces. 2011;86(1):169-75.
56. Hild N, Schneider OD, Mohn D, Luechinger NA, Koehler FM, Hofmann S, et al. Two-layer membranes of calcium phosphate/collagen/PLGA nanofibres: in vitro biomineralisation and osteogenic differentiation of human mesenchymal stem cells. Nanoscale. 2011;3(2):401-9.
57. Panzavolta S, Gioffre M, Focarete ML, Gualandi C, Foroni L, Bigi A. Electrospun gelatin nanofibers: optimization of genipin cross-linking to preserve fiber morphology after exposure to water. Acta biomaterialia. 2011;7(4):1702-9.
58. Jayakumar R, Ramachandran R, Divyarani VV, Chennazhi KP, Tamura H, Nair SV. Fabrication of chitin-chitosan/nano TiO2-composite scaffolds for tissue engineering applications. International journal of biological macromolecules. 2011;48(2):336-44.
59. Xie J, MacEwan MR, Schwartz AG, Xia Y. Electrospun nanofibers for neural tissue engineering. Nanoscale. 2010;2(1):35-44.
60. Bakhshandeh B, Soleimani M, Ghaemi N, Shabani I. Effective combination of aligned nanocomposite nanofibers and human unrestricted somatic stem cells for bone tissue engineering. Acta pharmacologica Sinica. 2011;32(5):626-36.
61. Kai D, Jin G, Prabhakaran MP, Ramakrishna S. Electrospun synthetic and natural nanofibers for regenerative medicine and stem cells. Biotechnology journal. 2013;8(1):59-72.
62. Bressan E, Carraro A, Ferroni L, Gardin C, Sbricoli L, Guazzo R, et al. Nanotechnology to drive stem cell commitment. Nanomedicine (Lond). 2013;8(3):469-86.
63. Barnes CP, Sell SA, Boland ED, Simpson DG, Bowlin GL. Nanofiber technology:

designing the next generation of tissue engineering scaffolds. Advanced drug delivery reviews. 2007;59(14):1413-33.
64. Pastorin G. Carbon Nanotubes: From Bench Chemistry to Promising Biomedical Applications. Singapore: Pan Stanford publishing Pte Ltd.; 2010.
65. Marrs B, Andrews R, Rantell T, Pienkowski D. Augmentation of acrylic bone cement with multiwall carbon nanotubes. Journal of biomedical materials research Part A. 2006;77(2):269-76.
66. Dai H. Carbon nanotubes: synthesis, integration, and properties. Accounts of chemical research. 2002;35(12):1035-44.
67. Nayak TR, Jian L, Phua LC, Ho HK, Ren Y, Pastorin G. Thin films of functionalized multiwalled carbon nanotubes as suitable scaffold materials for stem cells proliferation and bone formation. ACS nano. 2010;4(12):7717-25.
68. Kam NW, Jan E, Kotov NA. Electrical stimulation of neural stem cells mediated by humanized carbon nanotube composite made with extracellular matrix protein. Nano letters. 2009;9(1):273-8.
69. Crowder SW, Liang Y, Rath R, Park AM, Maltais S, Pintauro PN, et al. Poly(epsilon-caprolactone)-carbon nanotube composite scaffolds for enhanced cardiac differentiation of human mesenchymal stem cells. Nanomedicine (Lond). 2013;8(11):1763-76.
70. Barrientos-Duran A, Carpenter EM, Zur Nieden NI, Malinin TI, Rodriguez-Manzaneque JC, Zanello LP. Carboxyl-modified single-wall carbon nanotubes improve bone tissue formation in vitro and repair in an in vivo rat model. International journal of nanomedicine. 2014;9:4277-91.
71. Lin C, Wang Y, Lai Y, Yang W, Jiao F, Zhang H, et al. Incorporation of carboxylation multiwalled carbon nanotubes into biodegradable poly(lactic-co-glycolic acid) for bone tissue engineering. Colloids and surfaces B, Biointerfaces. 2011;83(2):367-75.
72. Xu B, Ju Y, Cui Y, Song G. Carbon nanotube array inducing osteogenic differentiation of human mesenchymal stem cells. Materials science & engineering C, Materials for biological applications. 2015;51:182-8.
73. Li X, Liu H, Niu X, Yu B, Fan Y, Feng Q, et al. The use of carbon nanotubes to induce osteogenic differentiation of human adipose-derived MSCs in vitro and ectopic bone formation in vivo. Biomaterials. 2012;33(19):4818-27.
74. Pan L, Pei X, He R, Wan Q, Wang J. Multiwall carbon nanotubes/polycaprolactone composites for bone tissue engineering application. Colloids and surfaces B, Biointerfaces. 2012;93:226-34.
75. Namgung S, Baik KY, Park J, Hong S. Controlling the growth and differentiation of human mesenchymal stem cells by the arrangement of individual carbon nanotubes. ACS nano. 2011;5(9):7383-90.
76. Ciapetti G, Granchi D, Devescovi V, Baglio SR, Leonardi E, Martini D, et al. Enhancing osteoconduction of PLLA-based nanocomposite scaffolds for bone regeneration using different biomimetic signals to MSCs. International journal of molecular sciences. 2012;13(2):2439-58.
77. Tay CY, Gu HG, Leong WS, Yu HY, Li HQ, Heng BC, et al. Cellular behavior of

human mesenchymal stem cells cultured on single-walled carbon nanotube film. Carbon. 2010;48(4):1095-104.
78. Chao TI, Xiang S, Lipstate JF, Wang C, Lu J. Poly(methacrylic acid)-grafted carbon nanotube scaffolds enhance differentiation of hESCs into neuronal cells. Adv Mater. 2010;22(32):3542-7.
79. Chao TI, Xiang S, Chen CS, Chin WC, Nelson AJ, Wang C, et al. Carbon nanotubes promote neuron differentiation from human embryonic stem cells. Biochemical and biophysical research communications. 2009;384(4):426-30.
80. Chen CS, Soni S, Le C, Biasca M, Farr E, Chen EY, et al. Human stem cell neuronal differentiation on silk-carbon nanotube composite. Nanoscale research letters. 2012;7(1):126.
81. Han IH, Sun F, Choi YJ, Zou F, Nam KH, Cho WH, et al. Cultures of Schwann-like cells differentiated from adipose-derived stem cells on PDMS/MWNT sheets as a scaffold for peripheral nerve regeneration. Journal of biomedical materials research Part A. 2015.
82. Guo JH, Liu Y, Lv ZJ, Wei WJ, Guan X, Guan QL, et al. Potential Neurogenesis of Human Adipose-Derived Stem Cells on Electrospun Catalpol-Loaded Composite Nanofibrous Scaffolds. Annals of biomedical engineering. 2015.
83. Kim T, Sridharan I, Zhu B, Orgel J, Wang R. Effect of CNT on collagen fiber structure, stiffness assembly kinetics and stem cell differentiation. Materials science & engineering C, Materials for biological applications. 2015;49:281-9.
84. Lee JH, Lee JY, Yang SH, Lee EJ, Kim HW. Carbon nanotube-collagen three-dimensional culture of mesenchymal stem cells promotes expression of neural phenotypes and secretion of neurotrophic factors. Acta biomaterialia. 2014;10(10):4425-36.
85. Chen YS, Hsiue GH. Directing neural differentiation of mesenchymal stem cells by carboxylated multiwalled carbon nanotubes. Biomaterials. 2013;34(21):4936-44.
86. Park SY, Kang BS, Hong S. Improved neural differentiation of human mesenchymal stem cells interfaced with carbon nanotube scaffolds. Nanomedicine (Lond). 2013;8(5):715-23.
87. Wickham AM, Islam MM, Mondal D, Phopase J, Sadhu V, Tamas E, et al. Polycaprolactone-thiophene-conjugated carbon nanotube meshes as scaffolds for cardiac progenitor cells. Journal of biomedical materials research Part B, Applied biomaterials. 2014;102(7):1553-61.
88. Mooney E, Mackle JN, Blond DJ, O'Cearbhaill E, Shaw G, Blau WJ, et al. The electrical stimulation of carbon nanotubes to provide a cardiomimetic cue to MSCs. Biomaterials. 2012;33(26):6132-9.
89. Zhang JCaY. Properties and Applications of Single-, Double- and Multi-Walled Carbon Nanotubes. Available from: http://www.sigmaaldrich.com/technical-documents/articles/materials-science/single-double-multi-walled-carbon-nanotubes.html.
90. Demczyk BGW, Y.M; Cumings, J; Hetman, M; Han, W; Zettl, A; Ritchie, R.O Direct mechanical measurement of the tensile strength and elastic modulus of multiwalled carbon nanotubes. Materials Science and Engineering A. 2002;334 (1–

2):173–8.
91. Meo MR, M. Prediction of Young's modulus of single wall carbon nanotubes by molecular-mechanics-based finite element modelling. Composites Science and Technology. 2006;66 (11–12):1597–605.
92. Lam CW, James JT, McCluskey R, Arepalli S, Hunter RL. A review of carbon nanotube toxicity and assessment of potential occupational and environmental health risks. Critical reviews in toxicology. 2006;36(3):189-217.
93. Cheng C, Muller KH, Koziol KK, Skepper JN, Midgley PA, Welland ME, et al. Toxicity and imaging of multi-walled carbon nanotubes in human macrophage cells. Biomaterials. 2009;30(25):4152-60.
94. Cui D, Tian F, Coyer SR, Wang J, Pan B, Gao F, et al. Effects of antisense-myc-conjugated single-walled carbon nanotubes on HL-60 cells. Journal of nanoscience and nanotechnology. 2007;7(4-5):1639-46.
95. Lam CW, James JT, McCluskey R, Hunter RL. Pulmonary toxicity of single-wall carbon nanotubes in mice 7 and 90 days after intratracheal instillation. Toxicological sciences : an official journal of the Society of Toxicology. 2004;77(1):126-34.
96. Mooney E, Dockery P, Greiser U, Murphy M, Barron V. Carbon nanotubes and mesenchymal stem cells: biocompatibility, proliferation and differentiation. Nano letters. 2008;8(8):2137-43.
97. Esfandiary E, Valiani A, Hashemibeni B, Moradi I, Narimani M. The evaluation of toxicity of carbon nanotubes on the human adipose-derived-stem cells in-vitro. Advanced biomedical research. 2014;3:40.
98. Prato M, Kostarelos K, Bianco A. Functionalized carbon nanotubes in drug design and discovery. Accounts of chemical research. 2008;41(1):60-8.
99. Sun YP, Fu K, Lin Y, Huang W. Functionalized carbon nanotubes: properties and applications. Accounts of chemical research. 2002;35(12):1096-104.
100. Wei W, Sethuraman A, Jin C, Monteiro-Riviere NA, Narayan RJ. Biological properties of carbon nanotubes. Journal of nanoscience and nanotechnology. 2007;7(4-5):1284-97.
101. Simmons TJ, Bult J, Hashim DP, Linhardt RJ, Ajayan PM. Noncovalent functionalization as an alternative to oxidative acid treatment of single wall carbon nanotubes with applications for polymer composites. ACS nano. 2009;3(4):865-70.
102. Allen BL, Kichambare PD, Gou P, Vlasova, II, Kapralov AA, Konduru N, et al. Biodegradation of single-walled carbon nanotubes through enzymatic catalysis. Nano letters. 2008;8(11):3899-903.
103. Dumortier H, Lacotte S, Pastorin G, Marega R, Wu W, Bonifazi D, et al. Functionalized carbon nanotubes are non-cytotoxic and preserve the functionality of primary immune cells. Nano letters. 2006;6(7):1522-8.
104. Voge CM, Stegemann JP. Carbon nanotubes in neural interfacing applications. Journal of neural engineering. 2011;8(1):011001.
105. Dubey N, Bentini R, Islam I, Cao T, Castro Neto AH, Rosa V. Graphene: A Versatile Carbon-Based Material for Bone Tissue Engineering. Stem cells international. 2015;2015:804213.
106. Gu M, Liu Y, Chen T, Du F, Zhao X, Xiong C, et al. Is graphene a promising nano-

material for promoting surface modification of implants or scaffold materials in bone tissue engineering? Tissue engineering Part B, Reviews. 2014;20(5):477-91.
107. Park SY, Park J, Sim SH, Sung MG, Kim KS, Hong BH, et al. Enhanced differentiation of human neural stem cells into neurons on graphene. Adv Mater. 2011;23(36):H263-7.
108. Nayak TR, Andersen H, Makam VS, Khaw C, Bae S, Xu X, et al. Graphene for controlled and accelerated osteogenic differentiation of human mesenchymal stem cells. ACS nano. 2011;5(6):4670-8.
109. Crowder SW, Prasai D, Rath R, Balikov DA, Bae H, Bolotin KI, et al. Three-dimensional graphene foams promote osteogenic differentiation of human mesenchymal stem cells. Nanoscale. 2013;5(10):4171-6.
110. Lee TJ, Park S, Bhang SH, Yoon JK, Jo I, Jeong GJ, et al. Graphene enhances the cardiomyogenic differentiation of human embryonic stem cells. Biochemical and biophysical research communications. 2014;452(1):174-80.
111. Wang EA, Israel DI, Kelly S, Luxenberg DP. Bone morphogenetic protein-2 causes commitment and differentiation in C3H10T1/2 and 3T3 cells. Growth Factors. 1993;9(1):57-71.
112. Park JS, Yang HN, Woo DG, Jeon SY, Park KH. Chondrogenesis of human mesenchymal stem cells in fibrin constructs evaluated in vitro and in nude mouse and rabbit defects models. Biomaterials. 2011;32(6):1495-507.
113. Chen YC, Lee DC, Tsai TY, Hsiao CY, Liu JW, Kao CY, et al. Induction and regulation of differentiation in neural stem cells on ultra-nanocrystalline diamond films. Biomaterials. 2010;31(21):5575-87.
114. Li W, Guo Y, Wang H, Shi D, Liang C, Ye Z, et al. Electrospun nanofibers immobilized with collagen for neural stem cells culture. Journal of materials science Materials in medicine. 2008;19(2):847-54.
115. Prabhakaran MP, Venugopal JR, Ramakrishna S. Mesenchymal stem cell differentiation to neuronal cells on electrospun nanofibrous substrates for nerve tissue engineering. Biomaterials. 2009;30(28):4996-5003.
116. Lee KD, Kuo TK, Whang-Peng J, Chung YF, Lin CT, Chou SH, et al. In vitro hepatic differentiation of human mesenchymal stem cells. Hepatology. 2004;40(6):1275-84.
117. Chivu M, Dima SO, Stancu CI, Dobrea C, Uscatescu V, Necula LG, et al. In vitro hepatic differentiation of human bone marrow mesenchymal stem cells under differential exposure to liver-specific factors. Translational research : the journal of laboratory and clinical medicine. 2009;154(3):122-32.
118. Banas A, Yamamoto Y, Teratani T, Ochiya T. Stem cell plasticity: learning from hepatogenic differentiation strategies. Developmental dynamics : an official publication of the American Association of Anatomists. 2007;236(12):3228-41.
119. Oh S, Brammer KS, Li YS, Teng D, Engler AJ, Chien S, et al. Stem cell fate dictated solely by altered nanotube dimension. Proceedings of the National Academy of Sciences of the United States of America. 2009;106(7):2130-5.
120. Lee MR, Kwon KW, Jung H, Kim HN, Suh KY, Kim K, et al. Direct differentiation of human embryonic stem cells into selective neurons on nanoscale ridge/groove

pattern arrays. Biomaterials. 2010;31(15):4360-6.
121. Huang C, Dai J, Zhang XA. Environmental physical cues determine the lineage specification of mesenchymal stem cells. Biochimica et biophysica acta. 2015;1850(6):1261-6.
122. Zhao B, Hu H, Yu A, Perea D, Haddon RC. Synthesis and characterization of water soluble single-walled carbon nanotube graft copolymers. Journal of the American Chemical Society. 2005;127(22):8197-203.
123. McKeon-Fischer KD, Flagg DH, Freeman JW. Coaxial electrospun poly(epsilon-caprolactone), multiwalled carbon nanotubes, and polyacrylic acid/polyvinyl alcohol scaffold for skeletal muscle tissue engineering. Journal of biomedical materials research Part A. 2011;99(3):493-9.
124. Ahadian S, Ramon-Azcon J, Estili M, Liang X, Ostrovidov S, Shiku H, et al. Hybrid hydrogels containing vertically aligned carbon nanotubes with anisotropic electrical conductivity for muscle myofiber fabrication. Scientific reports. 2014;4:4271.
125. Badylak SF. Regenerative medicine and developmental biology: the role of the extracellular matrix. Anatomical record Part B, New anatomist. 2005;287(1):36-41.
126. Guyton AC HJ. Textbook of Medical Physiology. 11th ed. Philadelphia: Elsevier Saunders 2006.
127. Egusa H, Kobayashi M, Matsumoto T, Sasaki J, Uraguchi S, Yatani H. Application of cyclic strain for accelerated skeletal myogenic differentiation of mouse bone marrow-derived mesenchymal stromal cells with cell alignment. Tissue engineering Part A. 2013;19(5-6):770-82.
128. Ma J, Holden K, Zhu J, Pan H, Li Y. The application of three-dimensional collagen-scaffolds seeded with myoblasts to repair skeletal muscle defects. Journal of biomedicine & biotechnology. 2011;2011:812135.
129. Kaariainen M, Kauhanen S. Skeletal muscle injury and repair: the effect of disuse and denervation on muscle and clinical relevance in pedicled and free muscle flaps. Journal of reconstructive microsurgery. 2012;28(9):581-7.
130. Riboldi SA, Sampaolesi M, Neuenschwander P, Cossu G, Mantero S. Electrospun degradable polyesterurethane membranes: potential scaffolds for skeletal muscle tissue engineering. Biomaterials. 2005;26(22):4606-15.
131. Saladin K. Anatomy & Physiology: The Unity of Form and Function (6th ed.). New York: McGraw-Hill; 2012.
132. De Bari C, Dell'Accio F, Vandenabeele F, Vermeesch JR, Raymackers JM, Luyten FP. Skeletal muscle repair by adult human mesenchymal stem cells from synovial membrane. The Journal of cell biology. 2003;160(6):909-18.
133. Hill M, Wernig A, Goldspink G. Muscle satellite (stem) cell activation during local tissue injury and repair. Journal of anatomy. 2003;203(1):89-99.
134. Li Y, Huard J. Differentiation of muscle-derived cells into myofibroblasts in injured skeletal muscle. The American journal of pathology. 2002;161(3):895-907.
135. Koning M, Harmsen MC, van Luyn MJ, Werker PM. Current opportunities and challenges in skeletal muscle tissue engineering. Journal of tissue engineering and regenerative medicine. 2009;3(6):407-15.
136. Kuang S, Gillespie MA, Rudnicki MA. Niche regulation of muscle satellite cell

self-renewal and differentiation. Cell stem cell. 2008;2(1):22-31.
137. Bach AD, Beier JP, Stern-Staeter J, Horch RE. Skeletal muscle tissue engineering. Journal of cellular and molecular medicine. 2004;8(4):413-22.
138. Dezawa M, Ishikawa H, Itokazu Y, Yoshihara T, Hoshino M, Takeda S, et al. Bone marrow stromal cells generate muscle cells and repair muscle degeneration. Science. 2005;309(5732):314-7.
139. Gang EJ, Jeong JA, Hong SH, Hwang SH, Kim SW, Yang IH, et al. Skeletal myogenic differentiation of mesenchymal stem cells isolated from human umbilical cord blood. Stem Cells. 2004;22(4):617-24.
140. Mohammad Hassan Heidari MN, Zinab Namjo, Reza Frahani, Abdolali Ebrahimi, Mojgan Bandepour, Zohreh Bahrami. Human Mesenchymal Stem Cells Differentiation to Skeletal Muscle cells in vitro Study. J Basic Appl Sci Res 2013;3(8):9.
141. Merrison AFA GD, Scolding NJ. Human Adult Bone Marrow-Derived Mesenchymal Stem Cells: Factors Influencing Skeletal Muscle Differentiation. J Cell Sci Ther. 2012;S4:001.
142. Bajek AD, Tomasz; Joachimiak, Romana; Spoz, Zaneta; Gagat, Maciej; Bodnar, Magdalena; Debski, Robert; Grzanka, Alina; Marszalek, Andrzej. Myogenic Differentiation of Mesenchymal Stem Cells is Induced by Striated Muscle Influences in vitro. Current Signal Transduction Therapy. 2012;Volume 7(Number 3):8.
143. Sirivisoot S, Harrison BS. Skeletal myotube formation enhanced by electrospun polyurethane carbon nanotube scaffolds. International journal of nanomedicine. 2011;6:2483-97.
144. Xu J, Xie Y, Zhang H, Ye Z, Zhang W. Fabrication of PLGA/MWNTs composite electrospun fibrous scaffolds for improved myogenic differentiation of C2C12 cells. Colloids and surfaces B, Biointerfaces. 2014;123:907-15.
145. Jaiswal RK, Jaiswal N, Bruder SP, Mbalaviele G, Marshak DR, Pittenger MF. Adult human mesenchymal stem cell differentiation to the osteogenic or adipogenic lineage is regulated by mitogen-activated protein kinase. The Journal of biological chemistry. 2000;275(13):9645-52.
146. Zhao B, Hu H, Yu A, Perea D, Haddon RC. Synthesis and characterization of water soluble single-walled carbon nanotube graft copolymers. Journal of the American Chemical Society. 2005;127(22):8197-203.
147. Engler AJ, Sen S, Sweeney HL, Discher DE. Matrix elasticity directs stem cell lineage specification. Cell. 2006;126(4):677-89.
148. Schmittgen TD, Livak KJ. Analyzing real-time PCR data by the comparative CT method. Nature protocols. 2008;3(6):1101-8.
149. Liu SQ, Tian Q, Hedrick JL, Po Hui JH, Ee PL, Yang YY. Biomimetic hydrogels for chondrogenic differentiation of human mesenchymal stem cells to neocartilage. Biomaterials. 2010;31(28):7298-307.
150. Levi B, James AW, Wan DC, Glotzbach JP, Commons GW, Longaker MT. Regulation of human adipose-derived stromal cell osteogenic differentiation by insulin-like growth factor-1 and platelet-derived growth factor-alpha. Plastic and reconstructive surgery. 2010;126(1):41-52.
151. Mohamed A. Sobh1 HIE-S, Soad A. Khalifa2, Eman H. Bakr2, Omnia K.R. El-

Sayyad2. IN VITRO COMPARATIVE STUDIES OF ADIPOCYTE STEM CELLS DERIVED FROM HUMAN ADIPOSE TISSUE AND AMNIOTIC FLUID CELLS. 2014.
152. Li X, Cai W, An J, Kim S, Nah J, Yang D, et al. Large-area synthesis of high-quality and uniform graphene films on copper foils. Science. 2009;324(5932):1312-4.
153. Lei B, Chen X, Wang Y, Zhao N, Du C, Fang L. Surface nanoscale patterning of bioactive glass to support cellular growth and differentiation. Journal of biomedical materials research Part A. 2010;94(4):1091-9.
154. Jian Yang JBaW. Improving cell affinity of poly(D,L-lactide) film modified by anhydrous ammonia plasma treatment. Polymers for Advanced Technologies. 2002;13(3-4):220–6.
155. Thomas M, Arora A, Katti DS. Surface hydrophilicity of PLGA fibers governs in vitro mineralization and osteogenic differentiation. Materials science & engineering C, Materials for biological applications. 2014;45:320-32.
156. Yang-Tse Cheng C-MC. Scaling, dimensional analysis, and indentation measurements. Materials Science and Engineering: R: Reports. 2004;Issues(4-5): 91-149.
157. Yu MF, Lourie O, Dyer MJ, Moloni K, Kelly TF, Ruoff RS. Strength and breaking mechanism of multiwalled carbon nanotubes under tensile load. Science. 2000;287(5453):637-40.
158. Treacy MM, Ebbesen, T.W., Gibson, J.M. Exceptionally high Young's modulus observed for individual carbon nanotubes. Nature. 1996; 38.
159. Yu MF, Kowalewski T, Ruoff RS. Investigation of the radial deformability of individual carbon nanotubes under controlled indentation force. Physical review letters. 2000;85(7):1456-9.
160. Moriyama QWaH. Carbon Nanotube-Based Thin Films: Synthesis and Properties. In: Yellampalli S, editor. Carbon Nanotubes - Synthesis, Characterization, Applications2011.
161. Zhu J. Bioactive modification of poly(ethylene glycol) hydrogels for tissue engineering. Biomaterials. 2010;31(17):4639-56.
162. Singh A ZJ, Ye Z, Elisseeff JH. Modular Multifunctional Poly(ethylene glycol) Hydrogels for Stem Cell Differentiation. Adv Funct Mater. 2013;23: 575–82.
163. Olbrich M, Rieger M, Reinert S, Alexander D. Isolation of osteoprogenitors from human jaw periosteal cells: a comparison of two magnetic separation methods. PloS one. 2012;7(10):e47176.
164. GM C. The Cell: A Molecular Approach. 2nd edition. . Associates SMS, editor2000.
165. Mariani E, Facchini A. Clinical applications and biosafety of human adult mesenchymal stem cells. Current pharmaceutical design. 2012;18(13):1821-45.
166. Al-Nbaheen M, Vishnubalaji R, Ali D, Bouslimi A, Al-Jassir F, Megges M, et al. Human stromal (mesenchymal) stem cells from bone marrow, adipose tissue and skin exhibit differences in molecular phenotype and differentiation potential. Stem cell reviews. 2013;9(1):32-43.
167. Wan Safwani WK, Makpol S, Sathapan S, Chua KH. The changes of stemness

biomarkers expression in human adipose-derived stem cells during long-term manipulation. Biotechnology and applied biochemistry. 2011;58(4):261-70.
168. Sartorelli V, Caretti G. Mechanisms underlying the transcriptional regulation of skeletal myogenesis. Current opinion in genetics & development. 2005;15(5):528-35.
169. Blais A, Tsikitis M, Acosta-Alvear D, Sharan R, Kluger Y, Dynlacht BD. An initial blueprint for myogenic differentiation. Genes & development. 2005;19(5):553-69.
170. Stewart JD, Masi TL, Cumming AE, Molnar GM, Wentworth BM, Sampath K, et al. Characterization of proliferating human skeletal muscle-derived cells in vitro: differential modulation of myoblast markers by TGF-beta2. Journal of cellular physiology. 2003;196(1):70-8.
171. Beier JP, Bitto FF, Lange C, Klumpp D, Arkudas A, Bleiziffer O, et al. Myogenic differentiation of mesenchymal stem cells co-cultured with primary myoblasts. Cell biology international. 2011;35(4):397-406.
172. Gahlmann R, Wade R, Gunning P, Kedes L. Differential expression of slow and fast skeletal muscle troponin C. Slow skeletal muscle troponin C is expressed in human fibroblasts. Journal of molecular biology. 1988;201(2):379-91.
173. Gang EJ, Darabi R, Bosnakovski D, Xu Z, Kamm KE, Kyba M, et al. Engraftment of mesenchymal stem cells into dystrophin-deficient mice is not accompanied by functional recovery. Experimental cell research. 2009;315(15):2624-36.
174. Wadhwa S, Rea C, O'Hare P, Mathur A, Roy SS, Dunlop PS, et al. Comparative in vitro cytotoxicity study of carbon nanotubes and titania nanostructures on human lung epithelial cells. Journal of hazardous materials. 2011;191(1-3):56-61.
175. Lee NK, Sowa H, Hinoi E, Ferron M, Ahn JD, Confavreux C, et al. Endocrine regulation of energy metabolism by the skeleton. Cell. 2007;130(3):456-69.
176. Song L, Tuan RS. Transdifferentiation potential of human mesenchymal stem cells derived from bone marrow. FASEB journal : official publication of the Federation of American Societies for Experimental Biology. 2004;18(9):980-2.
177. Merry K, Dodds R, Littlewood A, Gowen M. Expression of osteopontin mRNA by osteoclasts and osteoblasts in modelling adult human bone. Journal of cell science. 1993;104 (Pt 4):1013-20.
178. Tsai MT, Li WJ, Tuan RS, Chang WH. Modulation of osteogenesis in human mesenchymal stem cells by specific pulsed electromagnetic field stimulation. Journal of orthopaedic research : official publication of the Orthopaedic Research Society. 2009;27(9):1169-74.
179. Liu CF, Lefebvre V. The transcription factors SOX9 and SOX5/SOX6 cooperate genome-wide through super-enhancers to drive chondrogenesis. Nucleic acids research. 2015;43(17):8183-203.
180. Takahashi I, Nuckolls GH, Takahashi K, Tanaka O, Semba I, Dashner R, et al. Compressive force promotes sox9, type II collagen and aggrecan and inhibits IL-1beta expression resulting in chondrogenesis in mouse embryonic limb bud mesenchymal cells. Journal of cell science. 1998;111 (Pt 14):2067-76.
181. Nagase H, Kashiwagi M. Aggrecanases and cartilage matrix degradation. Arthritis research & therapy. 2003;5(2):94-103.
182. Baxa CA, Sha RS, Buelt MK, Smith AJ, Matarese V, Chinander LL, et al. Human

adipocyte lipid-binding protein: purification of the protein and cloning of its complementary DNA. Biochemistry. 1989;28(22):8683-90.
183. Seo JB, Moon HM, Noh MJ, Lee YS, Jeong HW, Yoo EJ, et al. Adipocyte determination- and differentiation-dependent factor 1/sterol regulatory element-binding protein 1c regulates mouse adiponectin expression. The Journal of biological chemistry. 2004;279(21):22108-17.
184. Enerback S, Ohlsson BG, Samuelsson L, Bjursell G. Characterization of the human lipoprotein lipase (LPL) promoter: evidence of two cis-regulatory regions, LP-alpha and LP-beta, of importance for the differentiation-linked induction of the LPL gene during adipogenesis. Molecular and cellular biology. 1992;12(10):4622-33.
185. Samuelsson L, Stromberg K, Vikman K, Bjursell G, Enerback S. The CCAAT/enhancer binding protein and its role in adipocyte differentiation: evidence for direct involvement in terminal adipocyte development. The EMBO journal. 1991;10(12):3787-93.
186. Gilbert PM, Havenstrite KL, Magnusson KE, Sacco A, Leonardi NA, Kraft P, et al. Substrate elasticity regulates skeletal muscle stem cell self-renewal in culture. Science. 2010;329(5995):1078-81.
187. Ghosh S, Laha M, Mondal S, Sengupta S, Kaplan DL. In vitro model of mesenchymal condensation during chondrogenic development. Biomaterials. 2009;30(33):6530-40.
188. Nam J, Johnson J, Lannutti JJ, Agarwal S. Modulation of embryonic mesenchymal progenitor cell differentiation via control over pure mechanical modulus in electrospun nanofibers. Acta biomaterialia. 2011;7(4):1516-24.
189. Woods A, Wang G, Beier F. RhoA/ROCK signaling regulates Sox9 expression and actin organization during chondrogenesis. The Journal of biological chemistry. 2005;280(12):11626-34.
190. Bai S, Han H, Huang X, Xu W, Kaplan DL, Zhu H, et al. Silk scaffolds with tunable mechanical capability for cell differentiation. Acta biomaterialia. 2015;20:22-31.
191. Tse JR, Engler AJ. Preparation of hydrogel substrates with tunable mechanical properties. Current protocols in cell biology / editorial board, Juan S Bonifacino [et al]. 2010;Chapter 10:Unit 10 6.
192. Cameron AR, Frith JE, Cooper-White JJ. The influence of substrate creep on mesenchymal stem cell behaviour and phenotype. Biomaterials. 2011;32(26):5979-93.
193. Vedula SR, Hirata H, Nai MH, Brugues A, Toyama Y, Trepat X, et al. Epithelial bridges maintain tissue integrity during collective cell migration. Nature materials. 2014;13(1):87-96.
194. Gao L, McBeath R, Chen CS. Stem cell shape regulates a chondrogenic versus myogenic fate through Rac1 and N-cadherin. Stem Cells. 2010;28(3):564-72.
195. Kim MH, Kino-oka M, Saito A, Sawa Y, Taya M. Myogenic induction of human mesenchymal stem cells by culture on dendrimer-immobilized surface with d-glucose display. Journal of bioscience and bioengineering. 2010;109(1):55-61.
196. Arnab Ghosh SG, Sukhen Das, Probal K. Das, Jonaki Mukherjee, Rajat Banerjee. Near infrared fluorescence and enhanced electrical conductivity of single walled

carbon nanotube-lead silicate glass composite. Journal of Non-Crystalline Solids 2014;385 7.
197. Michalopoulos GK, DeFrances MC. Liver regeneration. Science. 1997;276(5309):60-6.
198. Najimi MS, Fran ̧oise; Sokal, Etienne. Hepatocyte transplantation: current and future developments. Current Opinion in Organ Transplantation. 2007;12(5):503-8.
199. Miki T, Marongiu F, Dorko K, Ellis EC, Strom SC. Isolation of amniotic epithelial stem cells. Current protocols in stem cell biology. 2010;Chapter 1:Unit 1E 3.
200. Ghosh K, Kumar R, Singh J, Gahlawat SK, Kumar D, Selokar NL, et al. Buffalo (Bubalus bubalis) term amniotic-membrane-derived cells exhibited mesenchymal stem cells characteristics in vitro. In vitro cellular & developmental biology Animal. 2015.
201. Wang Q, Wu W, Han X, Zheng A, Lei S, Wu J, et al. Osteogenic differentiation of amniotic epithelial cells: synergism of pulsed electromagnetic field and biochemical stimuli. BMC musculoskeletal disorders. 2014;15:271.
202. Miki T, Lehmann T, Cai H, Stolz DB, Strom SC. Stem cell characteristics of amniotic epithelial cells. Stem Cells. 2005;23(10):1549-59.
203. Li H, Niederkorn JY, Neelam S, Mayhew E, Word RA, McCulley JP, et al. Immunosuppressive factors secreted by human amniotic epithelial cells. Investigative ophthalmology & visual science. 2005;46(3):900-7.
204. Takashima S, Ise H, Zhao P, Akaike T, Nikaido T. Human amniotic epithelial cells possess hepatocyte-like characteristics and functions. Cell structure and function. 2004;29(3):73-84.
205. Sakuragawa N, Enosawa S, Ishii T, Thangavel R, Tashiro T, Okuyama T, et al. Human amniotic epithelial cells are promising transgene carriers for allogeneic cell transplantation into liver. Journal of human genetics. 2000;45(3):171-6.
206. Moritoki Y, Ueno Y, Kanno N, Yamagiwa Y, Fukushima K, Gershwin ME, et al. Amniotic epithelial cell-derived cholangiocytes in experimental cholestatic ductal hyperplasia. Hepatology research : the official journal of the Japan Society of Hepatology. 2007;37(4):286-94.
207. Marongiu F, Gramignoli R, Dorko K, Miki T, Ranade AR, Paola Serra M, et al. Hepatic differentiation of amniotic epithelial cells. Hepatology. 2011;53(5):1719-29.
208. Che Abdullah CA, Lewis Azad C, Ovalle-Robles R, Fang S, Lima MD, Lepro X, et al. Primary liver cells cultured on carbon nanotube substrates for liver tissue engineering and drug discovery applications. ACS applied materials & interfaces. 2014;6(13):10373-80.
209. Fung J, Lee CK, Chan M, Seto WK, Wong DK, Lai CL, et al. Defining normal liver stiffness range in a normal healthy Chinese population without liver disease. PloS one. 2013;8(12):e85067.
210. Mueller S, Sandrin L. Liver stiffness: a novel parameter for the diagnosis of liver disease. Hepatic medicine : evidence and research. 2010;2:49-67.
211. TING CH. Evaluation of alternative in vivo and in vitro models for drug metabolism testing in drug discovery: National University of Singapore; 2013.
212. Li W, Wang D, Qin J, Liu C, Zhang Q, Zhang X, et al. Generation of functional hepatocytes from mouse induced pluripotent stem cells. Journal of cellular physiology.

2010;222(3):492-501.
213. Muller M, Jansen PL. The secretory function of the liver: new aspects of hepatobiliary transport. Journal of hepatology. 1998;28(2):344-54.
214. Berk PD, Stremmel W. Hepatocellular uptake of organic anions. Progress in liver diseases. 1986;8:125-44.
215. Baharvand H, Hashemi SM, Kazemi Ashtiani S, Farrokhi A. Differentiation of human embryonic stem cells into hepatocytes in 2D and 3D culture systems in vitro. The International journal of developmental biology. 2006;50(7):645-52.
216.Luo G, Guenthner T, Gan LS, Humphreys WG. CYP3A4 induction by xenobiotics: biochemistry, experimental methods and impact on drug discovery and development. Current drug metabolism. 2004;5(6):483-505.
217. Gerets HH, Tilmant K, Gerin B, Chanteux H, Depelchin BO, Dhalluin S, et al. Characterization of primary human hepatocytes, HepG2 cells, and HepaRG cells at the mRNA level and CYP activity in response to inducers and their predictivity for the detection of human hepatotoxins. Cell biology and toxicology. 2012;28(2):69-87.
218. Wang M, Pei H, Zhang L, Guan L, Zhang R, Jia Y, et al. Hepatogenesis of adipose-derived stem cells on poly-lactide-co-glycolide scaffolds: in vitro and in vivo studies. Tissue engineering Part C, Methods. 2010;16(5):1041-50.
219. Ghaedi M, Duan Y, Zern MA, Revzin A. Hepatic differentiation of human embryonic stem cells on growth factor-containing surfaces. Journal of tissue engineering and regenerative medicine. 2014;8(11):886-95.
220. Mizejewski GJ. Alpha-fetoprotein structure and function: relevance to isoforms, epitopes, and conformational variants. Experimental biology and medicine. 2001;226(5):377-408.
221. Mizejewski GJ. Physiology of alpha-fetoprotein as a biomarker for perinatal distress: relevance to adverse pregnancy outcome. Experimental biology and medicine. 2007;232(8):993-1004.
222. Arrieta O, Cacho B, Morales-Espinosa D, Ruelas-Villavicencio A, Flores-Estrada D, Hernandez-Pedro N. The progressive elevation of alpha fetoprotein for the diagnosis of hepatocellular carcinoma in patients with liver cirrhosis. BMC cancer. 2007;7:28.
223. Lin N, Lin J, Bo L, Weidong P, Chen S, Xu R. Differentiation of bone marrow-derived mesenchymal stem cells into hepatocyte-like cells in an alginate scaffold. Cell proliferation. 2010;43(5):427-34.
224. Moon YJ, Lee MW, Yoon HH, Yang MS, Jang IK, Lee JE, et al. Hepatic differentiation of cord blood-derived multipotent progenitor cells (MPCs) in vitro. Cell biology international. 2008;32(10):1293-301.
225. Babeu JP, Boudreau F. Hepatocyte nuclear factor 4-alpha involvement in liver and intestinal inflammatory networks. World journal of gastroenterology : WJG. 2014;20(1):22-30.
226. DeLaForest A, Nagaoka M, Si-Tayeb K, Noto FK, Konopka G, Battle MA, et al. HNF4A is essential for specification of hepatic progenitors from human pluripotent stem cells. Development. 2011;138(19):4143-53.
227. Ong SY, Dai H, Leong KW. Hepatic differentiation potential of commercially available human mesenchymal stem cells. Tissue engineering. 2006;12(12):3477-85.

228. Teckman JH, Qu D, Perlmutter DH. Molecular pathogenesis of liver disease in alpha1-antitrypsin deficiency. Hepatology. 1996;24(6):1504-16.
229. Van Eyken P, Desmet VJ. Cytokeratins and the liver. Liver. 1993;13(3):113-22.
230. Omary MB, Ku NO, Toivola DM. Keratins: guardians of the liver. Hepatology. 2002;35(2):251-7.
231. A. A. Gumerova MAT, and A. P. Kiassov. Expression of Different Liver Cell Markers During the Early Prenatal Human Development. Cell and Tissue Biology 2007;1(2):143–50.
232. Burchell A, Hume R. The glucose-6-phosphatase system in human development. Histology and histopathology. 1995;10(4):979-93.
233. Lea MA, Walker DG. The metabolism of glucose 6-phosphate in developing mammalian tissues. The Biochemical journal. 1964;91(3):417-24.
234. Kacevska M, Robertson GR, Clarke SJ, Liddle C. Inflammation and CYP3A4-mediated drug metabolism in advanced cancer: impact and implications for chemotherapeutic drug dosing. Expert opinion on drug metabolism & toxicology. 2008;4(2):137-49.
235. Zanger UM, Schwab M. Cytochrome P450 enzymes in drug metabolism: regulation of gene expression, enzyme activities, and impact of genetic variation. Pharmacology & therapeutics. 2013;138(1):103-41.
236. Tirona RG, Lee W, Leake BF, Lan LB, Cline CB, Lamba V, et al. The orphan nuclear receptor HNF4alpha determines PXR- and CAR-mediated xenobiotic induction of CYP3A4. Nature medicine. 2003;9(2):220-4.
237. Ince I, Knibbe CA, Danhof M, de Wildt SN. Developmental changes in the expression and function of cytochrome P450 3A isoforms: evidence from in vitro and in vivo investigations. Clinical pharmacokinetics. 2013;52(5):333-45.
238. Soars MG, Gelboin HV, Krausz KW, Riley RJ. A comparison of relative abundance, activity factor and inhibitory monoclonal antibody approaches in the characterization of human CYP enzymology. British journal of clinical pharmacology. 2003;55(2):175-81.
239. Lee CR, Goldstein JA, Pieper JA. Cytochrome P450 2C9 polymorphisms: a comprehensive review of the in-vitro and human data. Pharmacogenetics. 2002;12(3):251-63.
240. Treluyer JM, Gueret G, Cheron G, Sonnier M, Cresteil T. Developmental expression of CYP2C and CYP2C-dependent activities in the human liver: in-vivo/in-vitro correlation and inducibility. Pharmacogenetics. 1997;7(6):441-52.
241. Koukouritaki SB, Manro JR, Marsh SA, Stevens JC, Rettie AE, McCarver DG, et al. Developmental expression of human hepatic CYP2C9 and CYP2C19. The Journal of pharmacology and experimental therapeutics. 2004;308(3):965-74.
242. Esther Bui AMK, Autumn Klein. Women with Epilepsy: A Practical Management Handbook: Cambridge University Press.
243. Wells RG. The role of matrix stiffness in regulating cell behavior. Hepatology. 2008;47(4):1394-400.
244. Liu C, Liu Y, Xie H, Zhao S, Xu X, Fan L, et al. Role of three-dimensional matrix stiffness in regulating the chemoresistance of hepatocellular carcinoma cells.

Biotechnology and applied biochemistry. 2014.
245. You J, Park SA, Shin DS, Patel D, Raghunathan VK, Kim M, et al. Characterizing the effects of heparin gel stiffness on function of primary hepatocytes. Tissue engineering Part A. 2013;19(23-24):2655-63.
246. Yamazoe T, Shiraki N, Toyoda M, Kiyokawa N, Okita H, Miyagawa Y, et al. A synthetic nanofibrillar matrix promotes in vitro hepatic differentiation of embryonic stem cells and induced pluripotent stem cells. Journal of cell science. 2013;126(Pt 23):5391-9.
247. Ghaedi M, Soleimani M, Shabani I, Duan Y, Lotfi AS. Hepatic differentiation from human mesenchymal stem cells on a novel nanofiber scaffold. Cellular & molecular biology letters. 2012;17(1):89-106.
248. Piryaei A, Valojerdi MR, Shahsavani M, Baharvand H. Differentiation of bone marrow-derived mesenchymal stem cells into hepatocyte-like cells on nanofibers and their transplantation into a carbon tetrachloride-induced liver fibrosis model. Stem cell reviews. 2011;7(1):103-18.
249. Farzaneh Z, Pournasr B, Ebrahimi M, Aghdami N, Baharvand H. Enhanced functions of human embryonic stem cell-derived hepatocyte-like cells on three-dimensional nanofibrillar surfaces. Stem cell reviews. 2010;6(4):601-10.
250. Ber S, Torun Kose G, Hasirci V. Bone tissue engineering on patterned collagen films: an in vitro study. Biomaterials. 2005;26(14):1977-86.
251. Wang Y, Yao M, Zhou J, Zheng W, Zhou C, Dong D, et al. The promotion of neural progenitor cells proliferation by aligned and randomly oriented collagen nanofibers through beta1 integrin/MAPK signaling pathway. Biomaterials. 2011;32(28):6737-44.
252. Ma J, He X, Jabbari E. Osteogenic differentiation of marrow stromal cells on random and aligned electrospun poly(L-lactide) nanofibers. Annals of biomedical engineering. 2011;39(1):14-25.
253. Ball SG, Shuttleworth A, Kielty CM. Inhibition of platelet-derived growth factor receptor signaling regulates Oct4 and Nanog expression, cell shape, and mesenchymal stem cell potency. Stem Cells. 2012;30(3):548-60.
254. Pelham RJ, Jr., Wang Y. Cell locomotion and focal adhesions are regulated by substrate flexibility. Proceedings of the National Academy of Sciences of the United States of America. 1997;94(25):13661-5.
255. Lee J, Cuddihy MJ, Kotov NA. Three-dimensional cell culture matrices: state of the art. Tissue engineering Part B, Reviews. 2008;14(1):61-86.
256. Zhang S, Gelain F, Zhao X. Designer self-assembling peptide nanofiber scaffolds for 3D tissue cell cultures. Seminars in cancer biology. 2005;15(5):413-20.
257. Albrecht DR, Underhill GH, Wassermann TB, Sah RL, Bhatia SN. Probing the role of multicellular organization in three-dimensional microenvironments. Nature methods. 2006;3(5):369-75.
258. Lee GY, Kenny PA, Lee EH, Bissell MJ. Three-dimensional culture models of normal and malignant breast epithelial cells. Nature methods. 2007;4(4):359-65.

APPENDIXI: PUBLICATIONS AND CONFERENCE PRESENTATIONS

Publications

(1) C Zhao, JS Lin, M Choolanie, YY Dan, G Pastorin, HK Ho. Enhanced hepatic differentiation of human amniotic epithelial cells on poly-ethylene glycol linked multi-walled carbon nanotube coated hydrogel. Manuscript in preparation

(2) C Zhao, H Andersen, HK Ho, G Pastorin, B Özyilmaz. Enhanced myogenic differentiation of human mesenchymal stem cells on patterned graphene sheets. Manuscript in preparation

(3) C Zhao, H Andersen, B Özyilmaz, S Ramaprabhu, G Pastorin, HK Ho. Spontaneous and specific myogenic differentiation of human mesenchymal stem cells on polyethylene glycol-linked multi-walled carbon nanotube films for skeletal muscle engineering. Nanoscale (IF: 7.394). 2015, DOI: 10.1039/c5nr04303d.

(4) C Zhao, A Tan, G Pastorin, HK Ho. Nanomaterial scaffolds for stem cell proliferation and differentiation in tissue engineering. Biotechnol Adv (IF: 9.015). 2013, 31(5):654-68.

Conference presentations

(1) Oral presentation, "Spontaneous skeletal myogenic differentiation of human mesenchymal stem cells on films of polyethylene glycol-linked multi-walled carbon nanotubes". 2015 Global Conference on Polymer and Composite Materials (PCM 2015), Beijing, China. May 2015 (*Best Oral Presentation*)

(2) Oral presentation, "Films of polyethylene glycol-linked multi-walled carbon nanotubes favored myogenic differentiation of human mesenchymal stem cells for engineering skeletal muscle". 9th NUS-AAPS PharmSci@Asia Symposium, Shanghai, China. Jun 2014

(3) Poster presentation, "The effect of polyethylene glycol linked multi-walled carbon nanotubes on myogenic differentiation of human mesenchymal stem cells for skeletal muscle engineering". 4th International Conference on Stem Cell Engineering, Coronado, CA, USA. Mar 2014

(4) Poster presentation, "The effect of polyethylene glycol linked multi-walled carbon nanotubes on myogenic differentiation of human mesenchymal stem cells". 3rd Nano Today Conference, Singapore. Dec 2013